UC Riverside
UC Riverside Electronic Theses and Dissertations

Title

Implications of IFNβ and EphB2 mediated Ephrin-B Reverse Signaling on Inflammation, Antiviral Response and Neurotoxicity in HIV

Permalink

https://escholarship.org/uc/item/7t62w353

Author

Koury, Jeffrey

Publication Date

2024

UNIVERSITY OF CALIFORNIA
RIVERSIDE

Implications of IFNβ and EphB2 mediated Ephrin-B Reverse Signaling on Inflammation,
Antiviral Response and Neurotoxicity in HIV

A Dissertation submitted in partial satisfaction
of the requirements for the degree of

Doctor of Philosophy

in

Biomedical Sciences

by

Jeffrey Koury

March 2024

Dissertation Committee:
     Dr. Marcus Kaul, Chairperson
     Dr. Iryna Ethell
     Dr. Meera Nair

The Dissertation of Jeffrey Koury is approved:

_____

_____

_____

<div align="right">Committee Chairperson</div>

University of California, Riverside

ACKNOWLEDGEMENTS

The work in this dissertation would not be possible without the support of family, friends, professors, mentors, and pets.

I'd like to acknowledge my family and friends, who only asked a few times "when are you graduating?" Sorry for disappearing at times, I should have a little more time now.

I'd like to acknowledge my professor, Marcus Kaul, who helped provide me with the freedom to pursue the scientific questions I was passionate about.

I'd like to acknowledge my committee members Dr. Ethell and Dr. Nair for their continued guidance and effort in ensuring my success.

I'd like to acknowledge my cats, Pesto and Catarina, they are the best.

Finally, I'd like to acknowledge myself. Which I never do. For often taking the road less travelled and pressing onward even when the fruits of the labor seemed unattainable or distant.

DEDICATION

I dedicate this thesis to the dreamers and visionaries. Nobody ever changed the world

taking safe incremental steps. Dream big, find your passions, and sprint towards them

unabated.

Finally, I dedicate this thesis to my wife Samantha Koury, who provided endless support

in all forms throughout this program and always encouraged me to pursue my passions.

Successes are much easier when you have a supportive, encouraging, and intelligent

partner by your side.

ABSTRACT OF THE DISSERTATION

Implications of IFNβ and EphB2 mediated Ephrin-B Reverse Signaling on Inflammation, Antiviral Response and Neurotoxicity in HIV

by

Jeffrey Koury

Doctor of Philosophy, Graduate Program in Biomedical Sciences
University of California, Riverside, March 2024
Dr. Marcus Kaul, Chairperson

Human immunodeficiency virus-1 (HIV-1) is a retrovirus that can infiltrate and infect the central nervous system (CNS) leading to HIV-associated neurocognitive disorders (HAND). HAND is a condition behaviorally characterized by cognitive and neurological impairments, and pathologically characterized by rampant inflammation and loss of synaptic integrity. Although therapeutics exist to increase the lifespan of people living with HIV, the overall prevalence of HAND and the presence of HIV induced neuronal damage remains unchanged. Understanding the mechanisms underlying the neuropathology in HIV will guide the development of more efficacious therapeutics.

One hallmark response to HIV is the type I interferon antiviral response. HIV-1, and an HIVgp120 transgenic (HIVgp120tg) mouse model, both activate the innate immune system, including the production of type 1 interferons (IFNs) α and β, and induction of IFN-stimulated genes (ISG). In this dissertation, we characterize IFNβ's role in HIVgp120tg induced neuroHIV using an IFNβKO mouse model. The neuropathology observed in HIVgp120tg is only moderately affected by the KO of IFNβ but in a sex-

dependent fashion. Notably, IFNβKO results in an amelioration of neuronal presynaptic terminal damage but no protection of neuronal dendrites in the hippocampal CA1 region of HIVgp120tg mice. Additionally, female IFNβ-deficient HIVgp120tg mice display diminished microglial activation in the cortex and hippocampus. IFNβKO abrogates or diminishes the induction of type I interferon related genes including MX1, DDX58, IRF7, and IRF9 in HIVgp120tg brains. Additionally, the effects of IFNβKO on MAPK activities with a pronounced reduction of active ERK1/2 and active p38 in the HIVgp120tg brain. In summary, these findings show that IFNβ's absence in the presence of HIVgp120, is partially protective when assessing hippocampal pre-synaptic terminals and microglial counts, but partially damaging based on cortical dendritic assessment. Moreover, IFNβ plays a vital role in mediating the gp120 induced type I interferon response, expression of pro-inflammatory markers, and MAPK signaling.

Additionally, we highlight the activation of ephrin-B/EphB in the CNS of people living with HIV driven, at least in part, by gp120 viral envelope protein and type I interferon, IFNβ. Furthermore, EphB2 mediated ephrin-B reverse signaling onto microglia induces a prominent pro-inflammatory and antiviral signature with the capacity for this microglial specific pro-inflammatory secretome profile to induce non-contact dependent neurotoxicity. Finally, knockdown of microglial ephrin-B1, a binding partner for EphB2, shows a partial alleviation of the microglial pro-inflammatory signature and resulting neurotoxicity. Elevated EphB2 and its signaling onto microglia may present as a novel mechanism of neuroinflammation, and mediator of neurotoxicity, seen in the context of neuroHIV and potentially other neurodegenerative diseases.

TABLE OF CONTENTS

LIST OF FIGURES

Chapter 4

LIST OF TABLES

Chapter 4

Chapter 5

CHAPTER ONE:

Introduction to NeuroHIV, Microglial Models, Type I Interferons, and Ephrin-B/EphB

Signaling

1.1. HIV

Human Immunodeficiency Virus (HIV) is a single-stranded RNA (ssRNA) retrovirus with a global burden of 37 million people (*1*). HIV is transmitted through sexual contact across mucosal surfaces, fetal or infant exposure from the mother, and by inoculation through the skin (*2*). Early-stage clinical symptoms include generalized symptoms such as fever, headache, rash, sore throat and later progress to weight loss, cough, and swollen lymph nodes due to weakening of the immune system. HIV most prominently productively infects CD4+ T Cell, and as the infection progresses the CD4+ T Cell count diminishes from a normal 500-1200 cells per ul to <350 cells per ul, perpetuating opportunistic infection. Ultimately, the CD4+ T Cell count progressively diminishes to 200 cells per ul which is defined as Acquired Immunodeficiency Syndrome (AIDS) (*3*).

HIV Epidemiology

There are 2 main subtypes of the virus: HIV-1, the most prevalent and pathogenic subtype and HIV-2, primarily localized to western Africa, but less likely to progress to AIDS (*4*). HIV-1 can be sub-classified into 4 phylogenetic groups - M, N, O and P, based on separate instances of primate to human infections (*5*). Solely the M phylogenetic group resulted in a widespread pandemic (*5*). The M group is further divided into 9 different categories (A, B, C, D, F, G, H, J and K. (*6-8*). A consequence of this diversity is the increased difficulty in managing infections, as there is 25-35% molecular diversity between these subtypes in envelope (*env)* protein (*9*). Furthermore, antiretroviral therapies have not been designed and screened against all M subtypes, and thus exhibit poor fidelity against certain subtypes, for example, non-nucleoside transcriptase inhibitors might be less

efficacious against the F subtype (*10, 11*). However, regardless of the diversity, the group M HIV viruses don't show many differences in terms of transmissibility.

HIV Cell Binding and Entry

HIV viral entry requires the presence of CD4 and chemokine co-receptors CXCR4 or CCR5 on the host cell surface (*12*). Different strains of HIV have a preference towards leveraging different chemokine receptors. For example, HIVIIIB prefers CXCR4, while HIVBaL prefers CCR5, with the capacity of dual tropism in some strains (*2*).   Regardless of the strain or subtype, HIV binding and delivery of the viral payload into the cell requires engagement of viral protein, *env* (gp120 and gp41), and host cell receptor CD4. The virus initially attaches to the host by interacting with heparan sulfate proteoglycans, α4β7 integrins, adherens molecules and other proteins. This functionally allows the viral envelope protein, gp120, to come into proximity with CD4. Next, gp120, a tetramer comprised of 5 conserved domains (C1-C5) and 5 viral loops (V1-V5) binds to CD4, causing rearrangement of V1/V2 and subsequently V3. Following this conformational change, co-receptor (CCR5 or CXCR4) binding is allowed to progress mediated by the V3 loop. Membrane fusion is initiated as a peptide of gp41 inserts into the target membrane. Following fusion, the ssRNA virion genome enters the cytoplasm where it is reverse transcribed to synthesize the negative strand single strand DNA (ssDNA). RNase H degrades the ssRNA template and the positive strand DNA is synthesized. Following the extension of the second DNA strand, the pre-integration complex (PIC) is formed. It gets transported into the nucleus, potentially by a set of viral proteins involving Matrix (MA) and Capsid (CA) proteins. Integrase helps incorporate this DNA into the host genome,

where it is transcribed and translated and assembled using the host cell machinery and then exported out of the cell. (Reviewed in (*13*)).

This viral binding, entry and production can occur in the periphery by cells containing even low density CD4 receptors with either chemokine co-receptor. In the periphery, these primarily include CD4+ T cells and macrophages. The presumed route of entrance into the Central Nervous System (CNS) for HIV is via the trojan horse mechanism, primarily macrophages in the periphery traffic across the blood brain barrier into the CNS **(Fig 1.1)** (*14*). Once macrophages have trafficked into the CNS, the only other cell type expressing CD4 and chemokine co-receptors capable of being productively infected are microglia, which serve as a reservoir for HIV and critical mediators of neuroinflammation and neuronal damage (*15*). In fact, *in vitro* studies show depleting microglia alone can abrogate recombinant gp120 induced neurotoxicity and synaptic damage (*12, 16*).
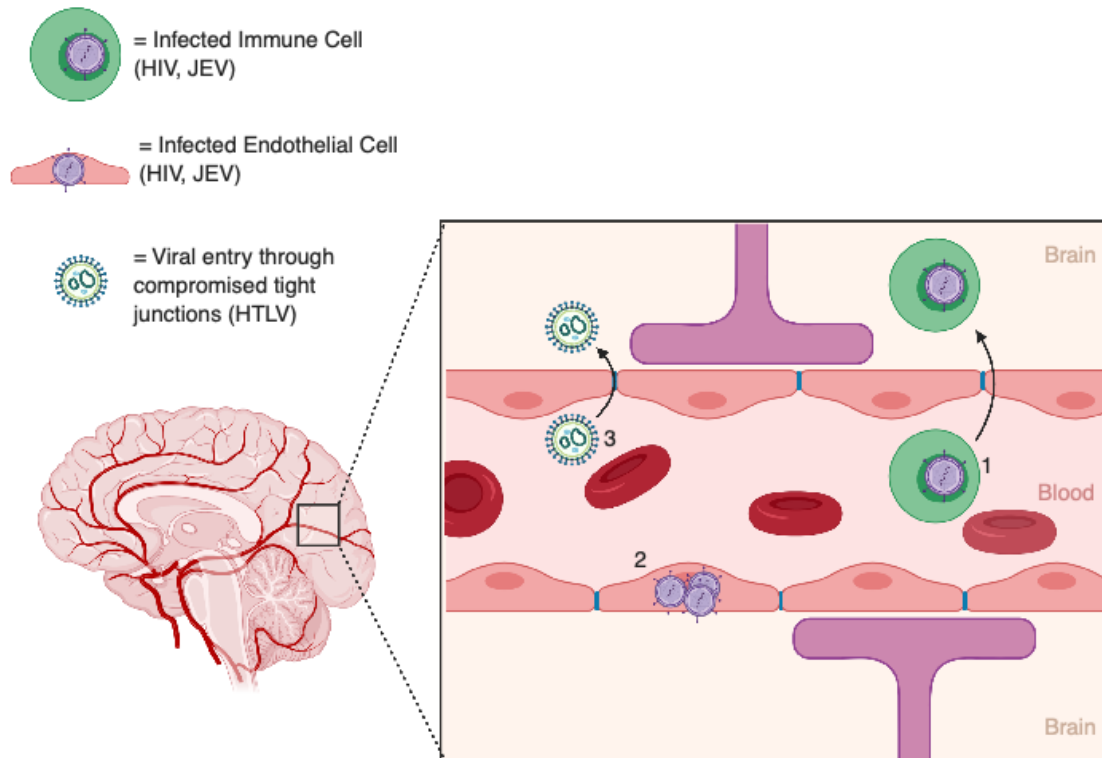
Figure 1.1. Mechanisms of viral entry through the blood brain barrier (BBB). Viral entry through the BBB can occur via 3 methods: (1) The Trojan Horse model where a virus leverages permissive host immune cells as a vehicle, (2) direct infection of brain microvascular endothelial cells (BMVECs) and (3) viral entry through dysregulation of tight junction proteins. Purple structures = astrocytic processes. HIV: Human immunodeficiency virus; JEV: Japanese encephalitis virus; HTLV: Human T Lymphotropic Virus.

NeuroHIV

Of the 37 million individuals living with HIV, an estimated 15-55% develop HIV-associated neurocognitive disorder (HAND) (*17, 18*). Symptomatically, this disorder manifests as cognitive impairment, motor dysfunction and speech impairments; while neuropathologically, it is characterized by synaptic degeneration and glial cell activation. The primary regions of neuronal damage in the brain include the frontal cortex, hippocampus, basal ganglia, substantia nigra, cerebellum and putamen (*19-23*).

In the CNS, the primary mediators of neurotoxicity and productive infection are microglia and macrophages. Some of the earliest pathological findings in HIV encephalitis were the presence of multinucleated giant cells and microglial nodules (*24, 25*). HIV infected microglia have been well described in generating a slew of secreted neurotoxic factors including excitotoxic substances, inflammatory cytokines, chemokines and viral proteins the release of which presumably results in neuroHIV (*26*). While existing antiretroviral therapies lower the viral load to levels below detection, there is currently no cure for HIV and the overall prevalence of HAND remains unchanged.

1.2. Microglia *in vitro* models

Microglial Ontogeny

Microglia are the resident immune cells of the central nervous system with several functions. The first is surveying the CNS environment for any perturbations including invading pathogens and internal danger signals. The second function is its communication and regulation of neuronal cell homeostasis (i.e. neuroinflammation, synaptic pruning etc.).

However, the origin of this cell type has been a point of contention for years. For decades, researchers were uncertain about the ontogeny of microglia, but recently, elegant in vivo lineage tracing studies have been employed to identify a primitive myeloid progenitor that contributes to the adult microglial population in the CNS (*27*). These primitive myeloid progenitors originate in the yolk sac before traversing the blood circulation to populate and differentiate in the developing CNS (*27-30*). Mouse embryonic studies revealed a microglial embryonic precursor at E7.5-E9.5 days from yolk sac blood islands, a stark ontological difference to hematopoietic stem cells in the fetal liver (E12.5) and bone marrow which give rise to hematopoietic derived macrophages (including peripheral, perivascular, choroid plexus and meningeal macrophages) (*31-33*). The transcription factor, Myb, was noted to be required for hematopoietic derived macrophage development, but not necessary for yolk sac derived macrophages which give rise to tissue resident macrophages, which includes microglia (*34*). Although Myb is not involved in microglia differentiation, PU.1 and IRF8 are crucial (*30, 34*). In fact, mice lacking the transcription factor, PU.1, were devoid of any microglia, which played a key role in identifying the mesodermal origin of microglia (*35, 36*). In addition, ablation of CSF1R in mice revealed the need for CSF1R signaling in the maintenance of microglia, as the CSF1R KO mouse lacked microglia, too (*37*). Factors such as IL-34 act as a ligand for the CSF-1 receptor, which functions to maintain microglia after development, primarily in the developed brain (*38, 39*).

Difficulties of Current Methodologies

Primary Microglia

One method of studying human microglia is via primary cultures. Collection of microglia from autopsy of postmortem adult or fetal samples is extremely limited and requires many layers of consent. Therefore, accessibility for most researchers is limited, stifling research on many neurodegenerative diseases. Beyond the barrier to access, uncertainty of the time of death affects cell viability, while variability due to comorbidities and coinfections are also a concern with postmortem tissue. There are some credible sources, such as normal and pathological tissues recovered from a rapid autopsy program which ensure a low median postmortem delay time to retain viability (*40*). In addition, isolation of microglial cells involves a series of processing steps including mechanical homogenization, enzymatic digestions and percoll gradient (*41-43*). A drawback is the potential for the harsh processing to modulate the resting microglial signature, further confounding downstream experiments (particularly at the transcriptome level). In fact, transcriptome analysis of surgically removed brain tissue later cultured in vitro revealed a significant down regulation of microglia-related genes (*44*). In addition, blood derived macrophages exist in the brain (i.e. perivascular, choroidal, meningeal macrophages etc.) that reduce the microglial purity as they are retained during the percoll gradient.

Cell Lines

Cell lines prove to be advantageous in many respects, including cost effectiveness, an unlimited supply as they are immortalized and thus the ability to bypass many of the regulatory hurdles for handling primary human tissue. Nearly all microglial immortalized

cell lines are generated by transforming lentiviral vector expressing SV40 T antigen into primary embryonic human microglia (*45-48*). For example, huglia 1A1 was the first immortalized microglial cortical cell line derived from embryonic telencephalon tissue (*49*). This preferentially shifted the microglial transcriptome away from an adult phenotype, and more towards a fetal one while also altering the overall phenotype. In fact, many studies have recently highlighted several functional and transcriptomic differences of *ex vivo* microglia (*46, 50, 51*). The human microglial clone 3 cell line (HMC3) is also an SV40 immortalized human microglial cell line that stains positively for canonical markers including CD68, CD14, and CD11b (*52*). HMC3 immortalized lines' basal production of IL-6 was increased following 24 hour treatment with IL-1a or by LPS (*53*). Additionally, HMC3 cells responded to activation by HIV viral protein TAT as observed by production and detection of reactive oxygen species. Additionally, HMC3 were activated by HIV-vectors resulting in detection of inflammatory factors IL-6, CCL2, CCL5, CXCL10) (*54*). Although HMC3s, and other immortalized lines, serve many benefits the immortalization process may skew their transcriptomic profile away from physiological microglia. Additionally, these lines are generated from the isolation and generation of primary microglial cultures which are not exclusively microglia and likely contain other myeloid populations such as brain perivascular macrophages. Stem cell derived human microglia can lower the barrier of entry into performing translatable neurodegenerative research while addressing many of the issues with other methods, including mechanical stress, viability, impurities from macrophages etc. In addition, it is

9

an extremely scalable approach as stem cell derived human microglia can be propagated and expanded *ex vivo*.

Methods for Deriving Stem Cell Induced Human Microglia

It is important to emphasize that the expression profile of microglia is variable even in normal physiology contingent on a multitude of factors. As described by Li et al., the expression profile of parenchymal microglia differs from perivascular, meningeal, and choroid plexus macrophages of the CNS (*55*). In addition, the transcriptome of microglia from varying anatomical regions of the brain also differs. The differential expression reflects the various functions certain microglia prefer, and the microenvironment cues they receive drive the expression of these genes. This is important when determining which stem cell derived microglial protocol should be used to mimic certain microglial phenotype and which cells to be used in co-cultures.

Reference Describing the Method	Origin of iPSC or ESC	Gene Expression	Protein Expression	Notable Genes/Proteins Not or Lowly Expressed	Diseases that can Potentially be Studied
Abud et al. Method (*56*)	10 iPSC lines from either fibrobasts or PBMC from healthy donors	Day 38 – P2RY12, GPR34, C1Q, CABLES1, BHLHE41, TREM2, ITAM, PROS1, APOE, SLOCO2B1, SLC7A8, PPARD, CRYBB1, CX3CR1, RGS10 AND GAS6	Day 10 – CD234a and CD41a Day 14 – PU.1 and TREM2 Day 38 – CD45low, CD11bint, PU.1, TREM2, MERTK, ITGB5, CX3CR1, TGFBR1, TMEM119, IBA1 and PROS1	FLT3 KLF2	*Alzheimer's Disease *Huntington's Disease *Amyotrophic Lateral Sclerosis (ALS) *Frontotemporal Dementia (FTD)
McQuade et al. Method (*57*)	4 iPSC lines and 1 ESC (H9)	Day 38 – P2RY12, GPR34, C1Q, CABLES1, BHLHE41, TREM2, ITAM, PROS1, APOE, SLOCO2B1, SLC7A8, PPARD, CRYBB1, CX3CR1, RGS10 AND GAS6	Day 10 – CD234a and CD41a Day 14 – PU.1 and TREM2 Day 38 – CD45low, CD11bint, PU.1, TREM2, MERTK, ITGB5, CX3CR1, TGFBR1, TMEM119, IBA1 and PROS1	FLT3 KLF2	*Alzheimer's Disease *Huntington's Disease *Amyotrophic Lateral Sclerosis (ALS) *Frontotemporal Dementia (FTD)
Mancuso et al. Method (*58*)	3 ESCs (H9)	CX3CR1, TMEM119, P2RY12, P2RY13, Elmo1 (Homeostatic microglia cluster) IL-1B, IL-6, CCL2, CCL4 (Cytokine microglia cluster)	CD11b CD45	N/A	*Alzheimer's Disease
Haenseler et al. Method (*59*)	6 iPSC lines from healthy donors	P2RY12, GPR34, MERTK, C1QA, PROS1, GAS6 (*50*)	IBA1, CD11B, CD45, CD14, MERTK	HLA-DR	*Alzheimer's Disease *Amyotrophic Lateral Sclerosis (ALS) *Parkinson's Disease (PD)
Pandya et al. Method (*60*)	NCRM-5 iPSCs and iNC-01 iPSCs from healthy donor	P2RY12, GPR34, MERTK, C1QA, PROS1, GAS6 (*50*)	Day 0 - Nanog and Tra-1-81 Day 15 – CD34, CD45, CD43 Day 30 – CD11b, Iba1, HLA-DR, CD45, TREM2, CX3CR1	CD206, CD200R, CD86, CD80	N/A
Douvaras et al. Method (*61*)	14 iPSC lines and 2 ESC lines (H9 and RUES1)	P2RY12, GPR34, MERTK, C1QA, PROS1, GAS6 (*50*)	CD11b, CD11C, TMEM119, CX3CR1, P2RY12, IBA1	Genes – TMEM119, CX3CR1 and LAG3	N/A

Table 1.1. **Gene expression and protein expression associated with mature microglial like cells**. Expression profile for each iPSC/ESC derived differentiation method, and the potential diseases they can model.

The first method, as outlined by Abud et al., is a 5 weeklong, two step procedure initially differentiating iPSCs into hematopoietic progenitors (iHPCs) and then to mature microglia. The iMicroglia used in this dissertation were based on the Abud et al. protocol. This initial step recapitulates microglial ontogeny since iHPCs represent a population of early progenitors derived from the yolk sac that become microglia. At day 10, the protocol yields iHPCs which are CD43+/CD235+/CD41+. Serum free differentiation media is then added to the iHPCs which include human recombinant CSF-1, IL34 and TGFB1, and by day 14 these cells present with an expression profile (PU.1 and TREM2) which indicates that the cells are committed to the microglial fate. By day 38, microglia have matured, resembling a microglial phenotype rather than a monocyte/macrophage phenotype with a series of markers being expressed. The genomic integrity of these iPSC derived microglia was maintained compared to the iPSCs with a strong $r^2 > 0.92$. Furthermore, principal component analysis and correlation analysis reveal a close resemblance of these iPSCs derived microglia with primary human fetal microglia and adult microglia. Beyond transcriptomic characterization, iPSC derived microglia using this method have shown to be physiologically functional secreting an assortment of cytokines, responding to adenosine diphosphate (ADP), attributed to their expression of P2RY12, and phagocytosing human synaptosomes. They were also able to respond to neuronal and astrocytic cues including CX3CL1, CD200 and TGFB. For example, when TGFB, a factor needed in maintaining the microglial specific transcriptome signature, was removed 1517 genes were differentially expressed as compared to 1262 genes with TGFB. iPSC induced microglia injected into 3D brain organoid lacking microglia but containing neurons,

astrocytes and oligodendrocytes were able to home in on a site of injury and adopted an activated amoeboid morphology (*56*).

The McQuade et al. method, published by the same group, is like the method described by Abud et al., but removes the hypoxic environment and the FACS/MACS sorting component. Importantly, at the transcriptome level, expression of nearly all genes is retained when using this updated method (*57*). Expression analysis revealed only 55 genes that were differentially expressed between the older Abud et al. method and the newer McQuade et al. method, albeit there was a stringent $p<0.001$ and fold change > 2 restriction to be classified as differentially expressed (*57*). Furthermore, this methodology brings logistical benefits including reduced cost and an increase in yield (approximately 60-fold from the Abud et al. method). Presumably, this methodology is a more streamlined way to model AD and potentially other neurodegenerative disease including Huntington's, ALS and FTD (*57*).

In the Pandya et al. method, the stem cell derived microglia function like microglia in that they can phagocytose pHrodo E. coli bioparticles. However, one drawback from this study is the lack of principal component analysis clustering of the human iPSC derived microglia with primary human fetal microglia. Despite this, the mature iPSC derived microglia did show a gene expression profile representative of microglia **(Table 1.1)**. The drawback of the Pandya et al. method is the requirement for co-culture with astrocytes, whereas other techniques can mature the microglia like cells by supplementing defined factors secreted by neurons and astrocytes to mimic the co-culture environment (*60*).

Similarly, the Haenseler et al. method requires co-culture with neurons. The author highlights the importance of this co-culture as the gene ontology analysis identified a downregulation in pathways associated with type 1 interferons, TLR1, TLR2 signaling, and antigen presentation compared to the monoculture population. The Haenseler et al. method also yields 10-43X its starting iPSC cell number and requires significantly less time (approximately 1 month) than the Pandya method (*59*). Although both techniques require the use of co-culture, the environment microglia are nurtured in define their function and therefore co-culturing may be important to model the *in vivo* environment.

The Reitboeck et al. paper utilizes a modified method of deriving iPSC induced microglial like cells, from a previous macrophage differentiation protocol (*62*) that mimics the MYB-independent developmental pathway like that of yolk sac derived microglia. Briefly, TREM2 variants fibroblasts were isolated from patients. iPSCs were generated using a 4 factor Sendai virus reprogramming (Oct4, Sox2, Klf4 and C-myc). iPSCs were differentiated into embryoid bodies using EBdiff medium, and on day 4 embryoid bodies were collected and left to settle in a new dish. Myeloid differentiation medium was added every 5-7 days, and after 3-4 weeks iPSC derived Microglia were collected by replacing 2/3 of the medium and filtered. iPSC derived Microglia were differentiated further after isolation (*63*).

Microglia, are a highly plastic cell type, and exhibit multiple alterations at the transcriptome level when cultured in isolation and removed from the brain microenvironment (*44*). This stresses the importance of coculturing these iPSC derived microglia with an astrocyte/neuronal culture. For example, when monocytes are placed in

an astrocytic conditioned media, after 10-12 days they acquire a typical ramified microglial morphology. In addition they begin to overexpress substance P and microglial marker Iba-1 (*64*). However, even more representative is engrafting human iPSC derived microglia into a humanized mouse brain to study human microglial role *in vivo* in health and disease. To this goal, Hasselmann et al. took GFP expressing iPSC derived hematopoietic stem cell (HSCs) from the McQuade et al. method and transplanted this into the lateral ventricle of P1 MITRG humanized mice (*65, 66*). After 2 months, microglia assessed via IHC showed robust engraftment throughout the forebrain with high expression of PU.1, P2RY12, Iba1, Ku80 and TMEM119. The GFP expression strongly overlaid with P2RY12 expression, and the morphology of the engrafted cells was ramified like that of quiescent mature microglia.

<u>Use Cases for Stem Cell Derived Microglia</u>

With all the research emphasizing the use of stem cell derived microglia in studying AD, it is essential to propose other neurodegenerative diseases that can potentially be studied with these microglial like cells. In fact, on a transcriptomic level, hundreds of genes in the microglia gene signature exhibited significant overlap with sets of genes that were positively correlated in AD, in frontotemporal lobar degeneration (FTLD), in HIV-associated neurocognitive disorder (HAND), and in Schizophrenia (Scz) making these likely diseases to model with iPSC derived microglia (*44*). According to Abud et al., iPSC derived microglia express other CNS disease related genes including APP, PSEN1/2, HTT, GRN, TARDBP, LRRK2, C9orf72, SOD1, VCP and FUS. These genes have implications in ALS, Huntington's disease, FTD and are expressed at similar levels as compared to primary fetal and adult microglia (*56, 67-70*).

In addition, stem cell derived microglia can be used to model neuropsychiatric disorders. Microglial dysregulation may potentially be implicated in neuropsychiatric conditions such as depression, anxiety, and obsessive-compulsive disorder (OCD) (*71*). Schizophrenia and autism spectrum disorder have been linked to dysregulation of synaptic pruning and phagocytosis by microglia (*72*). Many of the conclusions drawn regarding microglial implications in depression, for example, are done on postmortem tissue which may contain issues with viability of cells. Some results suggest the presence of microgliosis in depressed patients who committed suicide compared to patients who died of other reasons (*73*). Additionally, a study correlated an increase in quinolinic acid, an NMDA receptor agonist released from activated microglia, with an increased density of microglia in depressed patients who committed suicide as compared to normal healthy controls (*74*). However, other peer reviewed publications have claimed a lack of correlation between major depressive or bipolar disorder and microglial activation. In a study of six post mortem patients with depression, only one showed increased microglial activation in the hippocampus as measured by HLA-DR (*75*). Other studies assessed a multitude of regions in the brain for an increase in microglial density, including various regions of the cortex as well as the hippocampus, and found no difference as compared to healthy controls, but did however identify differential expression of TNFa (*76*). Ultimately, the role of the resident immune system of the CNS is still a point of contention with regards to depression and suicide. Stem cell derived microglia can serve to elucidate some of these disparities by addressing the concerns of using postmortem tissue as stated previously.

Outside of disease modeling, and because of its scalability, iPSC derived microglia may also be used in high throughput drug screens to determine the efficacy of small molecule inhibitors. Microglia are a driving force for neurodegenerative diseases, putting them in the spotlight as a target for therapeutics. For example, microglia are involved in mediating the conditional removal of TDP-43 leading to neurodegeneration (*77*). Additionally, IFITM3+ primary microglia and microglia-like cells have been implicated in inflammatory production in stroke and in regulating gamma-secretase resulting in amyloid beta production in AD (*78*). Particularly, the iPSC derived microglia and neurons can be co-cultured and used to study the effects of perturbations of microglia on the health of neurons. Presumably many drugs diminishing the activation state, number of microglia or microglia subtype can be screened, and the health or electrical activity of the co-cultured neuron can be determined.

1.3. The antiviral response and IFNβ

In the context of NeuroHIV, studies have identified a significant activation of the type I interferon response in the cortex and hippocampus in PLWH as well as Simian Immunodeficiency Virus (SIV) models or HIV mouse models (*79-82*). Microglia, along with the other cells in the CNS milieu, express type I interferon receptor heterodimer IFNAR1/2, and thus elicit a heightened antiviral response when activated by IFNβ/a. This response is characterized by an upregulation of hundreds of interferon-stimulated genes (ISGs), which play a vital effector role in reducing replicon activity, inhibiting viral cell binding/entry, preventing viral assembly and other mechanisms of action (*83*). Importantly,

the sustained activation of this pathway may have dual implications: while it aids in controlling viral replication and spread within the CNS, it could also contribute to neuroinflammation and neurodegeneration, further exacerbating the neurological complications in HIV. Therefore, it is prudent to investigate the type I interferon response in microglia, who are productively infected by HIV, in the CNS and present as a latent reservoir for the virus.

PAMPs and Viral Detectors

The antiviral response is an innate immune response which detects canonical signals of a pathogen, triggers a standardized response to mitigate the infection and alerts the neighboring cells. For a host to be able to detect the pathogen, there are conserved Pathogen-Associated Molecule Patterns (PAMPs) that are unique to the pathogen such that the host response is specific and targeted. These include single stranded RNA, CpG DNA, LPS, double stranded RNA 5'triphsophate, lipopeptides and more (*84*). The host contains a slew of detectors, known as Pathogen Recognition Receptors (PRRs) to detect these molecular motifs on pathogens. These include Toll Like Receptors (TLRs) which are membrane-bound receptors, Retinoic acid-inducible gene-I (RIG-I)-like Receptors (RLRs) which are cytoplasmic detectors, C-type lectin receptors (CLRs) and others. As HIV contains single stranded RNA, one of the most relevant viral detectors includes RIG-I (*84*). RLRs signaling syphons through an adaptor protein on mitochondria: IPS-1, also known as mitochondrial antiviral signaling protein (MAVS). Subsequently, TNFR1-associated death domain protein (TRADD), a protein that is recruited to IPS-1, can then propagate

signaling to NF-kB or to IRF3 and IRF7 to activate pro-inflammatory cytokines, type I interferons, and type I interferon stimulated genes (*85*).

TLR7 is another HIV detecting receptor present on the endosome. TLR7, after binding occurs, dimerizes, and signals through an adaptor protein MyD88 (*86*). MyD88, in TLR7 and TLR9 signaling, is necessary to mediate interferon production and it does so in concert with IRAK1/4, IRF7 and TRAF3/6 (*87*). MyD88 dependent signaling not only phosphorylates and activates IRF7, but also NF-kB and MAPKs. IRF5 is a downstream regulator of the MyD88 dependent pathway and induces inflammatory cytokines through TLR7 (*88-90*).

Type I Interferon Response

Viral detection converges signaling down to transcription factors NF-kB, IRF3 and IRF7 which translocate to the nucleus to directly activate type I interferons (IFNβ/a) resulting in an enhanced antiviral response. IFNβ is a small 23-kDa protein that signals to its heterodimeric receptor (IFNAR1/2) in an autocrine/paracrine like fashion, initiating JAK/STAT signaling forming a complex of STAT1/STAT2/IRF9 (*91*). This complex, called ISGF3, potentiates the antiviral response and an assortment of downstream Interferon Stimulated Genes (ISGs) and Interferon Response Factors (IRFs) which often have potent antiviral properties. Among them are two crucial homologous transcription factors, IRF3 and IRF7. IRF3 is constitutively expressed, while IRF7 is expressed at lower levels and is inducible, but both contain Serine/Threonine phosphorylation sites to for activation and translocation to the nucleus (*92*).

In HIV models, following detection by TLR7 or RIG-I, signaling cascades activate NF-kB and IRF7 leading to activation of IFNB, providing potent antiviral properties. In an SIV model, topical IFNB treatment mitigated SIV transmission following SIV challenge, which included 1) recruitment of CD4+ T Cells and macrophages, 2) upregulation of inflammatory and myeloid genes, and 3) antiviral interferon inducible genes. Additionally, a transient up-regulation of IFNB was noted in both an SIV and an HIVgp120 transgenic mouse model (*79, 82*).

Innate Immune Response in the CNS

The cellular processes involved in innate immunity occur rapidly to prevent viral infections from expanding. However, if the innate immune response fails to alleviate the infection or if the viral infection evades the immune system, an acute infection cannot be contained. The infection can become chronic and/or spread into other tissues, including the CNS. The persistent infection in the CNS results in inflammation of distinct anatomical regions including the meninges (meningitis), brain (encephalitis) and spinal cord (myelitis) caused by release of an assortment of pro-inflammatory cytokines and other deleterious factors (*93-95*). This release of cytokines can be massive, constituting what is called a 'cytokine storm' of the innate immune response in the CNS resulting in neuropathology and consequently behavioral and neurologic deficits (*96*). Generally, viruses enter the organism in the periphery, including neurotropic viruses, and if the innate immune response is insufficient, they can migrate into the CNS via a multitude of routes.

The innate immune response in the CNS includes the response of resident cells to viral infection of brain tissue (i.e., microglia and astrocytic responses) as well as resident

CNS innate cells dynamically interacting with trafficking T cells entering from the periphery (*97*). Beyond this, peripheral cells of the innate system (neutrophils, peripheral monocyte/macrophages etc.) can migrate into the CNS upon viral infection after receiving chemokine cues. In addition, from a molecular basis, many of the signaling pathways and PRRs, including TLRs and RIG-I, that exist in the periphery maintain relevance in the CNS. Although neuroinflammation is a necessity to alleviate damage from viral infection, it is a double-edged sword where excessive inflammation can be deleterious. Therefore, it is a constant push and pull by the host to regulate these inflammatory processes.

Microglia and Astrocytes

The innate immune response in the CNS differs from that of the periphery primarily based on a unique set of resident cell types: Microglia and Astrocytes. Based on fate mapping studies, microglia are embryonically derived from primitive myeloid progenitors originating from the yolk sac (*27, 98*). Microglia migrate into the brain parenchyma where they have several functions including phagocytosis, release of antiviral components and synaptic pruning. One of their functions include the sensing of extracellular ATP, which is released from virally infected neurons (*99*). Detection of ATP by P2Y12 and P2X7 receptors on the surface of microglia cue the microglia to migrate to the virally infected neuron and induce antiviral effects as well as phagocytic activity (*100*). Microglia also express PRRs, which ultimately induce a downstream type 1 interferon response through a cascade of intracellular signaling involving components MAVS, TRIF, STING, IRF3/7, STAT1, as discussed above (*84*). The type 1 interferon response has been shown to be neuroprotective in a chronic infection/inflammatory setting. For example, IFNAR

expression in the glomeruli of the olfactory bulb is crucial in preventing the spread of virus through the nasal epithelium and into the brain parenchyma (*101*). In addition, upon intranasal Vesicular Stomatitis Virus (VSV) infection, IFNβ was produced by the neuroectodermal cells (primarily astrocytes, and to a lesser extent neurons) and found to be protective of other IFNβ negative distal brain regions leading to a contained viral spread. (*102*). To corroborate this study, another study injected VSV into the caudate-putamen, and linked a type I interferon response to limiting viral spread at the site of inoculation, as well as inhibiting the spread to synaptically connected neurons (*103*). STING, a player in the canonical signaling for initiating type 1 interferon production against cytosolic DNA, plays a critical role in controlling CNS infection. STING knockout mice expressed increased neurological signs, as well as increased viral load and dissemination in the CNS of West Nile Virus (WNV) infected mice compared to WT (*104*).

Neurons

Neurons possess the ability to host an innate immune response as well. For example, in WNV the granule cell neurons of the cerebellum express a host defense pathway gene signature, including STAT1 and IFN dependent genes (*105*). Neurons express many PRR pathways that induce anti-viral responses in neurons. Among them is the NOD-like receptor NLRP3 which is capable of suppressing WNV replication in neurons via IL-1β production (*106*). Additionally, TLR3 is required for induction of type 1 IFN in WNV infected cortical neurons (*107*). RABV infections regulate other PRR players by activating viral detector RIG-I at the mRNA and protein level, shown *in vitro* by RABV infection of two neuronal lines - NT2N and SKNSH (*108*). In Zika Virus

(ZIKV), the clinical manifestation of microcephaly is thought to occur due to infection and apoptosis of neural progenitor cells (*109*). Studies using human embryonic stem cell-derived cerebral organoids to recapitulate early-stage brain development implicated TLR3 activation to neural progenitor depletion (*110*). Endosomal TLR7, RIG-I/MDA5 and cGas-STING also contribute to sensing of ZIKV pathogen signals (*111*).

Cytokine and Chemokines Regulating the Blood-Brain Barrier (BBB)

The release of proinflammatory cytokines/chemokines from the innate immune response are triggers to help regulate the tightness and permissiveness of the BBB as well as assist in trafficking peripheral immune cells into the CNS. The release of cytokines including TNFα, IL-1β and type 1 interferons can differentially regulate the permeability of the BBB. Increased TNFα and IL-1β expression compromise the tight junction proteins, claudin 5 and ZO-1, located between the BMVECs, allowing the BBB to be more permissive (*112*). This effect on the BBB is mediated by expression of MMP-9 in response to TNFα induced activation of p21-activated-kinase-1 (PAK1). Conversely, the loss of type 1 interferon specific signaling in cerebellar astrocytes promoted BBB permeability to the hindbrain in a WNV infection model (*113*). Viral entry increased specifically in the hindbrain, however, viral replication and tropism remained the same further indicating type 1 interferon's role specifically in modulating permeability at the level of the BBB (*113*).

1.4. Ephrin-B/EphB

Overview

Ephrins are a family of tyrosine receptor kinases that perform various functions generally mediated through contact dependent communication between cells. During development, they are often described in axon guidance and forming synaptic connections between neurons. During adulthood, they are often described to be involved in remodeling synapses, stem cell self-renewal, epithelial cell differentiation and recently immune function (*114, 115*). Ephrins and their receptors (Eph) can be classified as A or B and can signal bidirectionally. Forward signaling from the ephrin expressing cell to the Eph receptor expressing cell, or reverse signaling vice versa. There are nine EphA receptors that bind to five ephrin-A ligands, and five EphB receptors which bind three ephrin-B ligands (*116*). EphA4, and in the context of this dissertation EphB2, can bind ephrins outside of their traditional class (*117*). In this dissertation, EphB2 is described as a novel differentially expressed marker in the CNS of PLWH and further assessed for its role in neuroinflammation.

Structure

Ephrin/Eph are a family of tyrosine receptor kinases. Ephrin ligands have a general structure that includes an Eph receptor-binding domain and a linker to the plasma membrane (in the case of the A class) and a transmembrane segment with a cytoplasmic region (in the case of the B class). Eph receptors are larger and contain an ephrin ligand-binding domain, a single transmembrane segment and cytoplasmic region with a kinase domain. Eph receptors A and B are highly conserved, with the primary source of variability

coming from the ligand binding domain. As such, the diversity in their function and activation comes from the spatial and temporal signaling kinetics and clustering of ligand or receptor (*118*). Ephrin ligands have distinct structural differences near the transmembrane regions, with ephrin-A anchoring in the cell membrane via glycosylphosphatidylinositol and ephrin-B with a transmembrane segment that connects to the cytoplasmic tail (*119*).

Bidirectional Signaling

Eph receptor-ephrin complexes are unique in that they can initiate forward (to Eph expressing cell) and reverse signaling (to ephrin expressing cell). In forward signaling, ephrin binding can cause Eph receptors of different types and similar types to cluster based on Eph-Eph receptor cis domain clustering further potentiating signaling (*120, 121*). Phosphorylation of tyrosine residues in the juxtamembrane domain and kinase domain of most Eph receptors is necessary for kinase activity and subsequent biological activities of Eph receptors (*122*). Activation of Eph receptors recruit downstream signaling proteins that often have SH2 domains (including Src and Abl families and adaptors Nck and Crk) (*123, 124*). In the context of neurons, EphB2 cytoplasmic tail can phosphorylate NMDA receptors which promote cell surface localization and drives calcium currents (*125*). Additionally, EphB2, which is present on dendritic spines, tyrosine phosphorylates syndecan-2 a process required for normal spine formation (*126*).

In reverse signaling, the Eph receptor expressing cell can signal to the ligand expressing cell. For EphB, during EphB receptor binding, ephrin-B can be phosphorylated by Src kinase allowing SH2 domains to bind (*127, 128*). Furthermore, phosphorylation of

ephrin-B serine by reverse signaling stabilizes AMPA receptors in synapses (*129*). Reverse signaling to ephrin-B also recruits PDZ domain proteins regulating a variety of neuronal properties such as LTP and axon guidance (*130, 131*). Ephrin/Eph engagement is short lived given the immediate endocytosis that occurs, compromising this complex (*132*). Beyond cell-cell contact dependent signaling, EphB2 can be packaged and exported through small extracellular vesicles (EVs) and reverse signal onto ephrin-B expressing cells to induce STAT3, showing that full length unanchored EphB2 is sufficient to induce reverse signaling (*133*).

Regulators of ephrin-B/EphB

Little is known regarding the transcriptional regulators of the ephrin family. In the intestinal crypts, WNT-beta catenin plays a role in regulating ephrin-B1 and EphB receptor expression. Additionally, amyloid beta can bind to the fibronectin repeat domain of EphB2 and trigger EphB2 degradation into the proteosome. In the context of Alzheimer, overexpression of EphB2 lead to improved memory/anxiety behavioral problems via improved recruitment and phosphorylation of NMDA receptors (*134*). One study, has pointed to NF-kB binding sites in the enhancer region of EphB2 (*135*). Regulation of the signaling events occurs through multiple methods including 1) Eph receptor-ephrin complex internalization, or trans-endocytosis, 2) cell repulsion following cleavage by ADAMs or MMPs, 3) MMP or gamma secretase mediated Eph receptor cleavage, 4) cis-interactions attenuating signals or 5) dephosphorylation (*132, 136-141*).

Ephrin-B/EphB and the Immune Response

Ephrin-B/EphB signaling, to a lesser extent, has been described in promoting inflammation mainly in the periphery, but in only a handful of studies in the CNS. Ephrin-B1 expression was significantly elevated in fibroblasts and peripheral blood leukocytes of patients with rheumatoid arthritis (*142*). In the same study, animal models showed the production of TNFa and IL-6 following ephrin-B1-Fc treatment (*142*). In the liver, EphB2 knockout mice treated with liver fibrosis inducing chronic carbon tetrachloride (CCl_4) exposure were able to reduce liver fibrosis and significantly reduce an assortment of inflammatory factors such as TNFa, IL-1B, IL-6, CCL2 and CXCL10 (*143*). In the same vein, another study highlighted EphB2's role in kidney fibrosis, as EphB2 knockout mice ablated the pathology to renal structure and function, and a transcriptomic return to baseline (*144*). In the CNS of a mouse model for traumatic brain injury (TBI), EphB2 phosphorylation and subsequently CCL2 and IL-6 were induced, with ablation of EphB2 attenuating the expression of these inflammatory factors. The role of astrocytic ephrin-B1 was also reported in a mouse model of traumatic brain injury (TBI), showing suppression of TBI-induced STAT3 phosphorylation by astrocyte-specific ablation of ephrin-B1 and upregulation of STAT3 induced by the activation of ephrin-B1 in astrocytes (*145*). EphB2 binding to astrocytic ephrin-B1 induced NF-kB, as defined by NF-kB translocation, and the resulting cytokine expression was mediated by the MAPK pathway (*146*). Many of the inflammatory factors induced by ephrin-B/EphB in the periphery overlap with a hallmark inflammatory signature in neuroHIV and will be elaborated on more in Chapter Three of this dissertation.

REFERENCES FOR CHAPTER ONE

1.   Q. A. Karim, Current status of the HIV epidemic & challenges in prevention. *Indian J Med Res* **146**, 673-676 (2017).

2.   G. M. Shaw, E. Hunter, HIV transmission. *Cold Spring Harb Perspect Med* **2**, (2012).

3.   S. G. Deeks, J. Overbaugh, A. Phillips, S. Buchbinder, HIV infection. *Nature Reviews Disease Primers* **1**, 15035 (2015).

4.   O. T. Campbell-Yesufu, R. T. Gandhi, Update on human immunodeficiency virus (HIV)-2 infection. *Clin Infect Dis* **52**, 780-787 (2011).

5.   P. M. Sharp, B. H. Hahn, Origins of HIV and the AIDS pandemic. *Cold Spring Harb Perspect Med* **1**, a006841 (2011).

6.   F. E. McCutchan, Understanding the genetic diversity of HIV-1. *Aids* **14 Suppl 3**, S31-44 (2000).

7.   M. Peeters, P. M. Sharp, Genetic diversity of HIV-1: the moving target. *Aids* **14 Suppl 3**, S129-140 (2000).

8.   D. L. Robertson *et al.*, HIV-1 nomenclature proposal. *Science* **288**, 55-56 (2000).

9.   B. S. Taylor, M. E. Sobieszczyk, F. E. McCutchan, S. M. Hammer, The challenge of HIV-1 subtype diversity. *N Engl J Med* **358**, 1590-1602 (2008).

10.   C. Apetrei *et al.*, Human immunodeficiency virus type 1 subtype F reverse transcriptase sequence and drug susceptibility. *J Virol* **72**, 3534-3538 (1998).

11.   J. D. Church *et al.*, Analysis of HIV tropism in Ugandan infants. *Curr HIV Res* **8**, 498-503 (2010).

12.   K. E. Medders, M. Kaul, Mitogen-activated protein kinase p38 in HIV infection and associated brain injury. *Journal of neuroimmune pharmacology : the official journal of the Society on NeuroImmune Pharmacology* **6**, 202-215 (2011).

13.   C. B. Wilen, J. C. Tilton, R. W. Doms, HIV: cell binding and entry. *Cold Spring Harb Perspect Med* **2**, (2012).

14.   M. Kaul, G. A. Garden, S. A. Lipton, Pathways to neuronal injury and apoptosis in HIV-associated dementia. *Nature* **410**, 988-994 (2001).

15. D. Giulian, K. Vaca, C. Noonan, Secretion of neurotoxins by mononuclear phagocytes infected with HIV-1. *Science* **250**, 1593-1596 (1990).

16. W. Ru *et al.*, Microglia Mediate HIV-1 gp120-Induced Synaptic Degeneration in Spinal Pain Neural Circuits. *The Journal of Neuroscience* **39**, 8408-8421 (2019).

17. N. Sacktor *et al.*, Prevalence of HIV-associated neurocognitive disorders in the Multicenter AIDS Cohort Study. *Neurology* **86**, 334-340 (2016).

18. D. Saylor *et al.*, HIV-associated neurocognitive disorder--pathogenesis and prospects for treatment. *Nature reviews. Neurology* **12**, 234-248 (2016).

19. J. E. Bell, An update on the neuropathology of HIV in the HAART era. *Histopathology* **45**, 549-559 (2004).

20. M. Kaul, J. Zheng, S. Okamoto, H. E. Gendelman, S. A. Lipton, HIV-1 infection and AIDS: consequences for the central nervous system. *Cell Death Differ* **12 Suppl 1**, 878-892 (2005).

21. W. Ru, S. J. Tang, HIV-associated synaptic degeneration. *Mol Brain* **10**, 40 (2017).

22. V. E. Thaney *et al.*, IFNbeta Protects Neurons from Damage in a Murine Model of HIV-1 Associated Brain Injury. *Sci Rep* **7**, 46514 (2017).

23. V. E. Thaney *et al.*, Transgenic mice expressing HIV-1 envelope protein gp120 in the brain as an animal model in neuroAIDS research. *J Neurovirol* **24**, 156-167 (2018).

24. T. Kato, A. Hirano, J. F. Llena, H. M. Dembitzer, Neuropathology of acquired immune deficiency syndrome (AIDS) in 53 autopsy cases with particular emphasis on microglial nodules and multinucleated giant cells. *Acta Neuropathol* **73**, 287-294 (1987).

25. J. Michaels, R. W. Price, M. K. Rosenblum, Microglia in the giant cell encephalitis of acquired immune deficiency syndrome: proliferation, infection and fusion. *Acta Neuropathol* **76**, 373-379 (1988).

26. R. J. Ellis, M. J. Marquine, M. Kaul, J. A. Fields, J. C. M. Schlachetzki, Mechanisms underlying HIV-associated cognitive impairment and emerging therapies for its management. *Nature Reviews Neurology* **19**, 668-687 (2023).

27. F. Ginhoux *et al.*, Fate mapping analysis reveals that adult microglia derive from primitive macrophages. *Science* **330**, 841-845 (2010).

28.   F. Ginhoux, S. Lim, G. Hoeffel, D. Low, T. Huber, Origin and differentiation of microglia. *Frontiers in cellular neuroscience* **7**, 45 (2013).

29.   F. Ginhoux, M. Prinz, Origin of microglia: current concepts and past controversies. *Cold Spring Harbor perspectives in biology* **7**, a020537 (2015).

30.   K. Kierdorf *et al.*, Microglia emerge from erythromyeloid precursors via Pu.1- and Irf8-dependent pathways. *Nat Neurosci* **16**, 273-280 (2013).

31.   F. Alliot, I. Godin, B. Pessac, Microglia derive from progenitors, originating from the yolk sac, and which proliferate in the brain. *Brain research. Developmental brain research* **117**, 145-152 (1999).

32.   K. Ashwell, The distribution of microglia and cell death in the fetal rat forebrain. *Brain research. Developmental brain research* **58**, 1-12 (1991).

33.   E. Gomez Perdiguero *et al.*, Tissue-resident macrophages originate from yolk-sac-derived erythro-myeloid progenitors. *Nature* **518**, 547-551 (2015).

34.   C. Schulz *et al.*, A lineage of myeloid cells independent of Myb and hematopoietic stem cells. *Science* **336**, 86-90 (2012).

35.   S. R. McKercher *et al.*, Targeted disruption of the PU.1 gene results in multiple hematopoietic abnormalities. *The EMBO journal* **15**, 5647-5658 (1996).

36.   D. R. Beers *et al.*, Wild-type microglia extend survival in PU.1 knockout mice with familial amyotrophic lateral sclerosis. *Proceedings of the National Academy of Sciences of the United States of America* **103**, 16021-16026 (2006).

37.   X. M. Dai *et al.*, Targeted disruption of the mouse colony-stimulating factor 1 receptor gene results in osteopetrosis, mononuclear phagocyte deficiency, increased primitive progenitor cell frequencies, and reproductive defects. *Blood* **99**, 111-120 (2002).

38.   M. Greter *et al.*, Stroma-derived interleukin-34 controls the development and maintenance of langerhans cells and the maintenance of microglia. *Immunity* **37**, 1050-1060 (2012).

39.   H. Lin *et al.*, Discovery of a cytokine and its receptor by functional screening of the extracellular proteome. *Science* **320**, 807-811 (2008).

40.   L. F. Lue, T. G. Beach, D. G. Walker, Alzheimer's Disease Research Using Human Microglia. *Cells* **8**, (2019).

41. D. G. Walker, T. M. Tang, L. F. Lue, Studies on Colony Stimulating Factor Receptor-1 and Ligands Colony Stimulating Factor-1 and Interleukin-34 in Alzheimer's Disease Brains and Human Microglia. *Frontiers in aging neuroscience* **9**, 244 (2017).

42. A. M. Smith, H. M. Gibbons, C. Lill, R. L. Faull, M. Dragunow, Isolation and culture of adult human microglia within mixed glial cultures for functional experimentation and high-content analysis. *Methods in molecular biology (Clifton, N.J.)* **1041**, 41-51 (2013).

43. J. Rustenhoven *et al.*, Isolation of highly enriched primary human microglia for functional studies. *Scientific Reports* **6**, 19371 (2016).

44. D. Gosselin *et al.*, An environment-dependent transcriptional network specifies human microglia identity. *Science* **356**, eaal3222 (2017).

45. Y. Garcia-Mesa *et al.*, Immortalization of primary microglia: a new platform to study HIV regulation in the central nervous system. *Journal of neurovirology* **23**, 47-66 (2017).

46. A. Das *et al.*, Transcriptome sequencing reveals that LPS-triggered transcriptional responses in established microglia BV2 cell lines are poorly representative of primary microglia. *Journal of neuroinflammation* **13**, 182 (2016).

47. C. Dello Russo *et al.*, The human microglial HMC3 cell line: where do we stand? A systematic literature review. *Journal of neuroinflammation* **15**, 259 (2018).

48. V. S. Jadhav, K. H. Krause, S. K. Singh, HIV-1 Tat C modulates NOX2 and NOX4 expressions through miR-17 in a human microglial cell line. *Journal of neurochemistry* **131**, 803-815 (2014).

49. A. Nagai *et al.*, Generation and characterization of immortalized human microglial cell lines: expression of cytokines and chemokines. *Neurobiology of disease* **8**, 1057-1068 (2001).

50. O. Butovsky *et al.*, Identification of a unique TGF-beta-dependent molecular and functional signature in microglia. *Nat Neurosci* **17**, 131-143 (2014).

51. J. Melief *et al.*, Characterizing primary human microglia: A comparative study with myeloid subsets and culture models. *Glia* **64**, 1857-1868 (2016).

52. S. Peudenier, C. Hery, L. Montagnier, M. Tardieu, Human microglial cells: Characterization in cerebral tissue and in primary culture, and study of their susceptibility to HIV-1 infection. *Annals of Neurology* **29**, 152-161 (1991).

53. G. Sébire *et al.*, In vitro production of IL-6, IL-1 beta, and tumor necrosis factor-alpha by human embryonic microglial and neural cells. *Journal of immunology (Baltimore, Md. : 1950)* **150**, 1517-1523 (1993).

54. B. Ambrosius *et al.*, Teriflunomide and monomethylfumarate target HIV-induced neuroinflammation and neurotoxicity. *J Neuroinflammation* **14**, 51 (2017).

55. Q. Li, B. A. Barres, Microglia and macrophages in brain homeostasis and disease. *Nature Reviews Immunology* **18**, 225 (2017).

56. E. M. Abud *et al.*, iPSC-Derived Human Microglia-like Cells to Study Neurological Diseases. *Neuron* **94**, 278-293.e279 (2017).

57. A. McQuade *et al.*, Development and validation of a simplified method to generate human microglia from pluripotent stem cells. *Mol Neurodegener* **13**, 67 (2018).

58. R. Mancuso *et al.*, Stem cell derived human microglia transplanted in mouse brain to study genetic risk of Alzheimer's Disease. *bioRxiv*, 562561 (2019).

59. W. Haenseler *et al.*, A Highly Efficient Human Pluripotent Stem Cell Microglia Model Displays a Neuronal-Co-culture-Specific Expression Profile and Inflammatory Response. *Stem Cell Reports* **8**, 1727-1742 (2017).

60. H. Pandya *et al.*, Differentiation of human and murine induced pluripotent stem cells to microglia-like cells. *Nat Neurosci* **20**, 753-759 (2017).

61. P. Douvaras *et al.*, Directed Differentiation of Human Pluripotent Stem Cells to Microglia. *Stem Cell Reports* **8**, 1516-1524 (2017).

62. B. van Wilgenburg, C. Browne, J. Vowles, S. A. Cowley, Efficient, long term production of monocyte-derived macrophages from human pluripotent stem cells under partly-defined and fully-defined conditions. *PloS one* **8**, e71098 (2013).

63. P. Garcia-Reitboeck *et al.*, Human Induced Pluripotent Stem Cell-Derived Microglia-Like Cells Harboring TREM2 Missense Mutations Show Specific Deficits in Phagocytosis. *Cell reports* **24**, 2300-2311 (2018).

64. C. Leone *et al.*, Characterization of human monocyte-derived microglia-like cells. *Glia* **54**, 183-192 (2006).

65. A. Rongvaux *et al.*, Development and function of human innate immune cells in a humanized mouse model. *Nature biotechnology* **32**, 364-372 (2014).

66.   J. Hasselmann *et al.*, Development of a Chimeric Model to Study and Manipulate Human Microglia In Vivo. *Neuron* **103**, 1016-1033.e1010 (2019).

67.   A. D. Bachstetter *et al.*, Disease-related microglia heterogeneity in the hippocampus of Alzheimer's disease, dementia with Lewy bodies, and hippocampal sclerosis of aging. *Acta neuropathologica communications* **3**, 32 (2015).

68.   A. Crotti *et al.*, Mutant Huntingtin promotes autonomous microglia activation via myeloid lineage-determining factors. *Nat Neurosci* **17**, 513-521 (2014).

69.   H. Lui *et al.*, Progranulin Deficiency Promotes Circuit-Specific Synaptic Pruning by Microglia via Complement Activation. *Cell* **165**, 921-935 (2016).

70.   J. G. O'Rourke *et al.*, C9orf72 is required for proper macrophage and microglial function in mice. *Science* **351**, 1324-1329 (2016).

71.   L. R. Frick, K. Williams, C. Pittenger, Microglial dysregulation in psychiatric disease. *Clinical & developmental immunology* **2013**, 608654 (2013).

72.   R. M. Ransohoff, How neuroinflammation contributes to neurodegeneration. *Science* **353**, 777-783 (2016).

73.   J. Steiner *et al.*, Immunological aspects in the neurobiology of suicide: elevated microglial density in schizophrenia and depression is associated with suicide. *Journal of psychiatric research* **42**, 151-157 (2008).

74.   J. Steiner *et al.*, Severe depression is associated with increased microglial quinolinic acid in subregions of the anterior cingulate gyrus: evidence for an immune-modulated glutamatergic neurotransmission? *Journal of neuroinflammation* **8**, 94 (2011).

75.   T. A. Bayer, R. Buslei, L. Havas, P. Falkai, Evidence for activation of microglia in patients with psychiatric illnesses. *Neuroscience letters* **271**, 126-128 (1999).

76.   B. Dean *et al.*, Different changes in cortical tumor necrosis factor-alpha-related pathways in schizophrenia and mood disorders. *Molecular psychiatry* **18**, 767-773 (2013).

77.   R. C. Paolicelli *et al.*, TDP-43 Depletion in Microglia Promotes Amyloid Clearance but Also Induces Synapse Loss. *Neuron* **95**, 297-308.e296 (2017).

78.   E. Harmon *et al.*, Increased Expression of Interferon-Induced Transmembrane 3 (IFITM3) in Stroke and Other Inflammatory Conditions in the Brain. *Int J Mol Sci* **23**, (2022).

79.   V. E. Thaney *et al.*, IFNβ Protects Neurons from Damage in a Murine Model of HIV-1 Associated Brain Injury. *Sci Rep* **7**, 46514 (2017).

80.   B. B. Gelman *et al.*, The National NeuroAIDS Tissue Consortium brain gene array: two types of HIV-associated neurocognitive impairment. *PLoS One* **7**, e46178 (2012).

81.   R. Maung *et al.*, CCR5 knockout prevents neuronal injury and behavioral impairment induced in a transgenic mouse model by a CXCR4-using HIV-1 glycoprotein 120. *J Immunol* **193**, 1895-1910 (2014).

82.   L. Alammar, L. Gama, J. E. Clements, Simian immunodeficiency virus infection in the brain and lung leads to differential type I IFN signaling during acute infection. *J Immunol* **186**, 4008-4018 (2011).

83.   J. W. Schoggins, C. M. Rice, Interferon-stimulated genes and their antiviral effector functions. *Curr Opin Virol* **1**, 519-525 (2011).

84.   T. H. Mogensen, Pathogen recognition and inflammatory signaling in innate immune defenses. *Clin Microbiol Rev* **22**, 240-273, Table of Contents (2009).

85.   M. C. Michallet *et al.*, TRADD protein is an essential component of the RIG-like helicase antiviral pathway. *Immunity* **28**, 651-661 (2008).

86.   T. Kawai *et al.*, Lipopolysaccharide stimulates the MyD88-independent pathway and results in activation of IFN-regulatory factor 3 and the expression of a subset of lipopolysaccharide-inducible genes. *Journal of immunology (Baltimore, Md. : 1950)* **167**, 5887-5894 (2001).

87.   T. Kawai *et al.*, Interferon-alpha induction through Toll-like receptors involves a direct interaction of IRF7 with MyD88 and TRAF6. *Nat Immunol* **5**, 1061-1068 (2004).

88.   A. Paun *et al.*, Functional characterization of murine interferon regulatory factor 5 (IRF-5) and its role in the innate antiviral response. *J Biol Chem* **283**, 14295-14308 (2008).

89.   A. Schoenemeyer *et al.*, The interferon regulatory factor, IRF5, is a central mediator of toll-like receptor 7 signaling. *J Biol Chem* **280**, 17005-17012 (2005).

90.	A. Takaoka *et al.*, Integral role of IRF-5 in the gene induction programme activated by Toll-like receptors. *Nature* **434**, 243-249 (2005).

91.	R. Zawatzky, H. Jacobsen, in *Encyclopedia of Immunology (Second Edition),* P. J. Delves, Ed. (Elsevier, Oxford, 1998), pp. 1417-1421.

92.	M. Mori *et al.*, Identification of Ser-386 of interferon regulatory factor 3 as critical target for inducible phosphorylation that determines activation. *J Biol Chem* **279**, 9698-9702 (2004).

93.	D. Dionisio *et al.*, Encephalitis without meningitis due to sandfly fever virus serotype toscana. *Clin Infect Dis* **32**, 1241-1243 (2001).

94.	D. Ojeda-Juárez *et al.*, Lipocalin-2 mediates HIV-1 induced neuronal injury and behavioral deficits by overriding CCR5-dependent protection. *Brain Behav Immun*, (2020).

95.	O. Kincaid, H. L. Lipton, Viral myelitis: an update. *Curr Neurol Neurosci Rep* **6**, 469-474 (2006).

96.	O. O. Koyuncu, I. B. Hogue, L. W. Enquist, Virus infections in the nervous system. *Cell Host Microbe* **13**, 379-393 (2013).

97.	R. M. Ransohoff, M. A. Brown, Innate immunity in the central nervous system. *J Clin Invest* **122**, 1164-1171 (2012).

98.	E. Gomez Perdiguero *et al.*, Tissue-resident macrophages originate from yolk-sac-derived erythro-myeloid progenitors. *Nature* **518**, 547-551 (2015).

99.	P. Illes, J. Alexandre Ribeiro, Molecular physiology of P2 receptors in the central nervous system. *Eur J Pharmacol* **483**, 5-17 (2004).

100.	R. Fekete *et al.*, Microglia control the spread of neurotropic virus infection via P2Y12 signalling and recruit monocytes through P2Y12-independent mechanisms. *Acta Neuropathol* **136**, 461-482 (2018).

101.	C. N. Detje *et al.*, Local type I IFN receptor signaling protects against virus spread within the central nervous system. *J Immunol* **182**, 2297-2304 (2009).

102.	C. N. Detje *et al.*, Upon intranasal vesicular stomatitis virus infection, astrocytes in the olfactory bulb are important interferon Beta producers that protect from lethal encephalitis. *J Virol* **89**, 2731-2738 (2015).

103.   E. Drokhlyansky *et al.*, The brain parenchyma has a type I interferon response that can limit virus spread. *Proceedings of the National Academy of Sciences* **114**, E95 (2017).

104.   K. McGuckin Wuertz *et al.*, STING is required for host defense against neuropathological West Nile virus infection. *PLoS Pathog* **15**, e1007899 (2019).

105.   H. Cho *et al.*, Differential innate immune response programs in neuronal subtypes determine susceptibility to infection in the brain by positive-stranded RNA viruses. *Nat Med* **19**, 458-464 (2013).

106.   H. J. Ramos *et al.*, IL-1β signaling promotes CNS-intrinsic immune control of West Nile virus infection. *PLoS Pathog* **8**, e1003039 (2012).

107.   M. S. Suthar, M. S. Diamond, M. Gale, Jr., West Nile virus infection and immunity. *Nat Rev Microbiol* **11**, 115-128 (2013).

108.   D. Chopy *et al.*, Ambivalent Role of the Innate Immune Response in Rabies Virus Pathogenesis. *Journal of Virology* **85**, 6657 (2011).

109.   H. Tang *et al.*, Zika Virus Infects Human Cortical Neural Progenitors and Attenuates Their Growth. *Cell Stem Cell* **18**, 587-590 (2016).

110.   J. Dang *et al.*, Zika Virus Depletes Neural Progenitors in Human Cerebral Organoids through Activation of the Innate Immune Receptor TLR3. *Cell Stem Cell* **19**, 258-265 (2016).

111.   T. M. Serman, M. U. Gack, Evasion of Innate and Intrinsic Antiviral Pathways by the Zika Virus. *Viruses* **11**, (2019).

112.   L. Zhou *et al.*, Tumor necrosis factor-alpha induced expression of matrix metalloproteinase-9 through p21-activated kinase-1. *BMC Immunol* **10**, 15 (2009).

113.   B. P. Daniels *et al.*, Regional astrocyte IFN signaling restricts pathogenesis during neurotropic viral infection. *J Clin Invest* **127**, 843-856 (2017).

114.   M. Genander, J. Frisén, Ephrins and Eph receptors in stem cells and cancer. *Curr Opin Cell Biol* **22**, 611-616 (2010).

115.   E. B. Pasquale, Eph-ephrin bidirectional signaling in physiology and disease. *Cell* **133**, 38-52 (2008).

116.   E. B. Pasquale, Eph-ephrin promiscuity is now crystal clear. *Nat Neurosci* **7**, 417-418 (2004).

117. E. M. Lisabeth, G. Falivelli, E. B. Pasquale, Eph receptor signaling and ephrins. *Cold Spring Harb Perspect Biol* **5**, (2013).

118. J.-P. Himanen, M. Henkemeyer, D. B. Nikolov, Crystal structure of the ligand-binding domain of the receptor tyrosine kinase EphB2. *Nature* **396**, 486-491 (1998).

119. E. B. Pasquale, Eph–ephrin promiscuity is now crystal clear. *Nature Neuroscience* **7**, 417-418 (2004).

120. J. P. Himanen *et al.*, Architecture of Eph receptor clusters. *Proc Natl Acad Sci U S A* **107**, 10860-10865 (2010).

121. S. H. Wimmer-Kleikamp, P. W. Janes, A. Squire, P. I. Bastiaens, M. Lackmann, Recruitment of Eph receptors into signaling clusters does not require ephrin contact. *J Cell Biol* **164**, 661-666 (2004).

122. K. L. Binns, P. P. Taylor, F. Sicheri, T. Pawson, S. J. Holland, Phosphorylation of tyrosine residues in the kinase domain and juxtamembrane region regulates the biological and catalytic activities of Eph receptors. *Mol Cell Biol* **20**, 4791-4805 (2000).

123. E. Stein, U. Huynh-Do, A. A. Lane, D. P. Cerretti, T. O. Daniel, Nck recruitment to Eph receptor, EphB1/ELK, couples ligand activation to c-Jun kinase. *J Biol Chem* **273**, 1303-1308 (1998).

124. A. Pandey, H. Duan, V. M. Dixit, Characterization of a novel Src-like adapter protein that associates with the Eck receptor tyrosine kinase. *J Biol Chem* **270**, 19201-19204 (1995).

125. B. R. Groveman *et al.*, Roles of the SH2 and SH3 domains in the regulation of neuronal Src kinase functions. *Febs j* **278**, 643-653 (2011).

126. I. M. Ethell *et al.*, EphB/Syndecan-2 Signaling in Dendritic Spine Morphogenesis. *Neuron* **31**, 1001-1013 (2001).

127. C. A. Cowan, M. Henkemeyer, The SH2/SH3 adaptor Grb4 transduces B-ephrin reverse signals. *Nature* **413**, 174-179 (2001).

128. A. Palmer *et al.*, EphrinB phosphorylation and reverse signaling: regulation by Src kinases and PTP-BL phosphatase. *Mol Cell* **9**, 725-737 (2002).

129. C. L. Essmann *et al.*, Serine phosphorylation of ephrinB2 regulates trafficking of synaptic AMPA receptors. *Nat Neurosci* **11**, 1035-1043 (2008).

130. J. O. Bush, P. Soriano, Ephrin-B1 regulates axon guidance by reverse signaling through a PDZ-dependent mechanism. *Genes Dev* **23**, 1586-1599 (2009).

131. F. Bouzioukh *et al.*, Tyrosine phosphorylation sites in ephrinB2 are required for hippocampal long-term potentiation but not long-term depression. *J Neurosci* **27**, 11279-11288 (2007).

132. M. Zimmer, A. Palmer, J. Köhler, R. Klein, EphB-ephrinB bi-directional endocytosis terminates adhesion allowing contact mediated repulsion. *Nat Cell Biol* **5**, 869-878 (2003).

133. S. Sato *et al.*, EPHB2 carried on small extracellular vesicles induces tumor angiogenesis via activation of ephrin reverse signaling. *JCI Insight* **4**, (2019).

134. R. Hu *et al.*, Overexpression of EphB2 in hippocampus rescues impaired NMDA receptors trafficking and cognitive dysfunction in Alzheimer model. *Cell Death Dis* **8**, e2717 (2017).

135. P. D. Pozniak, M. K. White, K. Khalili, TNF-α/NF-κB signaling in the CNS: possible connection to EPHB2. *J Neuroimmune Pharmacol* **9**, 133-141 (2014).

136. G. Solanas, C. Cortina, M. Sevillano, E. Batlle, Cleavage of E-cadherin by ADAM10 mediates epithelial cell sorting downstream of EphB signalling. *Nat Cell Biol* **13**, 1100-1107 (2011).

137. S. Wei *et al.*, ADAM13 induces cranial neural crest by cleaving class B Ephrins and regulating Wnt signaling. *Dev Cell* **19**, 345-352 (2010).

138. C. Litterst *et al.*, Ligand binding and calcium influx induce distinct ectodomain/gamma-secretase-processing pathways of EphB2 receptor. *J Biol Chem* **282**, 16155-16163 (2007).

139. A. Georgakopoulos *et al.*, Metalloproteinase/Presenilin1 processing of ephrinB regulates EphB-induced Src phosphorylation and signaling. *Embo j* **25**, 1242-1252 (2006).

140. M. D. Antion, L. A. Christie, A. M. Bond, M. B. Dalva, A. Contractor, Ephrin-B3 regulates glutamate receptor signaling at hippocampal synapses. *Mol Cell Neurosci* **45**, 378-388 (2010).

141. A. Poliakov, M. L. Cotrina, A. Pasini, D. G. Wilkinson, Regulation of EphB2 activation and cell repulsion by feedback control of the MAPK pathway. *J Cell Biol* **183**, 933-947 (2008).

142. T. Kitamura *et al.*, Enhancement of lymphocyte migration and cytokine production by ephrinB1 system in rheumatoid arthritis. *Am J Physiol Cell Physiol* **294**, C189-196 (2008).

143. P. N. Mimche *et al.*, EphB2 receptor tyrosine kinase promotes hepatic fibrogenesis in mice via activation of hepatic stellate cells. *Scientific Reports* **8**, 2532 (2018).

144. Z. Huang *et al.*, Key role for EphB2 receptor in kidney fibrosis. *Clin Sci (Lond)* **135**, 2127-2142 (2021).

145. A. M. Nikolakopoulou *et al.*, Astrocytic Ephrin-B1 Regulates Synapse Remodeling Following Traumatic Brain Injury. *ASN Neuro* **8**, 1-18 (2016).

146. A.-S. Ernst *et al.*, EphB2-dependent signaling promotes neuronal excitotoxicity and inflammation in the acute phase of ischemic stroke. *Acta Neuropathologica Communications* **7**, 15 (2019).

CHAPTER TWO:

Interferon-β deficiency alters brain response to chronic HIV-1 envelope protein exposure

in a transgenic model of NeuroHIV

Hina Singh[1,2], Jeffrey Koury[1], Ricky Maung[1,2], Amanda J. Roberts[3], Marcus Kaul[1,2]*

[1]Division of Biomedical Sciences, School of Medicine, University of California,

Riverside, 900 University Ave, Riverside, CA, 92521, USA; email:

hsing@medsch.ucr.edu; jeffrey.koury@medsch.ucr.edu; ricky.maung@medsch.ucr.edu

[2]Infection and Inflammatory Disease Center, Sanford Burnham Prebys Medical

Discovery Institute, La Jolla, CA 92037, USA

[3] Animal Models Core, The Scripps Research Institute, 10550 North Torrey Pines Road,

MB6, La Jolla, CA 92037, USA; email: aroberts@scripps.edu

Corresponding author: Marcus Kaul, Division of Biomedical Sciences, School of

Medicine, University of California, Riverside, 900 University Ave, Riverside, CA,

92521, USA. Tel: (951) 827-7774. E-mail: marcus.kaul@medsch.ucr.edu

2.1. ABSTRACT

Human immunodeficiency virus-1 (HIV-1) infects the central nervous system (CNS) and causes HIV-associated neurocognitive disorders (HAND) in about half of the population living with the virus despite combination anti-retroviral therapy (cART). HIV-1 activates the innate immune system, including the production of type 1 interferons (IFNs) α and β. Transgenic mice expressing HIV-1 envelope glycoprotein gp120 (HIVgp120tg) in the CNS develop memory impairment and share key neuropathological features and differential CNS gene expression with HIV patients, including the induction of IFN-stimulated genes (ISG).

Here we show that knocking out IFNβ (IFNβKO) in HIVgp120tg and non-tg control mice impairs recognition and spatial memory, but does not affect anxiety-like behavior, locomotion, or vision. The neuropathology of HIVgp120tg mice is only moderately affected by the KO of IFNβ but in a sex-dependent fashion. Notably, in cerebral cortex of IFNβKO animals' presynaptic terminals are reduced in males while neuronal dendrites are reduced in females. The IFNβKO results in the hippocampal CA1 region of both male and female HIVgp120tg mice in an ameliorated loss of neuronal presynaptic terminals but no protection of neuronal dendrites. Only female IFNβ-deficient HIVgp120tg mice display diminished microglial activation in cortex and hippocampus and increased astrocytosis in hippocampus compared to their IFNβ-expressing counterparts. RNA expression for some immune genes and ISGs is also affected in a sex-dependent way. The IFNβKO abrogates or diminishes the induction of MX1, DDX58, IRF7 and IRF9 in HIVgp120tg brains of both sexes. Expression analysis of neurotransmission related genes reveals an influence of

IFNβ on multiple components with more pronounced changes in IFNβKO females. In contrast, the effects of IFNβKO on MAPK activities are independent of sex with pronounced reduction of active ERK1/2 but also of active p38 in the HIVgp120tg brain. In summary, our findings show that the absence of IFNβ impairs memory dependent behavior and modulates neuropathology in HIVgp120tg brains, indicating that its absence may facilitate development of HAND. Moreover, our data suggests that endogenous IFNβ plays a vital role in maintaining neuronal homeostasis and memory function.

Key words: Interferon beta (IFNβ); IFNβ knockout; HIVgp120-transgenic, HIV associated neurocognitive disorder; behavior deficits; P38 MAPK; ERK1/2 signaling; Sexual dimorphism.

2.2. INTRODUCTION

According to the World Health Organization (WHO) 38.4 million people were living with human immunodeficiency virus (HIV) worldwide as of 2021. Approximately 50% of people living with HIV develop HIV-associated neurocognitive disorder (HAND) in the era of combination anti-retroviral therapy (cART) (*1, 2*). Symptomatically, this disorder manifests as cognitive impairment, motor dysfunction and speech impairments; while neuropathologically, it is defined by synaptic degeneration and glial cell activation (*3-6*). Despite several decades of research, the cellular and molecular mechanisms involved in the pathogenesis of HAND remain only partially understood and no specific treatments are available (*6, 7*).

One model of brain injury inflicted by HIV infection is a HIVgp120 transgenic mouse (HIVgp120tg) expressing the viral gp120 envelope protein under the control of the glial fibrillary acidic protein (GFAP) promoter in astrocytes (*8*). This model recapitulates key neuropathological features observed in human NeuroHIV patients, namely those with HIV encephalitis, including neuronal damage, astrocytosis, microgliosis, similar differential gene expression profiles and memory-related behavioral deficits (*1, 6, 7, 9*). Employing the HIVgp120tg mice in previous studies we observed a crucial role of the innate immune system, specifically the type 1 interferon response, in promotion and amelioration of NeuroHIV (*9*). Type 1 interferons (IFNβ and IFNα) exert their biological function on the type 1 IFN receptor (IFNAR1/2 heterodimer), ultimately leading to activation of antiviral and neuroprotective components (*10*). In fact, we observed a transient increase of interferon beta (IFNβ), an anti-inflammatory and anti-viral type 1 interferon, preceding any behavioral or neuropathological signs in the HIVgp120tg mouse similar to what others observed in Simian Immunodeficiency Virus (SIV) models, suggesting a neuroprotective role for IFNβ in early HIV infection (*6, 11*). To prolong the antiviral and potential neuroprotective effects of IFNβ on HIV induced neuronal damage, previous studies from our lab intranasally administered mouse recombinant IFNβ to HIVgp120tg mice resulting in neuroprotection mediated by IFNAR1 and CCL4 (*6*). Later studies from our lab demonstrated that in the absence of neuroprotective amounts of exogenous IFNβ, IFNAR1 can contribute to neuronal injury in the presence of HIVgp120 in a sex dependent fashion (*7*), raising questions about the role of endogenous IFNβ in HIV induced neuronal injury.

Hence, in the present study, we characterize the role of the endogenous ligand IFNβ in the HIVgp120tg mouse utilizing a global IFNβ knockout (IFNβKO) (*12*).

We find that endogenous IFNβ is required to maintain neuronal homeostasis and memory function. However, genetic ablation of IFNβ also results in a partial reduction of HIV-induced injury, diminishing the loss of neuronal presynaptic terminals in CA1 of the hippocampus of both male and female mice. Interestingly, a reduction in microglial activation due to IFNβ knockout is only observed in cortex and hippocampus of females. The neurotransmission related gene expression and bioinformatics analysis further corroborates sexual dimorphism and alteration of comparably more components in females. In contrast, activities of mitogen-activated protein kinases (MAPK) and signal transducer and activator of transcription-3 (STAT3) are sex-independent. Altogether, the studies suggest a critical physiological and neuroprotective role of endogenous IFNβ in the brain which, however, is insufficient in the long-term to prevent neuronal injury caused by HIVgp120 exposure.

2.3. MATERIALS AND METHODS

Mouse models

HIVgp120tg mice expressing envelope glycoprotein gp120 of the HIV-1 strain LAV under the control of the GFAP promoter were kindly provided by Dr. Lennart Mucke (Gladstone Institute of Neurological Disease, University of California, San Francisco, CA) (*8*) and previously used to study the role of CCR5 in NeuroHIV. Mice deficient in IFNβ (IFNβKO) were kindly provided by Dr. Tomas Leanderson (Lund University, Lund, SE)

(*12*). IFNβKO and HIVgp120tg mice were cross-bred, and the F3 generation of the HIVgp120tg[het]- IFNβKO[het] mice was used to obtain four genotypes, all on the C57BL/6.129/SJL background: (1) IFNβKO-HIVgp120 (KOGP; IFNβKO^{-/-}gp120[+]), (2) HIVgp120 (GP; IFNβ^{+/+}gp120[+]), (3) IFNβKO (KO; IFNβ^{-/-}gp120[-]; control) and (4) wild-type (WT; IFNβ^{+/+}gp120[-], WT control). All procedures involving animals were performed in accordance and compliance with National Institute of Health *Guide for the Care and Use of Laboratory Animals* and approved by the Institutional Animal Care and Use Committees of the University of California, Riverside, Sanford-Burnham-Prebys Medical Discovery Institute and The Scripps Research Institute and this study follows the ARRIVE guidelines.

Behavioral testing

One cohort consisting of WT (male: 5, female: 7) HIVgp120tg (male: 5, female: 3), IFNβKO (male: 3, female: 6), and IFNβKO-HIVgp120 (male: 6, female: 7) mice were tested at 9-10 months of age by The Scripps Research Institute's (TSRI) Animal Models Core Facility. The behavioral tests were designed to examine cognitive abilities as well as other behaviors that could confound the interpretation of cognitive data, such as anxiety-like behavior, activity levels, and visual capability, and were performed in the following order: light/dark transfer (LDT), locomotor activity (LMA), optomotor (OM), novel object recognition (NOR), and Barnes maze test (BM). The behavioral tests were performed as previously published by our group (*1, 7, 9, 13*). The discrimination index for NOR was calculated using the formula, (time exploring the novel object – time exploring the familiar object) / (time exploring novel object + time exploring familiar object) * 100.

Immunohistology, quantitative fluorescence and deconvolution microscopy

Brain tissue harvest, immunofluorescence staining, deconvolution, and quantitative fluorescence microscopy (neuronal injury and astrocytic activation) and cell counting (microglial activation) were performed as previously described (*6, 7, 9, 13*). Briefly, 9 to 10 months-old mice were terminally anesthetized with isoflurane and immediately transcardially perfused on ice through the left ventricle with 0.9% saline. The brain was subsequently removed and divided into two hemispheres, with one fixed in 4% paraformaldehyde (72h at 4ºC) for histological analysis and the second dissected into hippocampus and cortex and subsequently snap frozen in liquid nitrogen for later RNA or protein extraction. Analysis of histopathology and RNA expression included 6 animals (3 females and 3 males) per group. For neuropathological assessment, 40 µm thick sagittal brain sections were prepared with a vibratome (Leica VT 1000S, Leica Biosystems, Buffalo Grove, IL) and immunostained using antibodies against synaptophysin (Syp; 1:50; Dako) and microtubule-associated protein 2 (MAP-2; 1:200; Sigma) as neuronal markers, or glial fibrillary acidic protein (GFAP; 1:250; Dako) and ionized calcium-binding adaptor molecule 1 (Iba1;1:125; Wako) as astrocytic and microglial markers, respectively. An Axiovert 200M fluorescence microscope (Carl Zeiss AG, Oberkochen, DE) with a motorized stage and Slidebook software (Intelligent Imaging Innovations version 6, Denver, CO) were used for image acquisition, deconvolution and quantitative analysis as recently published (*1, 6, 7, 9, 13*).

Isolation of mRNA and quantitative RT-PCR

Extraction, isolation and quantification of RNA of murine cerebral cortex and hippocampus was performed as previously described (*7*). Briefly, RNA of murine cerebral cortex and hippocampus was isolated using the Qiagen RNeasy Lipid Tissue Midi Kit (Qiagen, Cat# 75144) and Qiagen Mini Kit (Qiagen, Cat# 74104), respectively, according to the manufacturer's instructions. Quantitative RT-PCR (qRT-PCR) was performed as previously reported (*6, 9*). Firstly, RNA quality and concentration were determined using a NanoDrop DS-11 spectrophotometer (De Novix Inc., USA). 500ng of total RNA was reverse transcribed using SuperScript II reverse transcriptase (Invitrogen, USA) following the manufacturer's instructions. QRT-PCR was performed using 10µL of 2X Power PCR SYBR Green master mix (Applied Biosystems, USA), 1µL of cDNA (25ng), 8µL of PCR grade water and 0.5µL of forward and reverse primers. All qRT-PCR analysis was performed on the QuantStudio 6 flex Real-Time PCR System (Applied Biosystems/ Thermo Fisher Scientific, Carlsbad, CA) using the following protocol: 95ºC for 10 min, and for 40 cycles (95ºC for 30s, 59ºC for 1 min, 72ºC for 1 min) followed by a denaturation step for melting temperature (Tm) analysis. The relative amount of mRNA of every gene *versus* the internal control (GAPDH) was calculated following the $2^{-\Delta\Delta Ct}$ method. The primer sequences are listed in Supplementary Table S1.

GABA & Glutamate and Dopamine & Serotonin RT² Profiler™ PCR Array

Neurotransmission related gene expression analysis was performed using the GABA & Glutamate (PAMM-152Z) and Dopamine & Serotonin (PAMM-158Z) RT² Profiler™ Arrays following supplier's instructions (Qiagen, Germantown, MD).

Previously isolated RNA, procedure described above, was reverse transcribed using the RT^2 First-Strand kit (Qiagen) mixed with RT^2 qPCR Master Mix containing SYBR Green (Qiagen). A QuantStudio™ 6 Flex System (Applied Biosystems/Thermo Fisher Scientific) was used to run all PCR arrays. The RT^2 Profiler™ Array Data Analysis software package (version 3.5) used the $2^{-(\Delta\Delta CT)}$-based method (*14*) to calculate fold change and a modified Student's t-test to compute two-tail, equal variance *p*-values. This method calculates the difference between the gene of interest and the average of selected housekeeping genes (heat shock protein 90 alpha family class B member 1 (Hsp90ab1), Actin Beta (Actb), glyceraldehyde-3-phosphate dehydrogenase (Gapdh) and glucuronidase Beta (Gusb).

Ingenuity Pathway Analysis

Expression data for all 168 genes generated by RT^2 Profiler™ Arrays was further analyzed using Ingenuity Pathway Analysis (IPA; Ingenuity® Systems, www.ingenuity.com; build version: 486617M; content version: 46901286; release date: 2018–11-21) to generate the functional/biological gene networks. The IPA core analysis function was used and the same settings were employed as previously published with some minor changes in tissues and cell lines (inclusion of central nervous system cell line, immune cells and nervous system) (*7*).

Western blot analysis

Western blotting using lysates from mouse cortex and hippocampus was conducted as previously published with minor modifications (*7, 15*). Briefly, dissected cortex or hippocampus was lysed on ice with 400-600µL of lysis buffer (10mL of 1X RIPA buffer,

100uL of phosphatase inhibitor (Calbiochem/EMD Chemicals, San Diego, CA) and one tablet of complete protease inhibitor (Roche; Indianapolis, IN)). Tissue was homogenized first with an electric pestle followed by trituration in a 3mL syringe. After adjusting of protein concentration based on results of the bicinchoninic acid (BCA) protein assay kit (Pierce/Thermo Fisher Scientific), 25-50µg of protein were added to 4X LDS sample buffer and 10X reducing agent (Invitrogen) and boiled for 5 min. Samples were loaded in a 4-12% SDS-PAGE gel (Invitrogen) and electrophoretically separated, and then electro-transferred to PVDF membranes. Afterwards, the membranes were blocked with 4% bovine serum albumin (BSA) in Tris-buffered saline containing Tween (TBS-T) and sub-sequently incubated overnight at 4˚C with the primary antibodies. Membranes were then washed with TBS-T and incubated with anti-mouse-HRP (AP128P; Millipore Sigma) and anti-rabbit-HRP (111-036-045; Jackson Immuno Reseach) secondary antibodies. Membranes were imaged using the ChemiDoc™ XRS+ imager (Bio-Rad Laboratories, Hercules, CA). Densitometry analysis was performed using ImageJ 1.52a software (http://rsb.info.nih.gov/nih-image/) and normalized against α-Tubulin or GAPDH expression levels. The following antibodies were used: phospho-p38 (1°Ab- 1:1000; Cell Signaling; 9211; anti-rabbit 2°Ab- 1:5000), total p38 (1°Ab- 1:2000; Cell Signaling; 9212; anti-rabbit 2°Ab- 1:25,000), phospho-ERK1/2 (1°Ab- 1:1000; Cell Signaling; 9101S; anti-rabbit 2°Ab- 1:5000), total ERK1/2 (1°Ab- 1:2000; Cell Signaling; 9102; anti-rabbit 2°Ab- 1:5000), active JNK1/2 (1°Ab- 1:1000; Promega; V93A 20542917; anti-rabbit 2°Ab- 1:3000), total JNK1/2 (1°Ab- 1:1000; Cell Signaling; 9252; anti-rabbit 2°Ab- 1:3000) , phospho-STAT1 serine 727 (1°Ab- 1:1000, Cell Signaling 8826; anti-rabbit 2°Ab-

1:3000), total STAT1 (1°Ab- 1:1000, Cell Signaling, 14994S; anti-rabbit 2°Ab- 1:3000), phospho-STAT3 tyrosine 705 (1°Ab- 1:1000; Cell Signaling; 9145; anti-rabbit 2°Ab- 1:5000), total STAT3 (1°Ab- 1:1000; Cell Signaling; 9139S; anti-mouse 2°Ab- 1:5000) and housekeeping genes α-tubulin (1°Ab- 1:2000; Sigma T9026; anti-mouse 2°Ab- 1:10,000) or GAPDH (1°Ab- 1:20,000; Ambion; 4300; anti-mouse 2°Ab- 1:25,000).

Statistical analysis

The analysis of histopathological data, mRNA expression and Western blotting data were performed using Graphpad Prism 8 software (GraphPad Software, Inc., CA, USA), behavioral data were evaluated using StatView (SAS Institute, Cary, NC). Comparisons of two groups were made by unpaired Student t-test, whereas multiple groups were compared using a single-step procedure for multiple comparisons with analysis of variance (ANOVA) followed by Fisher's protected least significant difference (PLSD) post hoc test (*16*). P-values < 0.05 were considered statistically significant. CT values were measured using RT^2 Profiler™ PCR Arrays. QIAGEN data analysis center (http://www.qiagen.com/geneglobe) was used for $2^{-(\Delta\Delta CT)}$-based fold change calculations and a modified Student's test to compute two tails, equal variance p-values. For the gene enrichment analysis right-tailed Fisher's exact test was performed.

2.4. RESULTS

IFNβ is necessary for recognition memory and affects spatial learning

To investigate the effects of IFNβ on behavioral deficits associated with HIVgp120 expression in the brain, all four genotypes, WT; HIVgp120 (GP); IFNβKO (KO); and IFNβKO-HIVgp120 (KOGP), were subjected to behavioral testing at 9-10 months of age. There were no significant interactions between sex and genotype, therefore sexes were combined in the graphs. The LDT test showed no effects of HIVgp120 or IFNβ deficiency with or without gp120 on the time spent in the light compartment suggesting the absence of genotype-specific anxiety-like behavior (Fig. 2.1A). In the locomotor test there were no significant differences between genotypes in ambulation and rearing; however, HIVgp120 mice spent more time in the center of the arena relative to IFNβKO-HIVgp120 mice which suggests decreased anxiety-like behavior in the IFNβ-expressing mice (Fig. 2.1B). Indeed, while not significant, HIVgp120tg mice spent more time in the light compartment in the LDT test supporting this finding. There was no genotypic difference in head tracking behavior in the OPT test, signifying that the mice had intact vision (Supplementary Fig. 2.1). Overall, the results of these tests indicate that the mice are active, can see, and do not have impairments that would confound the results of the cognitive tests.

The NOR test was performed to assess short-term recognition memory. WT mice showed significantly more interest in the novel object than in the familiar object suggesting intact recognition memory. HIVgp120, IFNβKO and IFNβKO-HIVgp120 mice showed no significant differences in time spent with the familiar versus novel object, indicating impairment, and further suggesting a crucial role of IFNβ in recognition memory function

(Fig. 2.1C). However, the NOR discrimination indices did not detect any significant differences between the four tested genotypes (Supplementary Fig. 2.2)

The BM test revealed no significant effects of genotype or sex on latency to escape and the numbers of errors made before escape across the training trials (Supplementary Fig 2.2). In the BM probe test in which the escape tunnel was removed so that spatial memory could be assessed, WT mice spent significantly more time in the target quadrant (where the escape tunnel had been) than the average of the other quadrants indicating intact spatial learning and memory. HIVgp120 expression and IFNβ deficiency each alone did not significantly affect spatial memory but the combination of the two (i.e. IFNβKO-HIVgp120 mice) completely disrupted spatial memory suggesting that the baseline level of IFNβ is pivotal for maintaining spatial cognition in mice chronically exposed to HIVgp120 (Fig. 2.1D).

IFNβ deficiency affects presynaptic terminals in HIVgp120tg and non-tg mice

Previous studies analyzing the cerebral cortex and hippocampus of HIVgp120tg mice have shown damage to presynaptic terminals. To characterize the role of IFNβ in this neuroHIV model, we harvested the brains of 9-10 months old mice and performed histopathological analysis. Quantification using deconvolution microscopy identified a significant loss of pre-synaptic terminals in HIVgp120 mice compared to WT controls in layer III of the cortex and CA1 region of hippocampus in both males and females (Fig. 2.2, Synaptophysin). IFNβ deficiency alone also resulted in the loss of SYP^+ neuropil in both the cortex and hippocampus of males while the females were unaffected, with no additional loss due to IFNβKO in cortex of HIVgp120 mice. However, IFNβKO in HIVgp120 mice

partially diminished the loss of presynaptic terminals in hippocampus (CA1) of both the sexes (Fig. 2.2B & G).

IFNβ deficiency worsens loss of cerebrocortical neuronal dendrites in HIVgp120tg female mice

The HIVgp120 animals displayed a significant reduction in MAP2 fluorescence (P < 0.0001) in cortex and hippocampus (Fig. 2.2, MAP2). IFNβ deficiency did not affect the MAP2$^+$ neurites in male cortex and hippocampus. In female cortex, IFNβKO animals showed significant loss (P < 0.0001) of neuronal dendrites compared to WT controls. The IFNβKO-HIVgp120 animals showed significant decrease in MAP2+ neurites compared to all the other three genotypes. The female hippocampus remained unaffected by the IFNβ deficiency in the absence of HIVgp120 (Fig. 2.2C & H).

IFNβKO does not prevent astrocytosis but diminishes microglial activation in females

Quantitative fluorescence analysis of the immunofluorescence-stained brain section for astrocytic GFAP showed a significant increase in both cerebral cortex and CA1 of the hippocampus in the presence of HIVgp120 compared to the WT controls (Fig. 2.2, GFAP). IFNβ deficiency did not alter the expression of GFAP in male and female cortex but did so in the female hippocampus. On the other hand, IFNβKO mice showed a trend to a higher baseline level of GFAP in the female hippocampus, which did not reach significance compared to the WT control. The IFNβKO-HIVgp120 mice showed a significant increase the GFAP level compared to HIVgp120 mice suggesting the IFNβ deficiency may perpetuate astrocytosis in female hippocampus while having no such effect

in the cortex (Fig. 2.2D & I). IFNβ deficiency did not prevent, nor did it worsen the microglia activation in the male cortex and hippocampus (Fig. 2.2, IBA1). On the other hand, the IFNβKO in HIVgp120 mice partially reduced microgliosis in the female cortex and hippocampus (Fig. 2.2E & J). However, the IFNβKO showed significant higher count for microglial cells in female cortex compared to the WT controls.

IFNβ deficiency affects expression of the viral transgene and host immune response-related genes

To assess the effects of IFNβ ablation on the expression of HIVgp120 envelope protein, we compared the mRNA levels in cerebral cortex and hippocampus. Analysis by qRT-PCR revealed that the IFNβKO-HIVgp120 genotype resulted in enhanced expression of gp120 mRNA as compared to HIVgp120 mice in male but not in female cortex (Fig. 2.3A). On the other hand, while there was a trend to decrease in the expression of gp120 mRNA in hippocampus of both males and females due to IFNβ deficiency, the difference was not significant (Fig. 2.3B). HIVgp120 expression in the brain, similar to HIV. infection, is associated with enhanced expression of interferon-stimulated genes (ISGs), cytokines and chemokines (*6, 7, 9*). Therefore, we next investigated expression levels of CCL4 and CCL5, two anti-viral genes implicated in neuroprotection (*17*). CCL4 was significantly upregulated in HIVgp120 mice compared to the WT controls in cortex and hippocampus of male and only in female cortex (Fig. 2.3C). The knockout of IFNβ resulted in no significant differences on the expression level of CCL4. However, in the female hippocampus there was no significant change in the CCL4 expression level between HIVgp120 mice and WT mice, but the knockout of IFNβ resulted in increased levels of

CCL4 in IFNβKO-HIVgp120 mice compared to the other three genotypes (Fig. 2.3D). On the other hand, CCL5 levels were upregulated in HIVgp120 mice compared to the WT group; however, CCL5 expression was not changed by IFNβ deficiency in the cortex of males and females but the level of CCL5 in HIVgp120 and IFNβKO-HIVgp120 mice was higher in female cortex (Fig. 2.3E). In contrast, in male hippocampus IFNβKO-HIVgp120 mice showed significantly higher level of CCL5 compared to all the other three genotypes. Similarly, in female hippocampus the CCL5 level were upregulated in HIVgp120 compared to WT mice although not significantly and there was a trend increase in the level of CCL5 in IFNβKO-HIVgp120 mice compared to the other three genotypes (Fig. 2.3F).

We have previously shown that lipocalin-2 (LCN2) is one of the most up-regulated proteins in HIVgp120tg brains and contributes to neuronal damage and behavioral deficits in the HIVgp120 mice (*1*). Unsurprisingly, qRT-PCR analysis showed the elevated level of LCN2 in these 9-10-month HIVgp120 brains compared to the WT control group in the cortex and hippocampus of males and females (Fig. 2.3G, H). The knockout of IFNβ in the HIVgp120 mice significantly increased the expression level of LCN2 compared to other three genotypes in male and female cortex and female hippocampus. However, there was no significant effect of IFNβ deficiency on LCN2 level in the male hippocampus (Fig. 2.3H). The qRT-PCR results show that CCL2 expression was significantly upregulated in HIVgp120 mice in both the cortex and hippocampus of males and females (Fig. 2.4A & B). IFNβKO did not influence the expression of CCL2 in the cortex for both males and females, as well as in the female hippocampus. However, in the hippocampus, there was a significant decrease in the expression of CCL2 in IFNβKO-HIVgp120 mice compared to

the HIVgp120 mice, but this effect was observed only in males. The expression of CCL3 is upregulated due to HIVgp120 in the cortex of males and females regardless of IFNβ genotype (Fig. 2.4C). No significant differences in CCL3 expression were observed among the four tested genotypes in the male hippocampus. However, in female hippocampus, the increase in CCL3 expression was not able to reach significance in the HIVgp120tg mice compared to the WT but the knocking out IFNβ resulted in significant increase in CCL3 in the IFNβKO x HIVgp120 mice compared to the other three genotypes (Fig. 2.4D).

Expression of MX1, an interferon induced GTP-binding protein, was significantly upregulated in the presence of HIVgp120 in the female cortex and hippocampus in both sexes. However, this increase was not statistically significant in male cortex. The baseline level of MX1 in HIVgp120tg controls was higher in female cortex and hippocampus (male and females) compared to the male cortex (Fig. 2.4E & F). This upregulation of MX1 was absent in IFNβKO and IFNβKO- HIVgp120 mice, suggesting its increase to be completely dependent on this interferon. Like CCL2, CXCL10 has been implicated in HIV neuropathogenicity and higher expression levels of both CXCL10 and -11 were reported in the brain of HIVgp120 mice (*6, 7*). We observed significant upregulation in the expression of CXCL10 in HIVgp120 mice in both cortex and hippocampus consistent with our previous results (*1, 6, 7*). The CXCL10 upregulation was not affected by the absence of IFNβ gene in both male and female cortex and in male hippocampus. However, in female hippocampus, there was a significant decrease in the expression of CXCL10 in IFNβKO-HIVgp120 mice compared to the HIVgp120 mice (Fig. 2.4G & H). IFNβ deficiency did not affect the expression CXCL11 in the male cortex while in the female cortex there was

a significant increase in the CXCL11 expression in IFNβKO-HIVgp120 mice compared to the HIVgp120 mice (P < 0.05) (Fig. 2.4I). On the other hand, the mRNA expression of CXCL11 is not significantly different among the four tested genotypes in the hippocampus of either sex (Fig. 2.4J). The HIV-1 co-receptor CCR5 was also examined and the result revealed an upward trend in CCR5 levels due to HIVgp120 in the cortex of both males and females, regardless of IFNβ, although the increase was not statistically significant (Fig. 2.4K). While in the hippocampus, the RNA expression level of CCR5 was not significantly different between the four genotypes in either sex. However, an increase due to HIVgp120 was observed but without statistical significance (Fig. 2.4L). Additionally, STAT3 transcript levels were also assessed and showed that STAT3 expression was increased in the cortex and hippocampus of HIVgp120 mice. Specifically, in cortex, the expression of STAT3 was significantly higher in IFNβKO-HIVgp120 mice compared to HIVgp120 mice in both males and females (P < 0.01; P < 0.05) (Fig. 2.4M). However, in the female hippocampus the levels of STAT3 significantly decreased after knocking out IFNβ in HIVgp120 mice, while no such change was observed in the male hippocampus (Fig. 2.4N).

The comparably larger amounts of mRNA isolated from cortex allowed analyzing the mRNA expression levels of additional genes of the IFN system that have been implicated in HIV infection, namely DDX58 (RIG-I), IRF3, IRF7 and IRF9. HIV infection can activate the RIG-I signaling pathway which further leads to phosphorylation of IRF3 and IRF7 leading to production of type I IFNs (*18, 19*). We observed an elevated mRNA expression level of DDX58, IRF3 (P < 0.01 in females only) and IRF7 in the HIVgp120 mouse cortex for both males and females. Compared to the HIVgp120 mice, the IFNβKO-

gp120 mice exhibited a significant decrease in the expression level of DDX58 in males (P < 0.001) and females (P < 0.0001) (Fig. 2.5A). Interestingly, in male mice with HIVgp120 there was a trend increase in IRF3 levels compared to the wildtype controls, but it was not statistically significant. On the other hand, HIVgp120tg female mice had higher baseline IRF3 levels. Surprisingly, the absence of IFNβ did not have an impact on the mRNA expression level of IRF3 in either sex (Fig. 2.5B). In contrast, the absence of IFNβ resulted in a reduction of IRF7 expression in the HIVgp120 mice in both sexes. However, this decrease trend towards being higher than in IFNβKO mice but was not significant in females (Fig. 2.5C). Nevertheless, in males this decrease did reach a significance with a P < 0.05.

IRF9 also plays an important role in activating the transcription of ISGs upon binding with STAT1-STAT2 heterodimer (*20*). Hence, we assessed the expression level of IRF9 in cortex. HIVgp120 mice displayed a significant upregulation of IRF9 in both males and females, compared to all the other three genotypes. Interestingly, females had a higher baseline expression level than in males. However, the IFNβKO-HIVgp120 mice showed a significant reduction in the expression of IRF9 compared to the HIVgp120 mice in both males and females (P < 0.05; P< 0.001), although no significant difference was observed between WT control and IFNβKO mice (Fig. 2.5D).

Sex-dependent effects of IFNβ and HIVgp120 on neurotransmission-related gene networks

Next, we investigated whether the expression of genes involved in neurotransmission was affected by the deletion of the IFNβ gene in HIVgp120 brains. We used the RT2 Profiler™ PCR Arrays to analyze the GABA and glutamate (GG array: 84 genes) and dopamine and serotonin (DS array: 84 genes) neurotransmission systems and observed sex-dependent changes in expression of multiple neurotransmission related genes. The results indicated that when compared to their respective WT controls, the alterations in RNA expression in the cortex and hippocampus in association with HIVgp120 expression and the lack of IFNβ were greater in female than male mice. The results of the GABA and glutamate RT^2 Profiler PCR Arrays showed that in male cortex significant changes occurred in RNA expression of 15 genes while in female cortex of 26 genes (Fig. 2.6A & Supplementary Table 2.2). In the hippocampus, there were significant alteration in RNA expression level of 9 genes in males and 30 genes in females (Fig. 2.6B & Supplementary Table 2.3). The analysis of the dopamine and serotonin systems revealed in male cortex significantly altered RNA expression of 6 components as opposed to 27 components in females (Fig. 2.7A & Supplementary Table 2.4), while in the hippocampus 19 components were significantly altered in both males and females (Fig. 2.7B & Supplementary Table 2.5). The alteration of neurotransmission components from WT control differs in the presence of HIVgp120 with and without IFNβ and the IFNβKO itself, supporting the notion that IFNβ affects alone and in association with HIVgp120 neuronal integrity and behavioral performance. More pronounced changes in females are in line with

our histological findings where we observed a more pronounced effect of IFNβKO in this sex.

Further, bioinformatics employing IPA enables the identification of functional gene networks and upstream regulators using the differential gene expression data for males and females generated with the RT2-arrays. Two high scoring networks were identified each in males and females: In male HIVgp120 cortex (score: 66; molecules involved 35); in female HIVgp120 cortex (score: 64; molecules involved 35) in male HIVgp120 hippocampus (score: 65; molecules involved 35) and female HIVgp120 hippocampus (score: 65; molecules involved 35). These networks are affected by IFNβ ablation and are shown in Fig 2.8 & 2.9 & Supplementary Table 2.6. Interestingly, CREB1 (cAMP response element binding protein-1), down-stream of p38 and ERK1/2 signaling (*21*), was seen downregulated in the male cortical and hippocampal networks due to IFNβKO and HIVgp120, but with no further change due to IFNβ ablation in cortex in the presence of HIVgp120. However, in the hippocampus only IFNβ deficiency alone leads to downregulation whereas HIVgp120 expression results in upregulation. In contrast, in females, CREB1 did not score high enough to be included in the top scoring networks of cortex or hippocampus. Notably, IPA also predicted CREB-binding protein (Cyclic adenosine monophosphate Response Element Binding Protein; CREBBP) as an upstream regulator in both cortex and hippocampus of males and females, which is in line with our previous work suggesting the involvement of CREB in HIVgp120 neurotoxicity (*7*). The complete list of upstream regulators and their Z-scores is shown in Supplementary Table 2.7.

IFNβ modulates the effects of HIVgp120 on MAPK activity

Activation of p38 MAPK has been implicated in neuronal death and macrophage/micro-glia activation in HIV neurotoxicity (*15, 22*). Higher levels of phosphorylated p38 can be seen in cortex of HIVgp120 mice; however, we have reported earlier that the balance of all MAPK signaling is crucial to achieve complete neuroprotection in HIVgp120 mice (*1, 7*). To quantify active p38 MAPK, we performed Western blots for the phosphorylated kinase and its total protein. The immunoblotting results in the cortex revealed that there was a significant increase in the phospho-p38 level in HIVgp120 mice compared to the WT controls. This increase was absent in the IFNβKO-HIVgp120 mice suggesting that IFNβ deficiency permits neuronal injury without an increase and even at decreased levels of phosphorylated p38 in the cortex. We observed no sex differences and no significant difference in expression level of total p38 in any of the tested genotypes (Fig. 2.10 A-D).

The involvement of ERK1/2 in HIV-associated neuronal injury is well characterized and we have shown earlier in 11-14 months old HIVgp120 mice that reduction of hippocampal phosphorylated ERK1/2 (pERK1/2/) was associated with neuronal damage (*7, 23*). Therefore, pERK1/2 was also assessed and revealed that in the cortex there was a trend of an increase in the level of pERK1/2 in HIVgp120 mice compared to WT controls. However, IFNβ deficiency significantly reduced the level of pERK1/2 compared to the IFNβ-expressing genotypes and the decrease was consistent in IFNβKO-HIVgp120 mice, suggesting that IFNβ is crucial to maintain normal levels of

pERK1/2. Total ERK1/2 expression remained relatively unchanged in all the tested genotypes except for a significant drop in total ERK1/2 in IFNβKO-HIVgp120 mice compared to the WT and HIVgp120 mice expressing IFNβ. While no change was observed for pERK1/2 in hippocampus of 9-10 months old HIVgp120 compared to WT mice, a significant reduction was observed in IFNβKO mice compared to the IFNβKO-HIVgp120 mice at this age. There were no sex differences and no significant changes in the expression of total ERK1/2 in any of the tested genotypes (Fig. 2.10 E-H).

Next, levels of active and total cJun N-terminal kinase (JNK) 1/2 were assessed by western blotting. No significant changes were found for active JNK1/2 or total JNK1/2 in both cortex and hippocampus in HIVgp120 or IFNβKO genotypes, although average levels trended higher in cortex of IFNβKOs (Fig. 2.11 A-D).

Type 1 IFNs are one of the major players for activation of the Janus kinase-signal transducer and activator of transcription (JAK-STAT) pathway to activate ISGs (*24, 25*). HIVgp120 protein activates STAT1 in vitro, causing inflammation and blood brain barrier dysfunction (*26*), similarly we have reported higher level of STAT1 in brains of HIVgp120 mice (*7*). Consequently, phosphorylated-STAT1 and STAT1 was investigated through Western blot, the pSTAT1 analysis in the cortex showed that HIVgp120tg mice had significantly higher levels of pSTAT1 when comparted to the other three genotypes and this elevation was absent the IFNβKO-HIVgp120 mice. The expression of STAT1 protein was significantly higher in HIVgp120 mice compared to all the tested genotypes. However, IFNβ deficiency is associated with a significantly reduced level at baseline when compared to the WT controls. On the other hand, in hippocampus, pSTAT1 trended slightly above

the baseline level in the presence of HIVgp120 and IFNβ but without reaching significance (Fig. 2.12 A-D). Similarly, the total STAT1 expression was significantly increased in the HIVgp120 mice compared to all the other genotypes suggesting the absence of IFNβ signaling prevents an increase of pSTAT1 and STAT protein in both cortex and hippocampus.

STAT3 is one of the key factors promoting neuronal survival by inducing neuroprotective genes (*27*), therefore, we analyzed the levels STAT3 in cortex and hippocampus. In HIVgp120 mice, the levels of phosphorylated STAT3 were found to be significantly elevated when compared to the WT control group. The absence of IFNβ did not have any effect on the levels of pSTAT3. On the other hand, HIVgp120 mice exhibited a significant increase in the levels total STAT3, and the deletion of IFNβ did not affect these levels. In hippocampus, we observed an upregulation of pSTAT3 in the HIVgp120 mice, and even more so in IFNβKO-HIVgp120 mice (Fig. 2.12 E-H). The levels of total STAT3 were also elevated in the presence of HIVgp120, but IFNβ deficiency had no effect.

FIGURES

A. Light and Dark Transfer Test
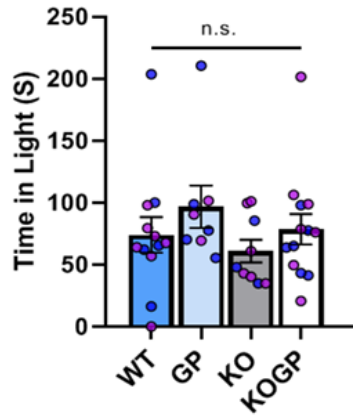
B. Locomotor Test
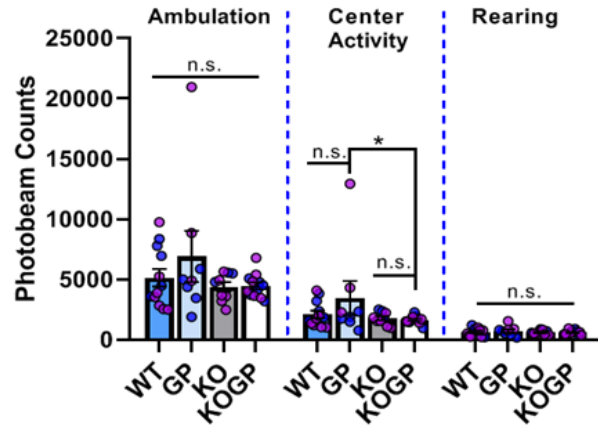
C. Novel Object Recognition Test
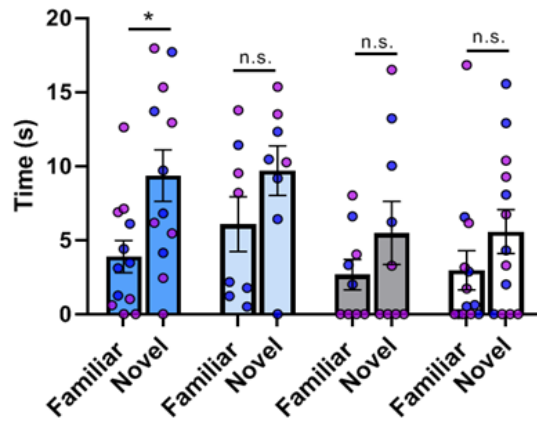
D. Barnes Maze Probe Test
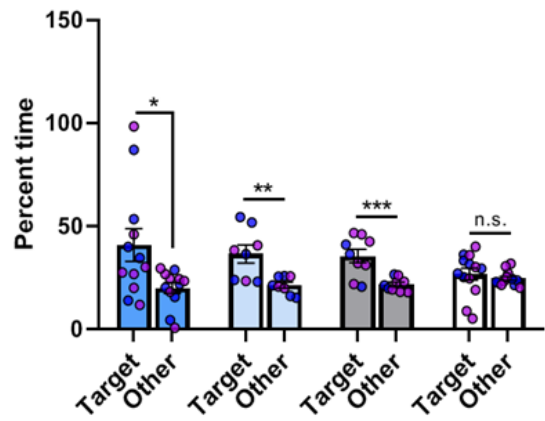
WT □ HIVgp120 □ IFNßKO □ IFNßKO-gp120

Fig. 2.1. **IFNβ affects recognition and spatial memory.** 9 to 10 month-old mice, WT (male:5; female:7), HIVgp120/GP (male:5; female:3), IFNβKO/KO (male:3; female:6) and IFNβKO-HIVgp120/KOGP (male:6; female:7) were behaviorally assessed as described in Materials and Methods. **(A)** Light/dark transfer test for anxiety like behavior. **(B)** Locomotor test showing ambulation, center activity and rearing. **(C)** Novel object recognition for recognition memory. **(D)** Barnes Maze probe test for spatial learning and memory. All data are represented as means ± SEM. Statistical analysis was performed as described in the methods section. *** $P < 0.001$, ** $P < 0.01$, * $P \leq 0.05$; ANOVAs and post hoc tests; n = 8-13 (females [pink dots] and males [blue dots]) per group/genotype; n.s., not significant.

Cortex

Hippocampus
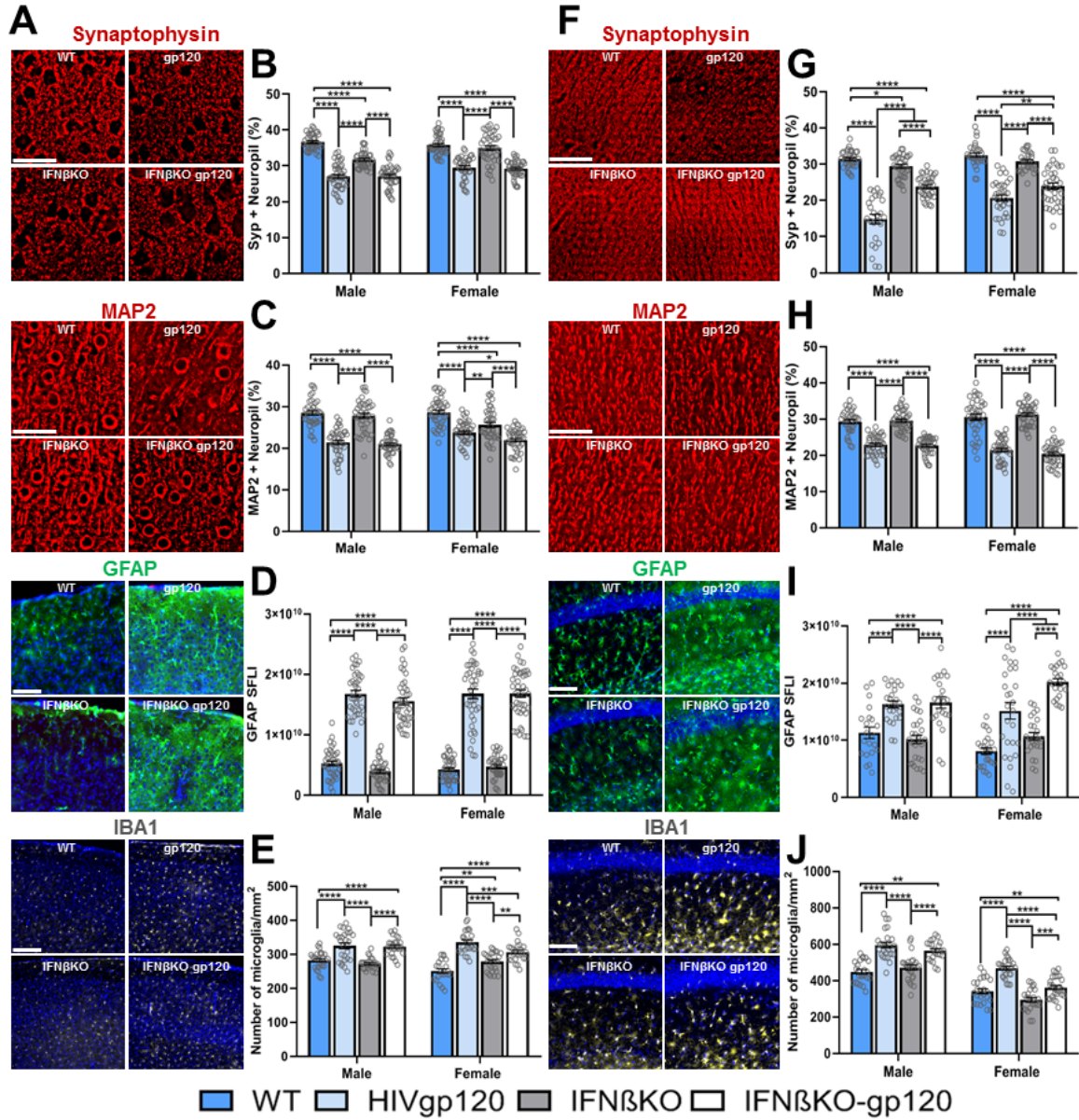
Fig. 2.2. Effect of IFNβ deficiency on presynaptic terminals, neuronal dendrites, astrocytosis and microgliosis. Brains of 9-10 months old mice were histologically analyzed as described in the methods. **(A & F)** Representative images of cortex (layer 3) and hippocampus (CA1) immunolabeled for neuronal synaptophysin (SYP) and MAP-2 (deconvolution microscopy; scale bar = 40 μm), astrocytic GFAP and Iba1 microglia (florescence microscopy; scale bar = 200 μm). **(B&G)** Quantification of neuropil positive for synaptophysin, **(C & H)** neuronal MAP-2, **(D & I)** fluorescence signal for astrocytic GFAP. **(E & J)** Counts for Iba1+ microglia. Genotypes: WT, HIVgp120 (GP), IFNβKO (KO), and IFNβKO-HIVgp120 (KOGP). Values are means ± SEM; **** $P < 0.0001$, *** $P < 0.001$, ** $P < 0.01$, * $P < 0.05$; ANOVA and Fisher's PLSD post hoc test; n = 6 animals (3 males and 3 females) per group/genotype.

Cortex   **Hippocampus**
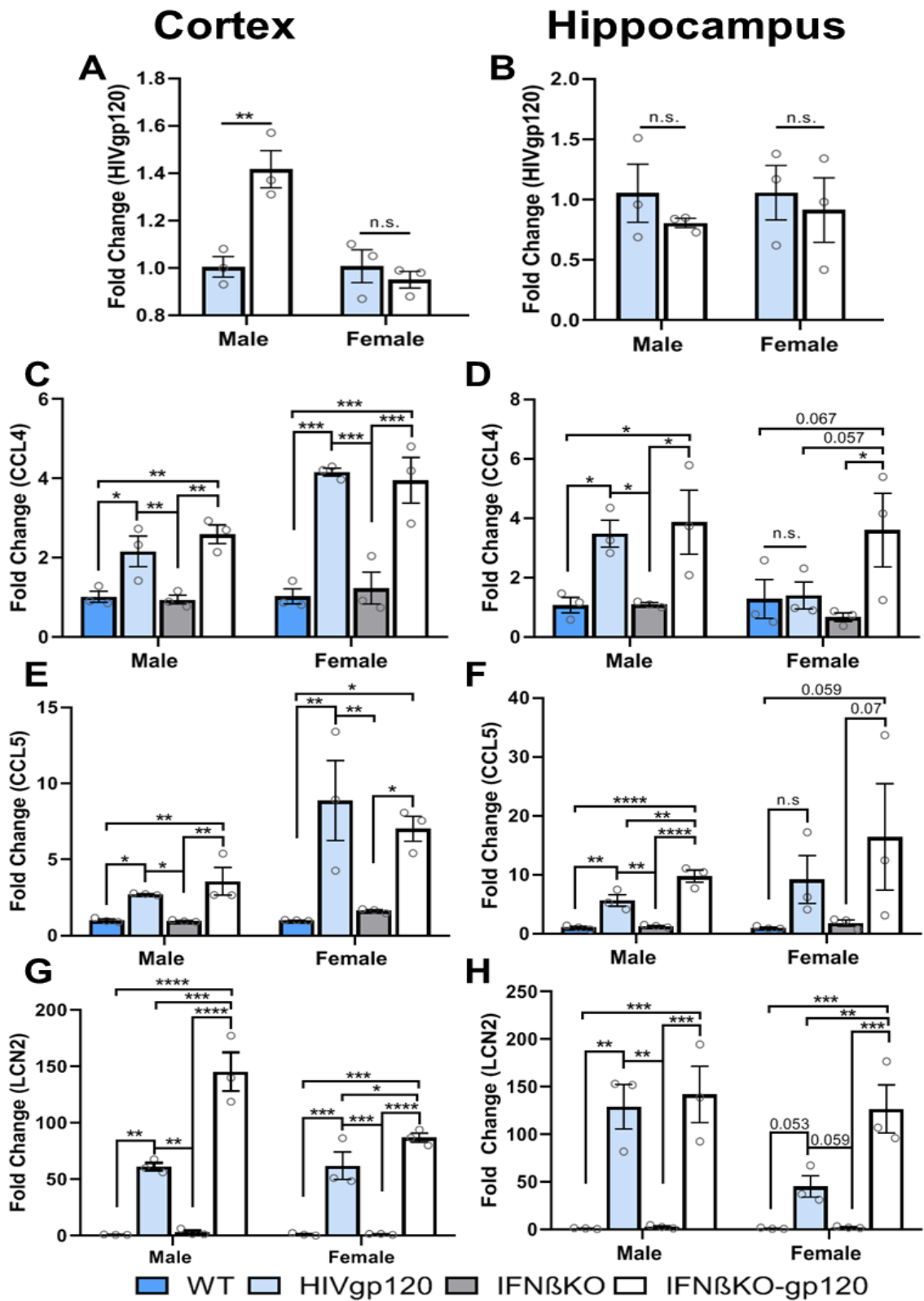
Fig. 2.3. Sex-dependent effects of IFNβ deficiency on RNA expression of transgenic viral HIVgp120 and host genes. The mRNA expression in the cortex and hippocampus of 9-10 months-old mice, were detected by quantitative RT-PCR as described in material and method section. (A & B) HIVgp120; (C & D) CCL4; (E & F) CCL5 and (G &H) LCN2. The obtained CT values were normalized to the level of GAPDH mRNA. Values are means ± SEM; **** $P < 0.0001$, *** $P < 0.001$, ** $P < 0.01$, * $P < 0.05$; ANOVA and Fisher's PLSD post hoc test; n = 3 mice per group/genotype; n.s., not significant.

Cortex
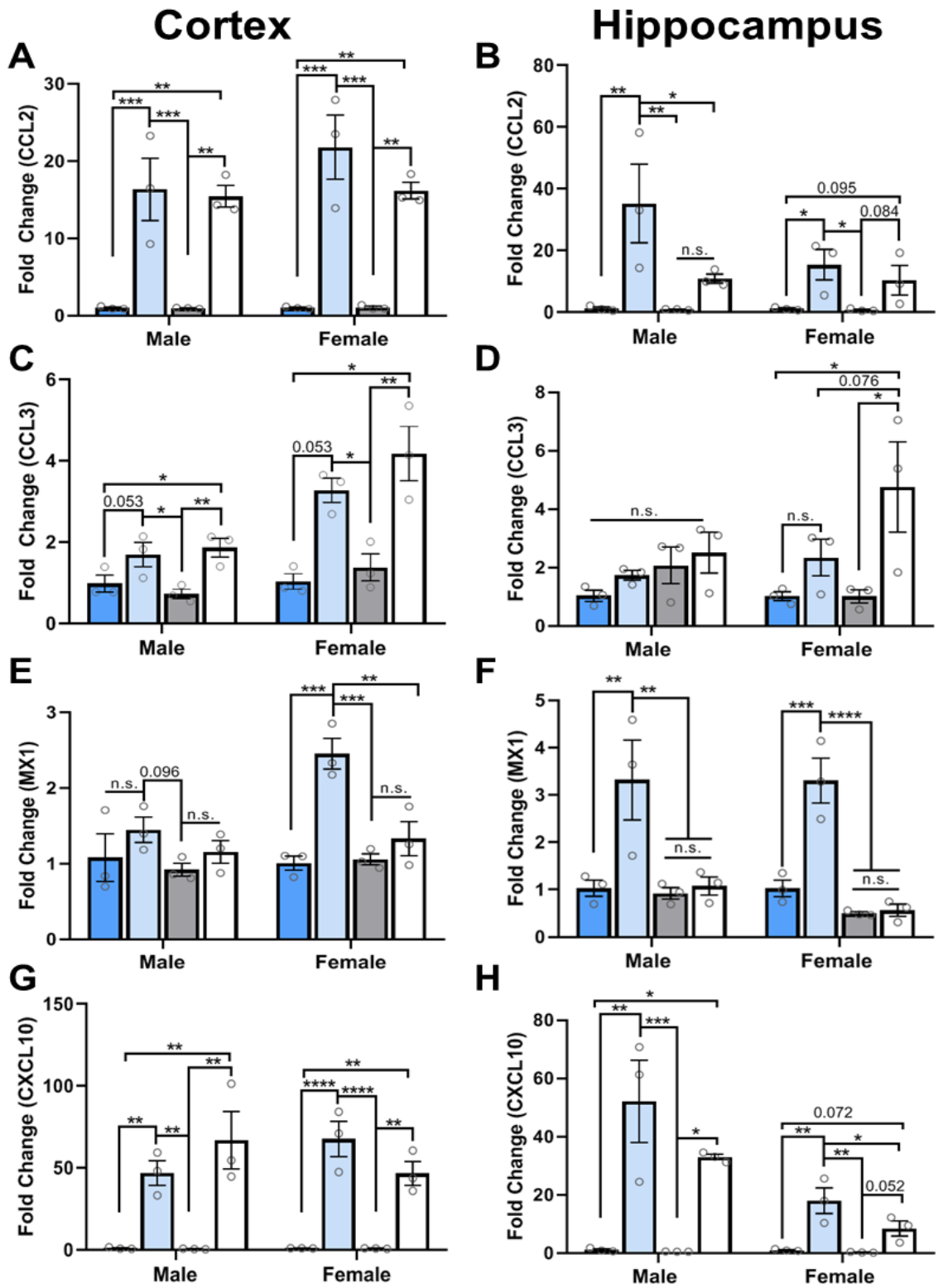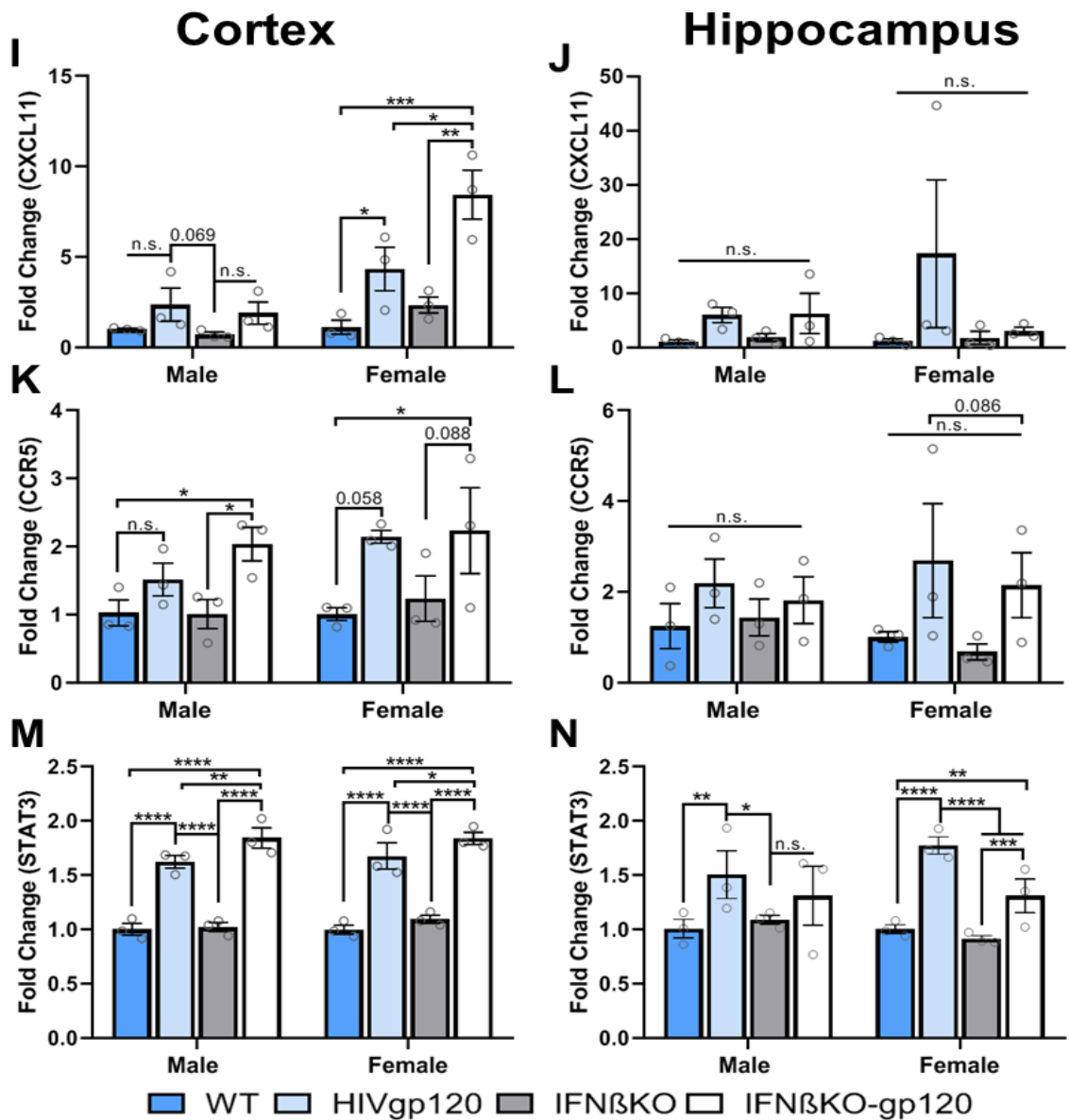
Hippocampus

Fig. 2.4. Effects of IFNβ deficiency on RNA expression of host genes. The mRNA expression in the cortex and hippocampus of 9-10 months-old mice, were detected by quantitative RT-PCR as described in material and method section. **(A & B)** CCL2; **(C & D)** CCL3; **(E & F)** MX1; **(G & H)** CXCL10; **(I & J)** CXCL11; **(K & L)** CCR5 and **(M & N)** STAT3. The obtained CT values were normalized to the level of GAPDH mRNA. Values are means ± SEM; **** $P < 0.0001$, *** $P < 0.001$, ** $P < 0.01$, * $P < 0.05$; ANOVA and Fisher's PLSD post hoc test; n = 3 mice per group/genotype/sex; n.s., not significant.

70
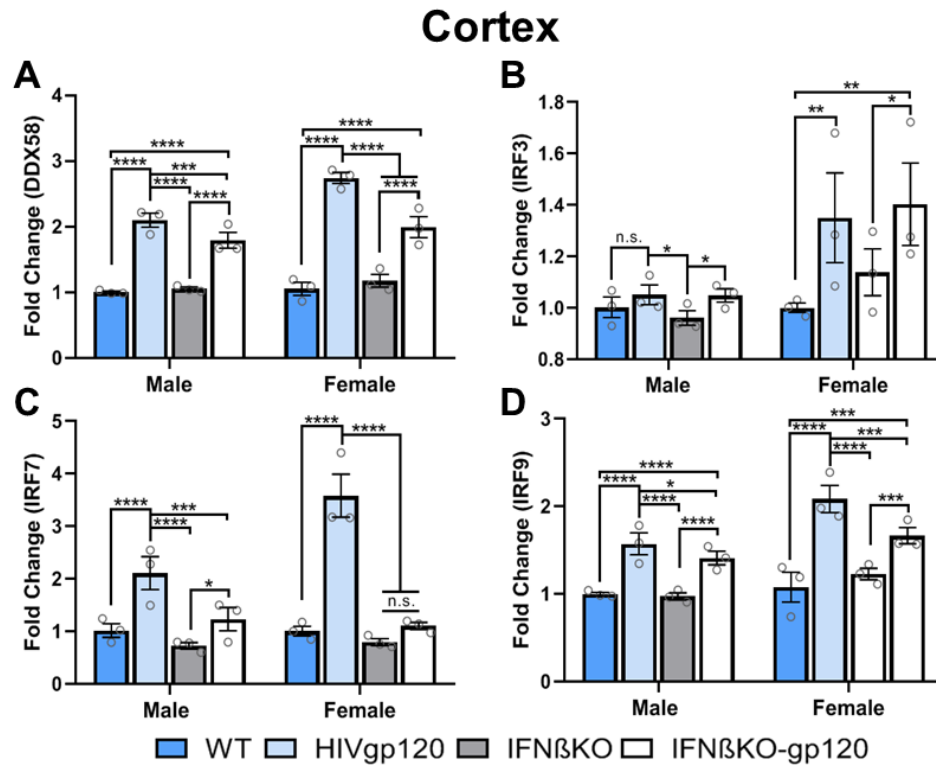
Fig. 2.5. Effects of IFNβ deficiency on RNA expression of DDX58, IRF3, IRF7 and IRF9. The mRNA expression levels of DDX58 **(A)**, IRF3 **(B)**, IRF7 **(C)**, and IRF9 **(D)** were measured in the cortex of 9-10-month-old mice using quantitative RT-PCR. The obtained CT values were then normalized to the level of GAPDH mRNA. The values are presented as means ± SEM; **** $P < 0.0001$, *** $P < 0.001$, ** $P < 0.01$, * $P < 0.05$; ANOVA and Fisher's PLSD post hoc test; n = 3 mice per group/genotype; n.s., not significant.

A. Cortex

GABA Glutamate

B. Hippocampus

Magnitude of gene expression

min · avg · max
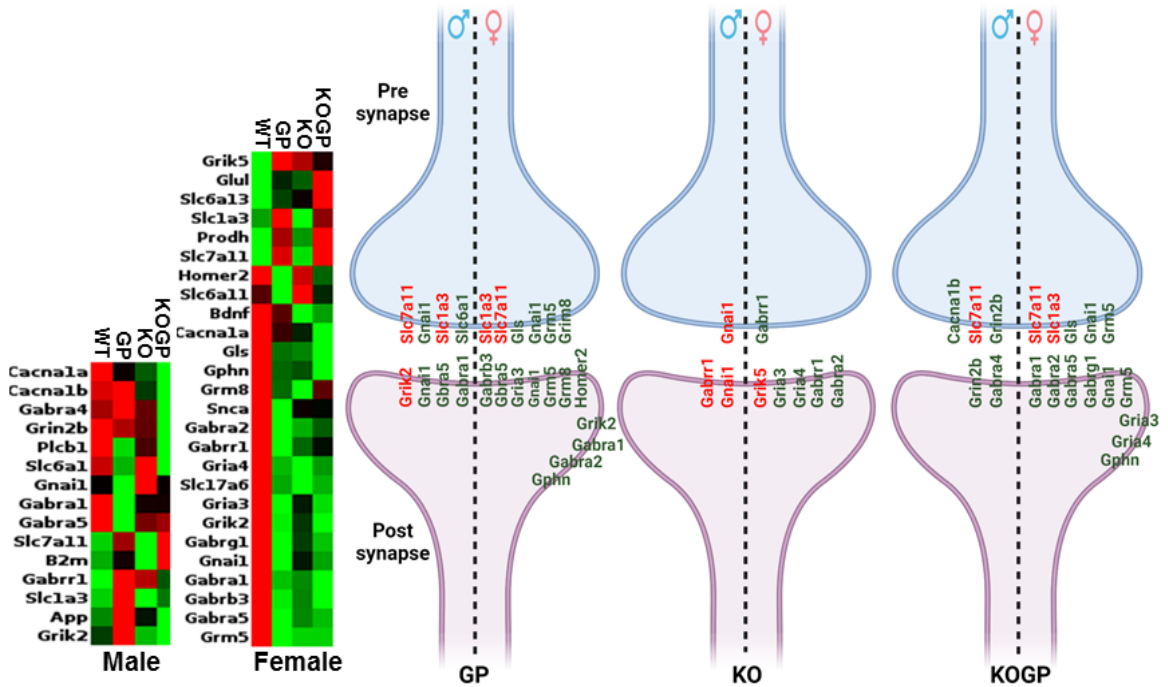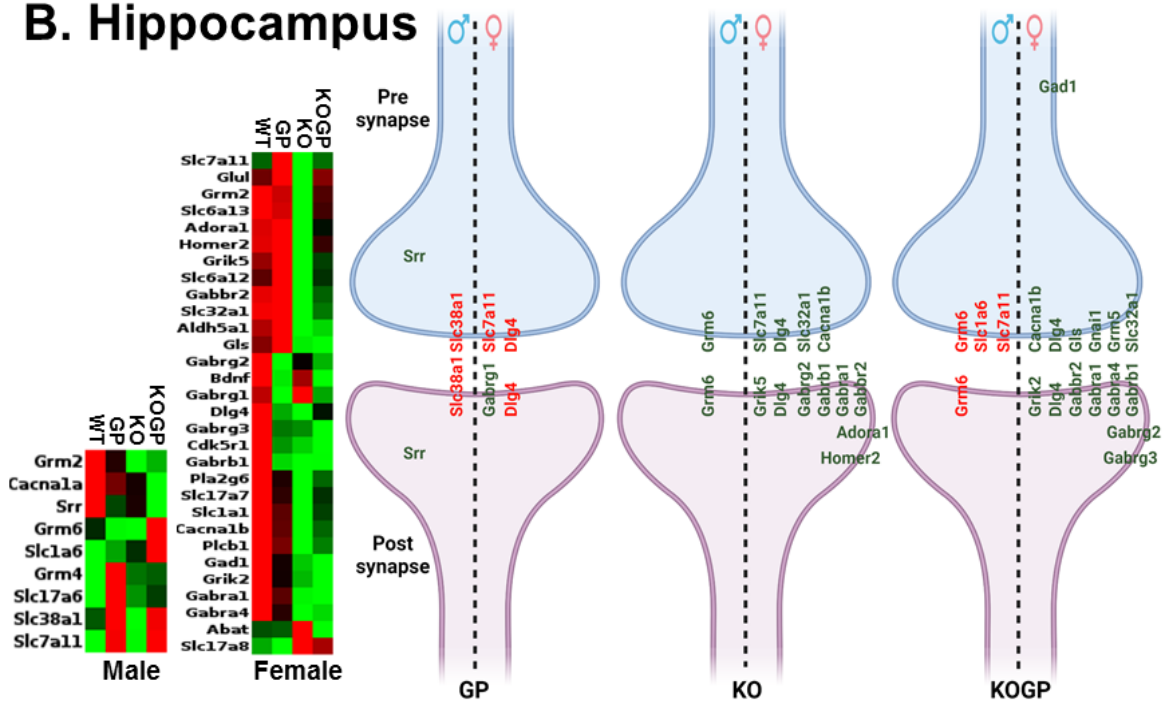
Fig. 2.6. Differential gene expression associated with GABA and glutamate neurotransmission systems in the cortex and hippocampus. Clustergram heat map of mRNA expression of the GABA/Glutamate system in the cortex **(A)** and in the hippocampus **(B)** showing gene expression profile of WT, HIVgp120, and IFNβ-deficient mice with or without HIVgp120. Red indicates higher gene expression while green indicates the lower expression in the sample set normalized by rows. RNA was analyzed using RT^2 Profiler PCR Array and the associated Qiagen data analysis software. The heat maps represent significantly changed genes as the averages of three biological replicates. The figure on the right is a schematic representation of the pre- and post-synaptic distribution of differentially expressed genes in neurons of each genotype. Genotypes: WT, HIVgp120 (GP), IFNβKO (KO), and IFNβKO-HIVgp120 (KOGP).

A. Cortex — Dopamine & Serotonin
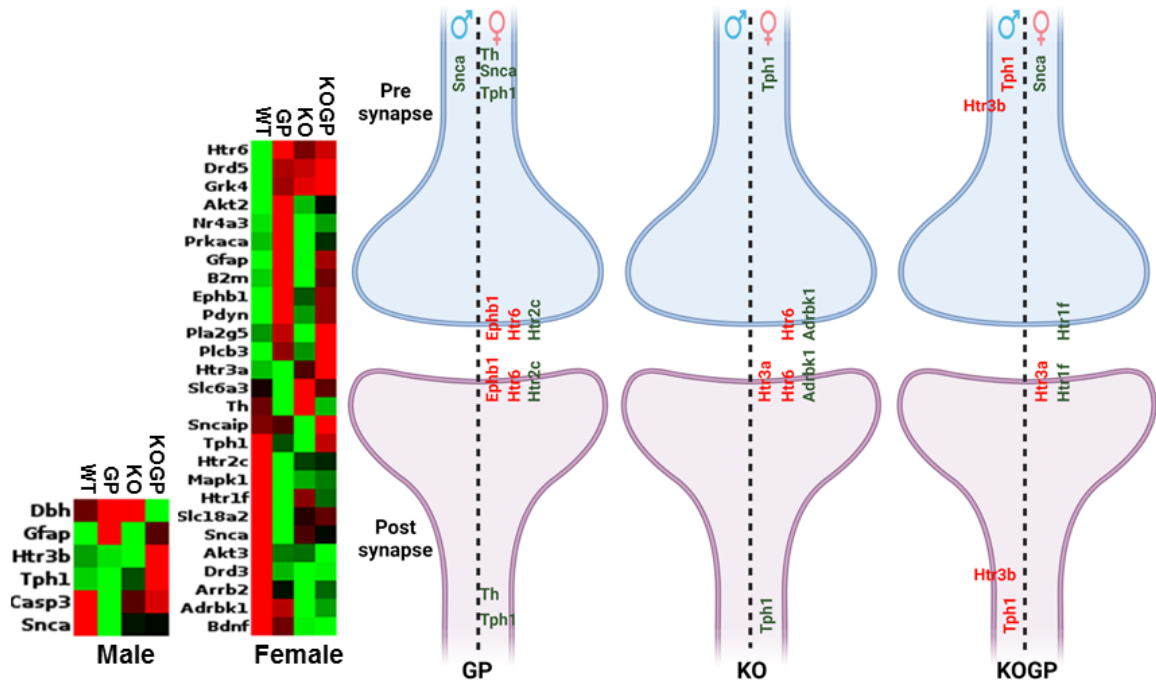
B. Hippocampus
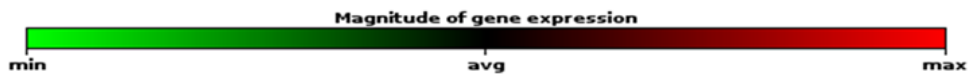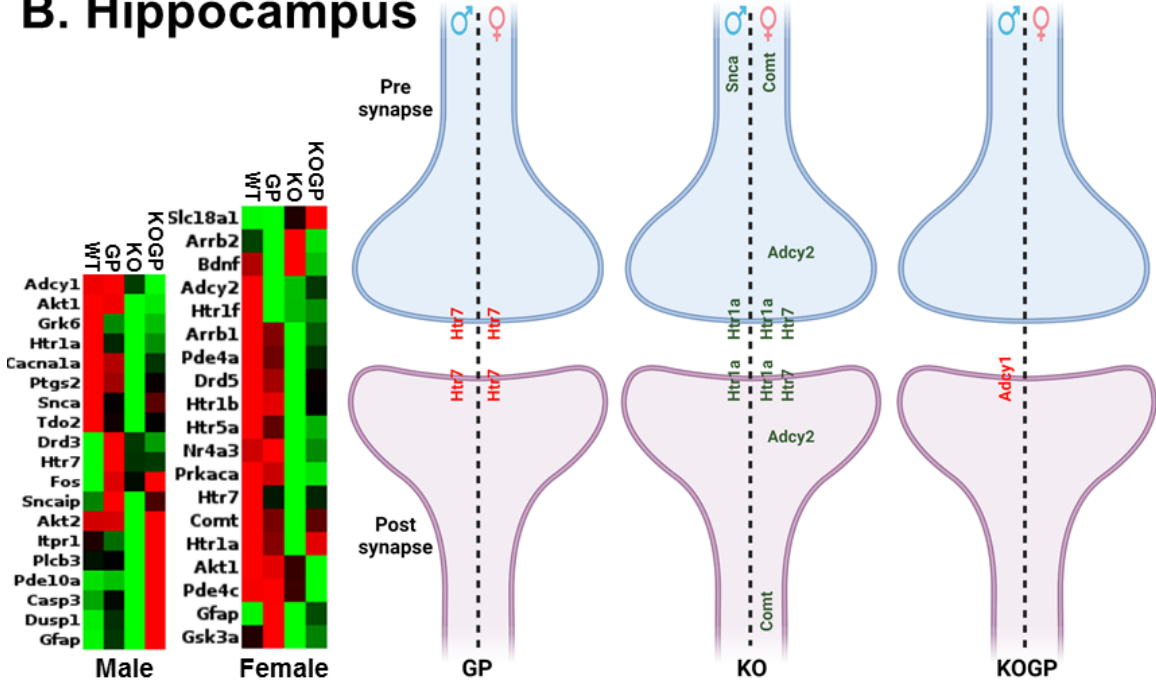
Fig. 2.7. Differential gene expression associated with dopamine serotonin neurotransmission systems in the cortex and hippocampus. Clustergram heat map of dopamine/serotonin systems in the cortex **(A)** and in the hippocampus **(B)** showing gene expression profile of WT, HIVgp120-transgenic, IFNβ-deficient mice with or without HIVgp120. Red indicates the higher gene expression while green indicate the lower gene expression in the sample set. RNA was analyzed using RT^2 Profiler PCR Array and the associated Qiagen data analysis software. The heat maps represent significantly changed genes as the averages of three biological replicates. The figure on the right is a schematic representation of the pre- and post-synaptic distribution of differentially expressed genes in neurons of each genotype. Genotypes: WT, HIVgp120 (GP), IFNβKO (KO), and IFNβKO-HIVgp120 (KOGP).

Male Cortex

Female Cortex

A. HIVgp120 vs WT
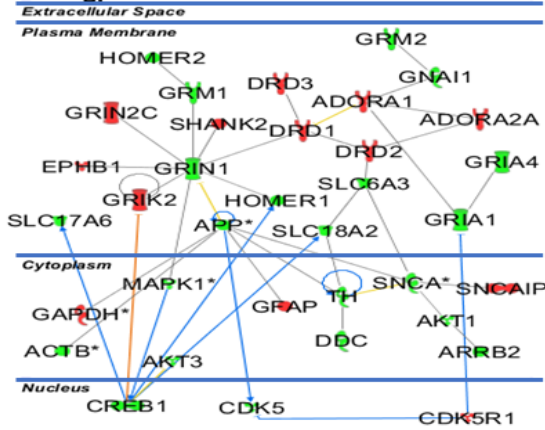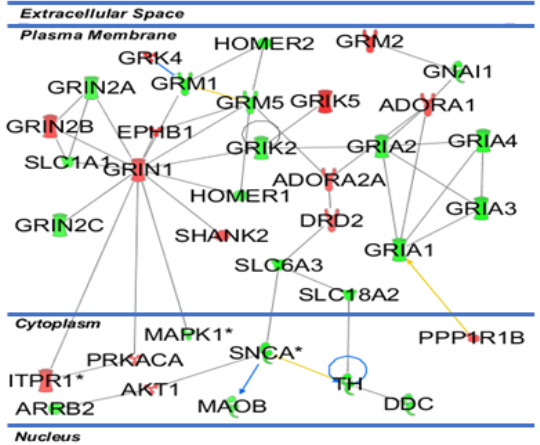
B. IFNβKO vs WT
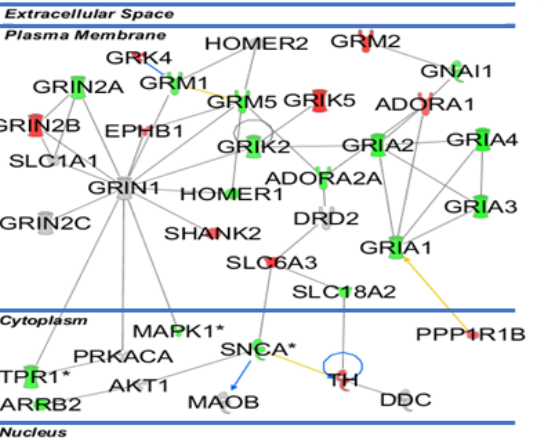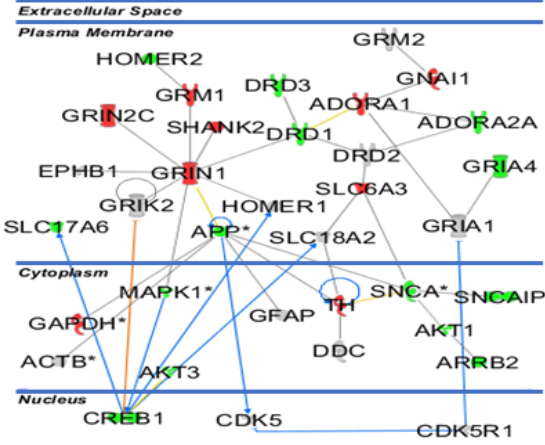
C. IFNβKO x gp120 vs WT
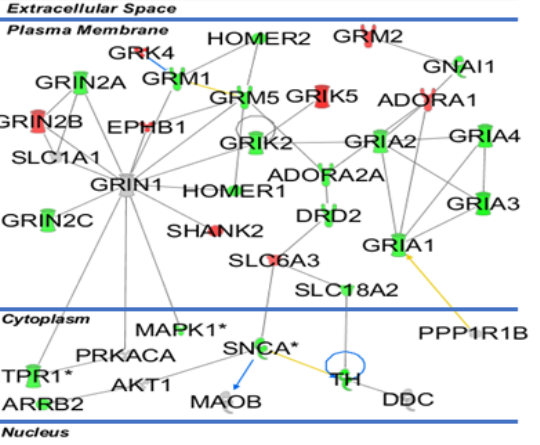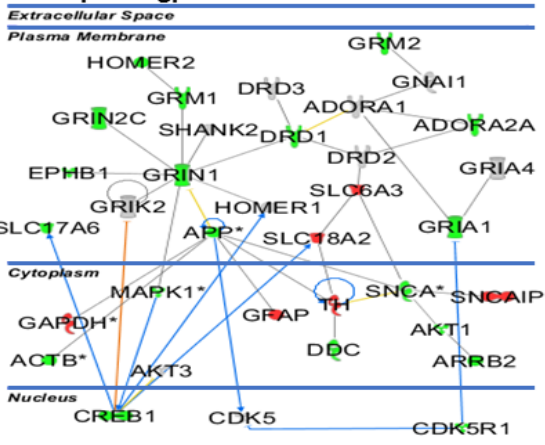
Chemical/Toxicant
Enzyme
G-protein Coupled Receptor
Growth factor
Ion Channel
Kinase
Ligand-dependent Nuclear Receptor
Transcription Regulator
Transporter
Undefined
Direct Relationship

Leads to activation
Leads to Inhibition
Effect not predicted
Findings inconsistent with state of downstream molecules

Fig. 2.8. Functional neural gene networks of neurotransmission affected by HIVgp120 and IFNβ deficiency in the cortex. RNA expression data obtained with the GABA/glutamate RT^2 Profiler PCR Array were analyzed using IPA software. **(A)** HIVgp120 versus WT, **(B)** IFNβKO versus WT, **(C)** IFNβKO-HIVgp120 versus WT. Green indicates down-regulated while red reflects up-regulated genes respectively. The components without color represent genes were include by IPA without experimentally determined expression levels. IPA identified for each sex a different highest scoring gene direct interaction network in which alterations on expression levels were driven by HIVgp120 in the absence or presence of IFNβ. * Indicates genes for which differential regulation reached significance in the RT^2 Profiler PCR Array (* $P < 0.05$; modified t-test).

Male Hippocampus

A. HIVgp120 vs WT

B. IFNβKO vs WT

C. IFNβKO x gp120 vs WT

Female Hippocampus

Legend:

⊖ Chemical/Toxicant	⅋ Growth factor	♋ Ligand-dependent Nuclear Receptor	⬭ Transporter	
℥ Enzyme	⎅ Ion Channel	⤳ Transcription Regulator	○ Undefined	
Ⅴ G-protein Coupled Receptor	⅋ Kinase		― Direct Relationship	

— Leads to activation   — Leads to Inhibition   — Effect not predicted   — Findings inconsistent with state of downstream molecules
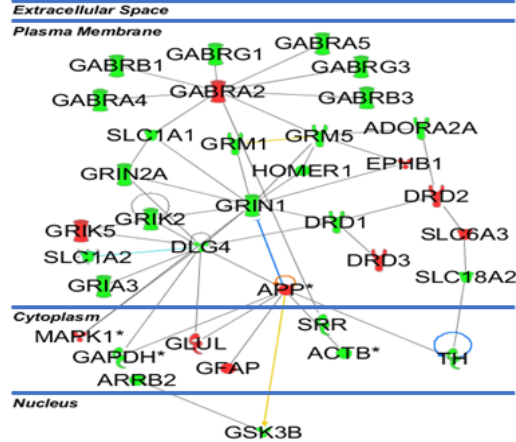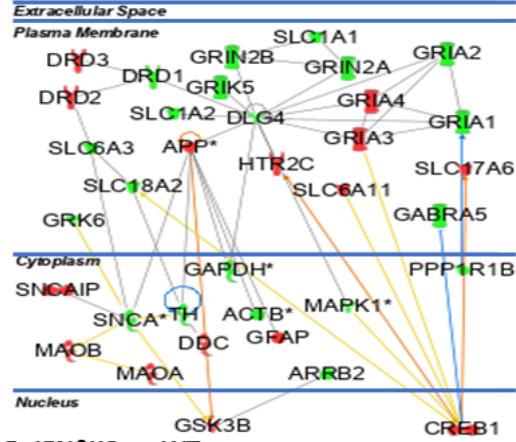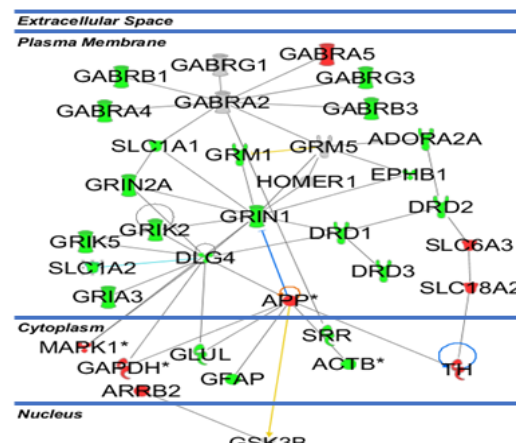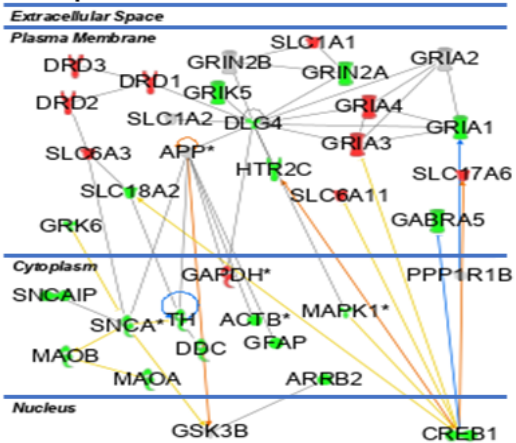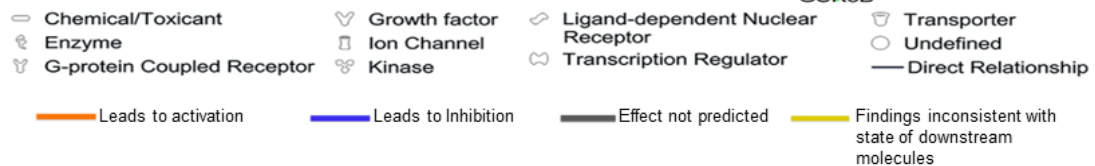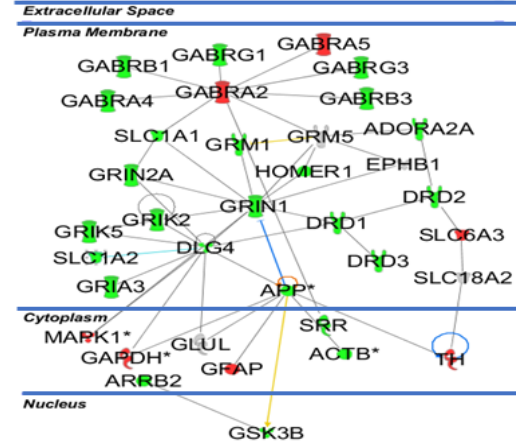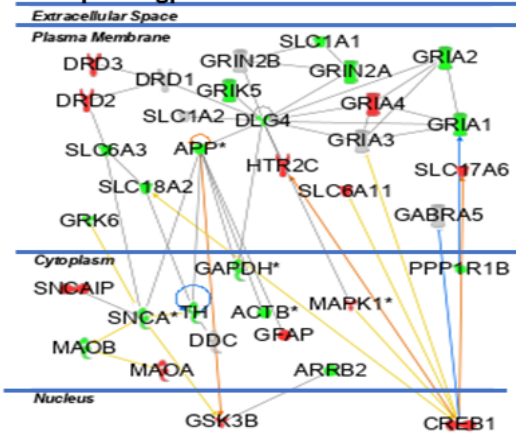
Fig. 2.9. Functional neural gene networks of neurotransmission affected by HIVgp120 and IFNβ deficiency in the hippocampus. RNA expression data obtained with the dopamine/serotonin RT^2 Profiler PCR Array were analyzed using IPA software. **(A)** HIVgp120 versus WT, **(B)** IFNβKO versus WT, **(C)** IFNβKO-HIVgp120 versus WT. Green indicates down-regulated while red reflects up-regulated genes respectively. Components without color represent genes without experimentally determined expression levels. IPA identified for each sex a different highest scoring gene network in which alterations on expression levels were driven by HIVgp120 in the absence or presence of IFNβ. * Indicates genes for which differential regulation reached significance in the RT^2 Profiler PCR Array (* $P < 0.05$; modified t-test).
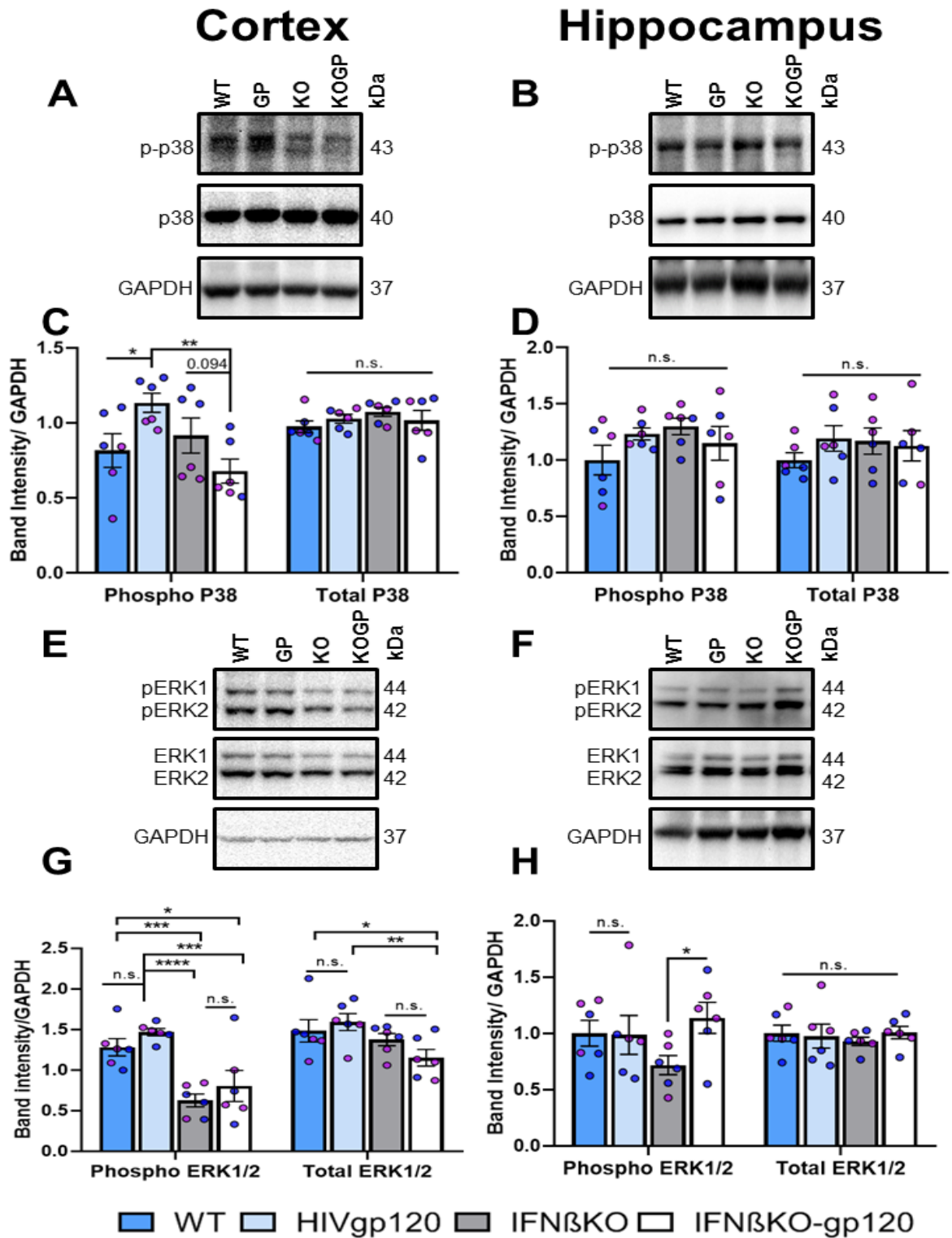
Fig. 2.10. The effect of HIVgp120 and IFNβ deficiency on the phosphorylation levels of p38 MAPK and ERK1/2. The phosphorylation level of p38 and ERK1/2 in the cortex and hippocampus were measured using Western blotting. Representative Western blot of phospho-p38(p-p38), p38 protein, and GAPDH in cortex **(A)** and hippocampus **(B)**. The graph shows quantification of p-p38 and p38 by densitometry using normalization to GAPDH in the cortex **(C)** and hippocampus **(D)**. Representative Western blot of phospho-ERK1/2 (pERK1/2), ERK1/2 total protein, and GAPDH in cortex **(E)** and hippocampus **(F)**. The graph shows densitometry analysis of pERK1/2 and ERK1/2 normalized to GAPDH in the cortex **(G)** and hippocampus **(H)**. Values are means $\pm$ SEM; **** $P < 0.0001$, *** $P < 0.001$, ** $P < 0.01$, * $P < 0.05$; ANOVA and Fisher's PLSD post hoc test; n = 6 animals (3 males and 3 females) 9-10 months-old animals per group/genotype; females [pink dots] and males [blue dots]; n.s., not significant). Genotypes: Wildtype (WT), HIVgp120tg (GP), IFNβKO (KO), and IFNβKO × HIVgp120 (KOGP).
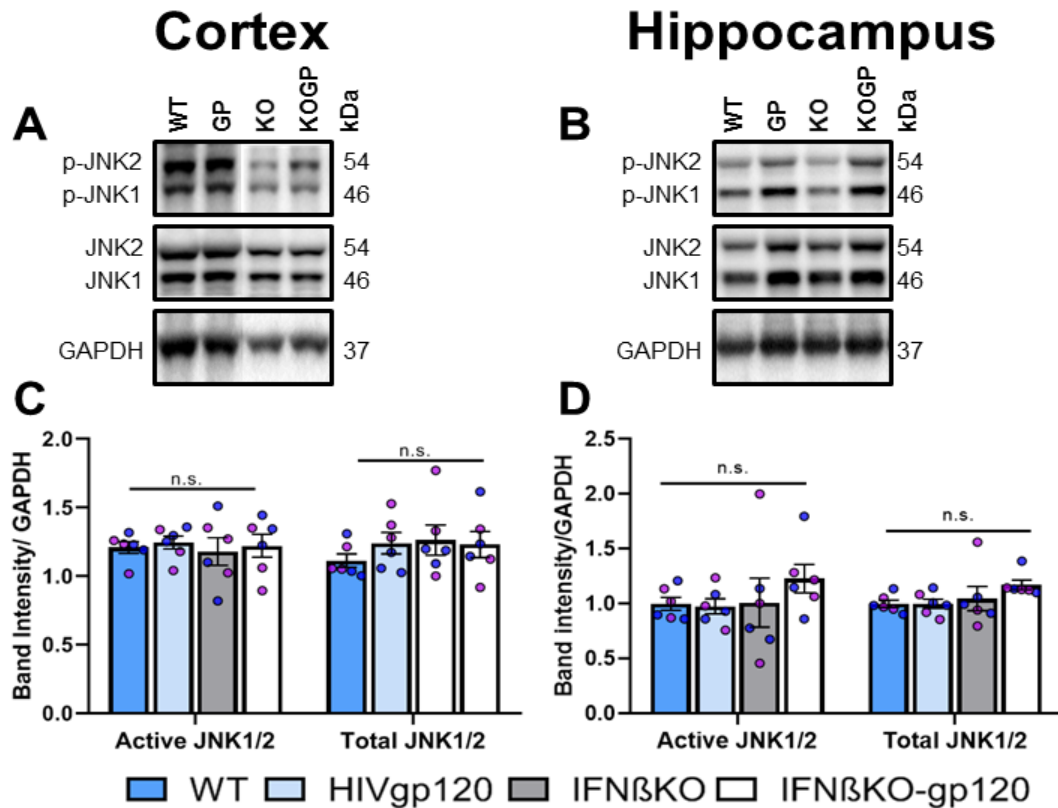
Fig. 2.11. IFNβ deficiency does not alter the expression of JNK in cortex and hippocampus of HIVgp120 mice. The protein expression of phospho-JNK1/2 and JNK1/2 were assessed using immunoblotting. Representative western blot images and densitometry analysis of p-JNK1/2 and JNK1/2 normalized to GAPDH in the cortex (**A** and **C**) and hippocampus (**B** and **D**). Genotypes: WT (WT), HIVgp120tg (GP), IFNβKO (KO) and IFNβKO x HIVgp120 (KOGP). Values are means ± SEM; ANOVA and Fisher's PLSD post hoc test; n = 6 animals (3 males and 3 females) 9-10 months-old animals per group/genotype; females [pink dots] and males [blue dots]; n.s., not significant). Genotypes: Wildtype (WT), HIVgp120tg (GP), IFNβKO (KO), and IFNβKO × HIVgp120 (KOGP).

Cortex
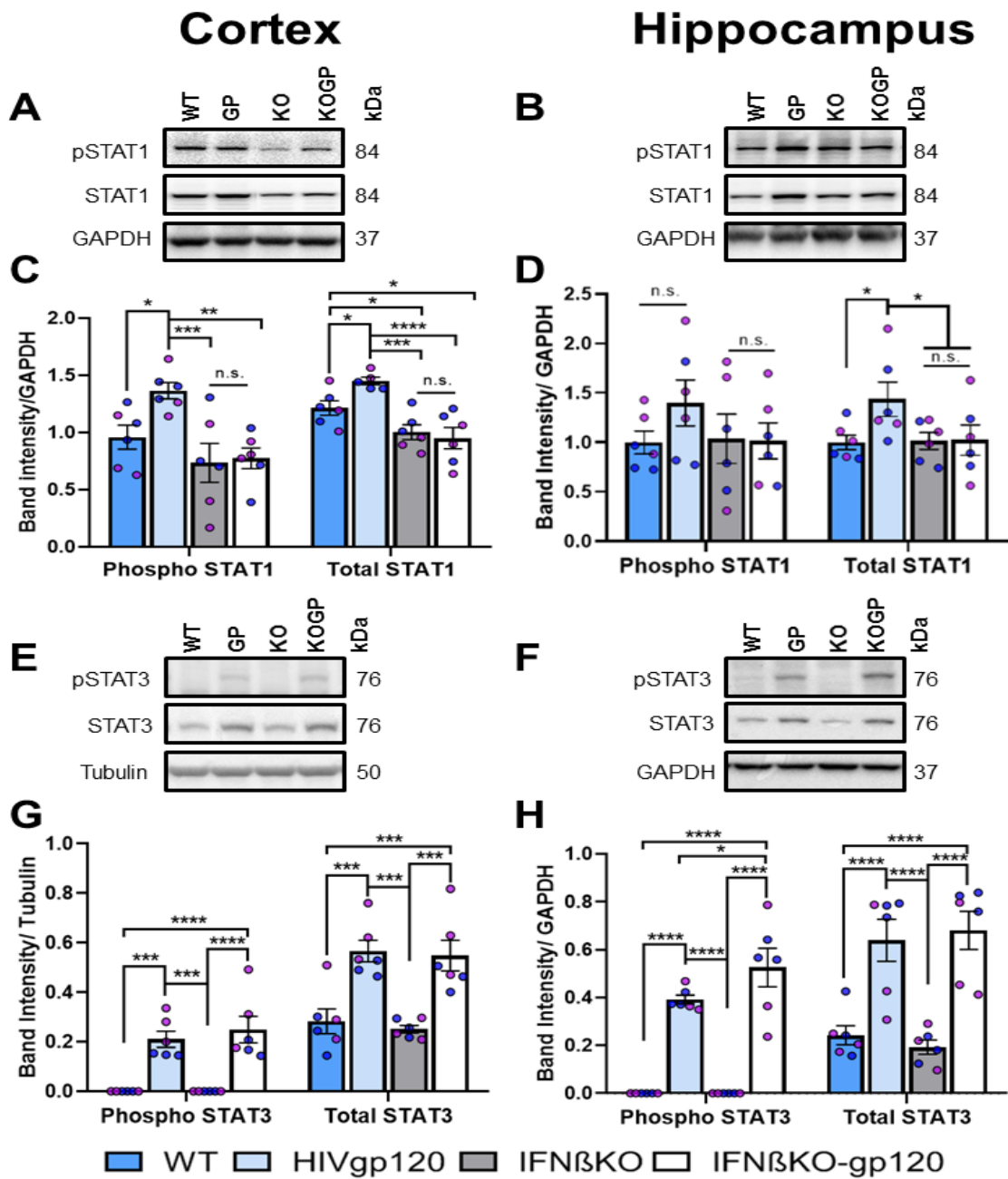
Hippocampus

Fig. 2.12. The effect of HIVgp120 and IFNβ deficiency on the phosphorylation levels of STAT1 and STAT3. The phosphorylation level of STAT1 and STAT3 in the cortex and hippocampus were measured using Western blotting. Representative Western blot of pSTAT1, STAT1, and GAPDH in cortex **(A)** and hippocampus **(B)**. The graph shows quantification of pSTAT1 and STAT1 by densitometry using normalization to GAPDH in the cortex **(C)** and hippocampus **(D)**. Representative Western blot of pSTAT3, STAT3, and tubulin in cortex (**E**) and hippocampus (**F**). The graph shows densitometry analysis of pSTAT3 and STAT3 normalized to tubulin in the cortex (**G**) and hippocampus (**H**). Values are means ± SEM; **** $P < 0.0001$, *** $P < 0.001$, ** $P < 0.01$, * $P < 0.05$; ANOVA and Fisher's PLSD post hoc test; n = 6 animals (3 males and 3 females) 9-10 months-old animals per group/genotype; females [pink dots] and males [blue dots]; n.s., not significant). Genotypes: WT, HIVgp120 (GP), IFNβKO (KO), and IFNβKO-HIVgp120 (KOGP).

Gene	Primer Sequence (5′-3′)
HIV-1 gp120	Fwd: TGAGCCAATTCCCATACATTATTG Rev: CCTGTTCCATTGAACGTCTTATTATTAC
Ccl2	Fwd: CCCAATGAGTAGGCTGGAGA Rev: TCTGGACCCATTCCTTCTTG
Ccl3	Fwd: GCGCCATATGGAGCTGACA Rev: GATGAATTGGCGTGGAATCTTC
Ccl4	Fwd: AGGGTTCTCAGCACCAATGG Rev: AGCTGCCGGGAGGTGTAAG
Ccl5	Fwd: ACACCACTCCCTGCTGCTTT Rev: TGCTGCTGGTGTAGAAATACTCCTT
Ccr5	Fwd: CGAAAACACATGGTCAAACG Rev: GTTCTCCTGTGGATCGGGTA 20
Mx1	Fwd: AGAGCAAGTCTTCTTCAAGGATCAC Rev: GTGGCCTTCCCATCTTCCA
Cxcl10 (5uM)	Fwd: GCCGTCATTTTCTGCCTCAT Rev: GGCCCGTCATCGATATGG
Cxcl11	Fwd: GGCTTCCTTATGTTCAAACAGGG Rev: GCCGTTACTCGGGTAAATTACA
Stat3	Fwd: AGGAGTCTAACAACGGCAGCCT Rev: GTGGTACACCTCAGTCTCGAAG
Lcn2	Fwd: GCCCCATCTCTGCTCACTGT Rev: TTTTTTCTGGACCGCATTGC
Ddx58	Fwd: AAGGAAAACTGGCCAAAGGT Rev: TGGTTTCAATGGGCTGTGTA
Irf3 (15uM)	Fwd: CAGATCTGATTGCCTTCATGGA Rev: ACATTCCCCCATGCAGAAC
Irf7 (5uM)	Fwd: CACCCCCATCTTCGACTTCA Rev: CCAAAACCCAGGTAGATGGTGTA
Irf9	Fwd: GTCTGGAAGACTCGCCTACG Rev: TGGTCCTCCCATTTTCCATA
Gapdh	Fwd: AGGTCGGTGTGAACGGATTTG Rev: TGTAGACCATGTAGTTGAGGTCA

Supplementary Table 2.1: Primer sequences. 20µM concentration was used for all the primers except Cxcl10 (5µM), Irf3 (15µM) and IRF7 (5µM).

GABAergic & Glutamatergic Neurotransmission Systems (Male Cortex)						
	HIVgp120		IFNβKO		IFNβKO x HIVgp120	
Gene	Fold Regulation	P value	Fold Regulation	P value	Fold Regulation	P value
App	1.28	0.045737	1.08	0.395693	-1.09	0.369092
Cacna1a	-1.36	0.140437	-1.61	0.050348	-2.26	0.017629
Cacna1b	1.03	0.893342	-1.27	0.216394	-1.56	0.038233
Gabra1	-1.64	0.017735	-1.22	0.185619	-1.22	0.106868
Gabra4	1.04	0.720303	-1.03	0.567412	-1.23	0.004854
Gabra5	-1.54	0.047297	-1.10	0.561933	-1.07	0.673668
Gabra6	4.14	0.693538	2.61	0.816322	3.82	0.557310
Gabrr1	1.66	0.180286	1.56	0.024112	1.22	0.371398
Gnai1	-1.14	0.004990	1.12	0.029280	1.00	0.946042
Grik2	1.13	0.022947	-1.05	0.706982	-1.08	0.546507
Grin2b	-1.04	0.842543	-1.09	0.631950	-1.36	0.003964
Plcb1	-1.24	0.074064	-1.08	0.260654	-1.26	0.048581
Slc1a3	1.56	0.013274	-1.06	0.788425	1.11	0.503408
Slc6a1	-1.28	0.021295	1.03	0.507437	-1.36	0.132682
Slc7a11	2.15	0.001121	-1.16	0.310051	2.45	0.000814
B2m	1.42	0.025992	-1.22	0.478154	1.93	0.000389

GABAergic & Glutamatergic Neurotrasmission Systems (Female Cortex)					
	HIVgp120		IFNβKO		IFNβKO x HIVgp120	
Gene	Fold Regulation	P value	Fold Regulation	P value	Fold Regulation	P value
Bdnf	-1.21	0.177534	-2.07	0.016867	-1.73	0.022998
Cacna1a	-1.21	0.069015	-1.33	0.035562	-1.77	0.018145
Gabra1	-1.37	0.004827	-1.31	0.080963	-1.44	0.009029
Gabra2	-1.99	0.016051	-1.73	0.019073	-1.51	0.016274
Gabra5	-1.70	0.016550	-1.47	0.144925	-1.57	0.037888
Gabrb3	-1.26	0.030168	-1.19	0.371397	-1.27	0.051665
Gabrg1	-1.90	0.068954	-1.42	0.077836	-1.73	0.041465
Gabrr1	-1.80	0.284434	-1.45	0.019649	-1.31	0.301961
Gls	-1.19	0.035321	-1.20	0.053959	-1.28	0.028031
Glul	1.13	0.217767	1.10	0.324954	1.31	0.014554
Gnai1	-1.34	0.003463	-1.16	0.122459	-1.27	0.024548
Gphn	-1.37	0.018256	-1.34	0.056699	-1.63	0.019458
Gria3	-1.97	0.000663	-1.37	0.043163	-1.87	0.000586
Gria4	-1.38	0.053599	-1.46	0.042447	-1.34	0.044709
Grik2	-1.22	0.045541	-1.12	0.076390	-1.22	0.057291
Grik5	1.98	0.053126	1.83	0.010308	1.55	0.109787
Grm5	-1.29	0.017293	-1.26	0.112044	-1.26	0.033738
Grm8	-1.22	0.030155	-1.34	0.129706	-1.09	0.609097
Homer2	-1.32	0.042153	-1.02	0.740380	-1.20	0.175304
Prodh	1.37	0.063752	1.09	0.596124	1.45	0.044387
Slc17a6	-1.76	0.052508	-2.06	0.002359	-1.79	0.004946
Slc1a3	1.47	0.007451	-1.11	0.506605	1.35	0.030084
Slc6a11	-1.33	0.016028	1.12	0.051352	-1.10	0.157670
Slc6a13	1.22	0.028434	1.31	0.167500	1.59	0.015563
Slc7a11	2.81	0.006727	1.11	0.339012	2.94	0.000277
Snca	-1.70	0.016516	-1.24	0.169463	-1.27	0.006578
B2m	1.93	0.010466	-1.26	0.532607	1.64	0.082569

Supplementary Table 2.2: Differential gene expression in males and females in the GABA/glutamate neurotransmission systems in cortex.

GABAergic & Glutamatergic Neurotransmission Systems (Female Hippocampus)

Gene	HIVgp120		IFNβKO		IFNβKO x HIVgp120	
	Fold Regulation	P value	Fold Regulation	P value	Fold Regulation	P value
Abat	-1.02	0.955505	1.60	0.326682	-1.46	0.005687
Adora1	1.02	0.794662	-1.47	0.044878	-1.19	0.080789
Aldh5a1	1.10	0.559845	-2.38	0.028979	-2.13	0.081029
Bdnf	-1.54	0.003698	-1.07	0.734813	-1.57	0.003297
Cacna1b	-1.15	0.325915	-1.72	0.044366	-1.41	0.019001
Cdk5r1	-1.35	0.230099	-1.42	0.056800	-1.48	0.046268
Dlg4	-1.35	0.014020	-1.45	0.025593	-1.20	0.008023
Gabbr2	1.04	0.826423	-5.45	0.024388	-2.23	0.032782
Gabra1	-1.17	0.531610	-1.82	0.000614	-1.84	0.013037
Gabra4	-1.29	0.168111	-2.16	0.073956	-2.00	0.023355
Gabrb1	-1.23	0.193384	-1.25	0.043229	-1.25	0.049472
Gabrg1	-1.48	0.048500	1.05	0.735771	-1.35	0.083545
Gabrg2	-1.32	0.137893	-1.13	0.017730	-1.26	0.023332
Gabrg3	-1.28	0.096623	-1.30	0.082762	-1.43	0.035803
Gad1	-1.19	0.278865	-1.46	0.178666	-1.54	0.041672
Gls	1.06	0.584003	-1.25	0.149807	-1.27	0.011147
Glul	1.10	0.491897	-1.36	0.025572	1.02	0.753134
Grik2	-1.17	0.339889	-1.37	0.084762	-1.45	0.021034
Grik5	1.19	0.442854	-3.88	0.011878	-1.65	0.083425
Grm2	-1.05	0.997000	-1.80	0.043357	-1.18	0.291352
Homer2	1.03	0.862765	-1.92	0.031506	-1.21	0.182905
Pla2g6	-1.21	0.298295	-1.62	0.019112	-1.37	0.034450
Plcb1	-1.15	0.265593	-1.94	0.021120	-1.57	0.015981
Slc17a7	-1.20	0.286544	-1.68	0.038702	-1.32	0.071226
Slc17a8	-1.10	0.767562	1.46	0.037502	1.36	0.264008
Slc1a1	-1.14	0.348816	-1.64	0.023002	-1.32	0.002288
Slc32a1	1.01	0.945940	-2.74	0.031409	-1.87	0.013690
Slc6a12	1.35	0.381709	-3.92	0.043164	-1.43	0.426865
Slc6a13	-1.04	0.832997	-1.99	0.016150	-1.23	0.705345

Supplementary Table 2.3: Differential gene expression in males and females in the GABA/glutamate neurotransmission systems in hippocampus.

GABAergic & Glutamatergic Neurotransmission Systems (Male Hippocampus)

Gene	HIVgp120		IFNβKO		IFNβKO x HIVgp120	
	Fold Regulation	P value	Fold Regulation	P value	Fold Regulation	P value
Cacna1a	-1.35	0.100642	-1.76	0.032035	-20.13	0.053689
Grm2	-1.20	0.590753	-1.64	0.023390	-1.51	0.067692
Grm4	1.51	0.022574	1.14	0.558689	1.16	0.534173
Grm6	-2.03	0.072749	-2.08	0.038792	1.72	0.036582
Slc17a6	3.34	0.018332	1.49	0.352942	1.88	0.353422
Slc1a6	1.14	0.325995	1.32	0.352752	1.78	0.014775
Slc38a1	1.38	0.045238	-1.23	0.063052	1.37	0.356444
Slc7a11	2.49	0.105830	1.02	0.917190	2.51	0.017559
Srr	-1.51	0.025798	-1.31	0.082851	-2.11	0.289386

Dopaminergic & Serotonergic Neurotransmission Systems (Male Cortex)

Gene	HIVgp120		IFNβKO		IFNβKO X HIVgp120	
	Fold Regulation	P-Value	Fold Regulation	P-Value	Fold Regulation	P-Value
Casp3	-1.38	0.005821	-1.10	0.627135	-1.02	0.903975
Dbh	1.08	0.138727	1.08	0.639513	-1.24	0.039718
Gfap	28.14	0.000302	1.05	0.784071	19.11	0.004091
Htr3b	-1.49	0.378335	-1.85	0.306631	3.07	0.032722
Snca	-1.33	0.023729	-1.15	0.303824	-1.15	0.393783
Tph1	-1.05	0.847388	1.14	0.582536	1.51	0.014876

Dopaminergic & Serotonergic Neurotransmission Systems (Female Cortex)

Gene	HIVgp120 Fold Regulation	P-value	IFNβKO Fold Regulation	P-value	IFNβKO X HIVgp120 Fold Regulation	P-value
Adrbk1	-1.02	0.863136	-1.16	0.042706	-1.13	0.218704
Akt2	1.28	0.027409	1.04	0.726793	1.13	0.166490
Akt3	-1.31	0.015898	-1.30	0.055655	-1.47	0.000647
Arrb2	-1.10	0.176396	-1.21	0.017491	-1.14	0.145872
Bdnf	-1.12	0.393272	-1.56	0.036063	-1.58	0.040492
Drd3	-1.46	0.493424	-1.57	0.049965	-1.55	0.186732
Drd5	1.54	0.356990	1.57	0.063411	1.64	0.041046
Ephb1	1.55	0.013147	1.18	0.178321	1.44	0.090538
Gfap	30.24	0.000079	1.15	0.184940	25.15	0.001862
Grk4	1.52	0.039580	1.61	0.011884	1.64	0.038123
Htr1f	-1.37	0.050611	-1.07	0.258866	-1.23	0.000449
Htr2c	-1.56	0.043937	-1.29	0.095003	-1.26	0.104865
Htr3a	-1.08	0.941389	1.31	0.000052	1.51	0.000015
Htr6	1.46	0.017499	1.34	0.032673	1.42	0.071015
Mapk1	-1.34	0.015693	-1.27	0.059846	-1.23	0.023230
Nr4a3	1.40	0.039301	-1.02	0.884908	1.06	0.626531
Pdyn	1.59	0.022020	1.11	0.369905	1.47	0.008502
Pla2g5	1.54	0.097828	-1.19	0.079424	1.63	0.030374
Plcb3	1.38	0.033023	1.10	0.493638	1.49	0.018538
Prkaca	1.11	0.018360	-1.01	0.991324	1.03	0.634648
Snca	-1.77	0.024336	-1.18	0.065793	-1.29	0.017595
Sncaip	-1.04	0.675392	-1.37	0.044200	1.09	0.439822
Th	-2.51	0.015463	1.25	0.378774	-1.97	0.534379
Tph1	-1.80	0.045712	-3.06	0.005478	-1.09	0.964680
B2m	2.11	0.008420	-1.12	0.677162	1.77	0.051016

Supplementary Table 2.4: Genes differentially regulated in males and females in the dopamine/serotonin neurotransmission systems in the cortex

Dopaminergic & Serotonergic Neurotransmission Systems (Male Hippocampus)						
	HIVgp120		IFNβKO		IFNβKO x HIVgp120	
Gene	Fold Regulation	P-value	Fold Regulation	P-value	Fold Regulation	P-value
Adcy1	1.01	0.945657	-1.29	0.276612	-1.58	0.048488
Akt1	-1.01	0.979375	-1.26	0.039318	-1.25	0.031203
Akt2	1.00	0.821887	-1.51	0.009263	1.03	0.661958
Cacna1a	-1.06	0.966422	-1.69	0.011063	-1.33	0.425483
Casp3	1.27	0.349559	-1.17	0.572993	1.71	0.031930
Drd3	2.77	0.010060	1.69	0.361777	1.34	0.474535
Dusp1	1.22	0.157338	-1.02	0.981012	1.57	0.013936
Fos	1.77	0.099613	1.39	0.310168	1.83	0.028539
Gfap	5.36	0.126037	-1.22	0.397022	12.42	0.015644
Grk6	-1.38	0.178237	-1.56	0.042218	-1.46	0.122750
Htr1a	-1.25	0.284441	-1.53	0.020782	-1.37	0.099623
Htr7	1.52	0.013202	1.21	0.213102	1.20	0.299095
Itpr1	-1.13	0.521322	-1.32	0.007207	1.19	0.129981
Pde10a	1.04	0.584958	-1.04	0.839280	1.56	0.034081
Plcb3	1.02	0.833039	-1.34	0.034679	1.29	0.055315
Ptgs2	-1.08	0.691396	-1.72	0.003498	-1.25	0.184759
Snca	-1.22	0.162212	-1.58	0.047995	-1.13	0.505023
Sncaip	1.68	0.003183	-1.27	0.478172	1.36	0.068818
Tdo2	-1.30	0.697132	-1.98	0.044388	-1.33	0.848806

Dopaminergic & Serotonergic Neurotransmission Systems (Female Hippocampus)

Gene	HIVgp120		IFNβKO		IFNβKO x HIVgp120	
	Fold Regulation	P-value	Fold Regulation	P-value	Fold Regulation	P-value
Adcy1	-1.30	0.351440	-2.04	0.139294	-1.58	0.237268
Adcy2	-1.58	0.012334	-1.48	0.021582	-1.29	0.064721
Akt1	-1.05	0.512890	-1.59	0.042097	-17.18	0.215736
Arrb1	-1.13	0.368283	-1.88	0.024994	-1.47	0.095320
Arrb2	-1.43	0.016191	1.51	0.201890	-1.34	0.013053
Bdnf	-1.60	0.041505	1.07	0.709451	-1.48	0.047503
Comt	-1.11	0.437947	-1.60	0.037327	-1.13	0.301419
Drd5	-1.16	0.627559	-4.06	0.035163	-1.57	0.037298
Fos	1.01	0.936162	1.12	0.798231	-2.34	0.114270
Gfap	8.96	0.001634	-1.18	0.561229	3.69	0.158939
Gsk3a	1.31	0.080315	-1.69	0.037113	-1.30	0.221146
Htr1a	-1.10	0.429452	-1.68	0.022863	-1.02	0.891747
Htr1b	-1.04	0.762767	-3.60	0.023628	-1.56	0.213371
Htr1d	-2.09	0.238363	-3.86	0.120079	-2.20	0.220123
Htr1f	-1.89	0.046105	-1.70	0.152866	-1.59	0.109672
Htr5a	-1.23	0.291316	-2.47	0.008075	-2.02	0.033119
Htr7	-1.25	0.175801	-1.58	0.039440	-1.27	0.125837
Nr4a3	1.04	0.635842	-1.59	0.072681	-1.39	0.007741
Pde4a	-1.19	0.310189	-2.32	0.042235	-1.50	0.116767
Pde4c	1.01	0.823463	-1.25	0.593573	-2.15	0.039142
Prkaca	-1.05	0.534703	-1.78	0.010555	-1.71	0.025134
Slc18a1	-1.01	0.966170	1.68	0.403607	2.21	0.039987

Supplementary Table 2.5: Genes differentially regulated in males and females in the dopamine/serotonin neurotransmission systems in the hippocampus

Sex/Brain region	Molecules in Network	Score	Focus Molecules	Top Diseases and
Male Cortex	ACTB,ADORA1,ADORA2A,AKT1,AKT3,APP,ARRB2,CDK5,CDK5R1,CREB1,DDC,DRD1,DRD2,DRD3,EPHB1,GAPDH,GFAP,GNAI1,GRIA1,GRIA4,GRIK2,GRIN1,GRIN2C,GRM1,GRM2,HOMER1,HOMER2,MAPK1,SHANK2,SLC17A6,SLC18A2,SLC6A3,SNCA,SNCAIP,TH	66	35	Behavior, Cell-To-Cell Signaling and Interaction, Nervous System Development and Function
Female Cortex	ADORA1,ADORA2A,AKT1,ARRB2,DDC,DRD2,EPHB1,GNAI1,GRIA1,GRIA2,GRIA3,GRIA4,GRIK2,GRIK5,GRIN1,GRIN2A,GRIN2B,GRIN2C,GRK4,GRM1,GRM2,GRM5,HOMER1,HOMER2,ITPR1,MAOB,MAPK1,PPP1R1B,PRKACA,SHANK2,SLC18A2,SLC1A1,SLC6A3,SNCA,TH	64	35	Behavior, Cell-To-Cell Signaling and Interaction, Nervous System Development and Function
Male Hippocampus	ACTB,APP,ARRB2,CREB1,DDC,DLG4,DRD1,DRD2,DRD3,GABRA5,GAPDH,GFAP,GRIA1,GRIA2,GRIA3,GRIA4,GRIK5,GRIN2A,GRIN2B,GRK6,GSK3B,HTR2C,MAOA,MAOB,MAPK1,PPP1R1B,SLC17A6,SLC18A2,SLC1A1,SLC1A2,SLC6A11,SLC6A3,SNCA,SNCAIP,TH	66	35	Behavior, Cell-To-Cell Signaling and Interaction, Nervous System Development and Function
Female Hippocampus	ACTB,ADORA2A,APP,ARRB2,DLG4,DRD1,DRD2,DRD3,EPHB1,GABRA2,GABRA4,GABRA5,GABRB1,GABRB3,GABRG1,GABRG3,GAPDH,GFAP,GLUL,GRIA3,GRIK2,GRIK5,GRIN1,GRIN2A,GRM1,GRM5,GSK3B,HOMER1,MAPK1,SLC18A2,SLC1A1,SLC1A2,SLC6A3,SRR,TH	66	35	Behavior, Organismal Injury and Abnormalities, Psychological Disorders

Supplementary Table 2.6: List of molecules comprising the top scoring networks predicted by Ingenuity Pathway analysis (IPA).

Cortex Upstream Regulators

Male	Upstream Regulator	Molecule Type	Predicted Activation State	Activation z-score	p-value
HIVgp120	None Scored				
IFNβKO	CREBBP	Transcription regulator	Activated	2.236	2.22E-10
IFNβKO X HIVgp120	CREBBP	Transcription regulator	Inhibited	-2.236	7.38E-14
	HTT	Transcription regulator	Activated	2.395	3.58E-28

Female	Upstream Regulator	Molecule Type	Predicted Activation State	Activation z-score	p-value
HIVgp120	NR3C1	ligand-dependent nuclear receptor	Activated	2.933	2.34E-22
IFNβKO	EGR2	transcription regulator	Inhibited	-2.236	0.000319
	CREBBP	transcription regulator	Inhibited	-2	1.48E-08
IFNβKO X HIVgp120	CREBBP	transcription regulator	Inhibited	-2.236	5.95E-12

Hippocampus Upstream Regulators

Male	Upstream Regulator	Molecule Type	Predicted Activation State	Activation z-score	p-value
HIVgp120	PIAS1	Transcription regulator	Inhibited	-2.449	7.35E-08
IFNβKO	None Scored				
IFNβKO X HIVgp120	IRF8	transcription regulator	Inhibited	-2.407	6.46E-08
	PIAS1	transcription regulator	Inhibited	-2.828	1.33E-10
	CREBBP	transcription regulator	Inhibited	-2	4.93E-08

Female	Upstream Regulator	Molecule Type	Predicted Activation State	Activation z-score	p-value

HIVgp120	ASCL1	transcription regulator	Inhibited	-2.213	0.000000621
	FEV	transcription regulator	Inhibited	-2.646	0.000000647
	MECP2	transcription regulator	Inhibited	-2.414	2.1E-09
	ZFPM1	transcription regulator	Inhibited	-2	6.33E-09
	CREBBP	transcription regulator	Inhibited	-2	4.49E-10
IFNβKO	HTT	transcription regulator	Activated	2.724	1.48E-30
	CREBBP	transcription regulator	Inhibited	-2.449	1.1E-14
IFNβKO X HIVgp120	HTT	transcription regulator	Activated	2.329	3.35E-34
	ESR1	ligand-dependent nuclear receptor	Activated	2.213	4.98E-08
	CREBBP	transcription regulator	Inhibited	-2.449	6.14E-15

Supplementary Table 2.7: Ingenuity Pathway analysis (IPA) generated predictions regarding potential upstream regulators in cortex and hippocampus of both males and females.
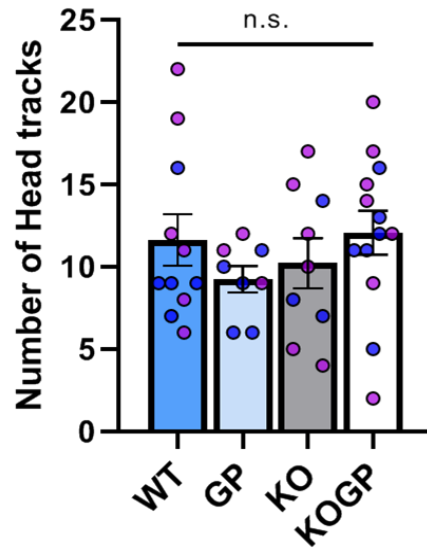
Supplementary Fig 2.1: Optomotor test for vision was performed on 9-10 month-old mice: WT (male:5; female:7), HIVgp120/GP (male:5; female:3), IFNβKO/KO (male:3; female:6 and IFNβKO-HIVgp120/KOGP (male:6; female:7). All data are represented as means ± SEM. Statistical analysis was performed as described in the methods section. n = 8-13 (males and females) per group/genotype; females [pink dots] and males [blue dots]; n.s., not significant.
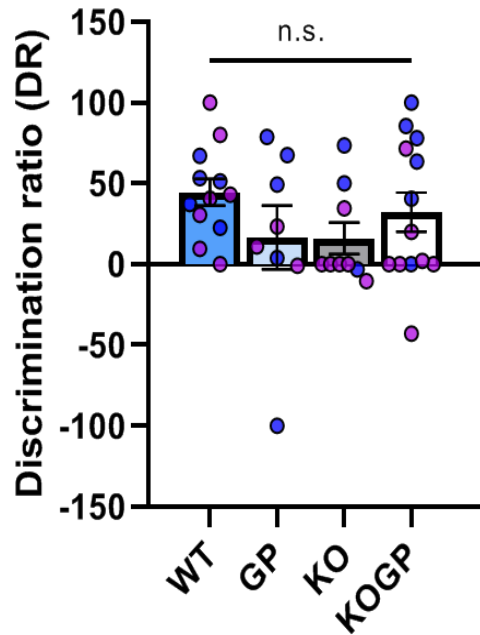
Supplementary Fig 2.2: Novel object recognition test as discrimination ratio (DR). Novel object recognition test was performed on 9-10 month-old mice: WT (male:5; female:7), HIVgp120/GP (male:5; female:3), IFNβKO/KO (male:3; female:6 and IFNβKO-HIVgp120/KOGP (male:6; female:7). All data are represented as means ± SEM. Statistical analysis was performed as described in the methods section. n = 8-13 (males and females) per group/genotype; females [pink dots] and males [blue dots]; n.s., not significant.

(A) Barnes maze latencies to escape   **(B) Barnes maze error**
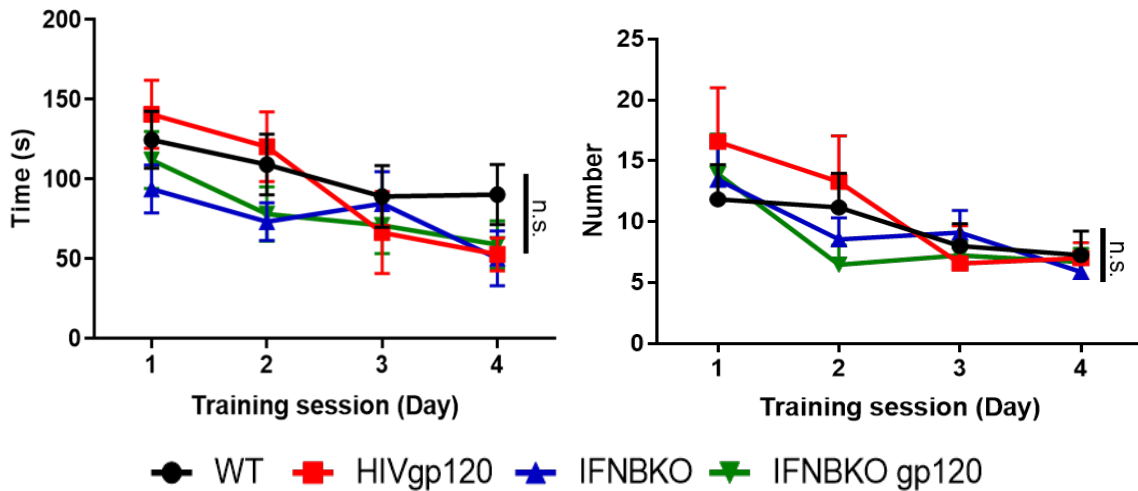
Supplementary Fig 2.3: Behavioral assessment of WT, HIVgp120, IFNβKO and IFNβKO-HIVgp120 mice. Barnes maze test: The latencies to enter the escape hole over 4 days of acquisition (A); and the number of errors made to enter the correct escape hole over 4 days of training session (B). Statistical analysis was performed as described in the methods section. Genotypes: WT (WT), HIVgp120 (GP), IFNβKO (KO) and IFNβKO-HIVgp120 (KOGP). Values are presented in line graphs (A, B). n = 8-13 animals (males and females) per group/genotype; n.s., not significant.

2.5. DISCUSSION

HIV-1 enters the CNS early in infection and continues to cause HAND, but the pathogenic mechanism of HAND and HIV-associated dementia (HAD), the most severe neurological complication of HIV/AIDS, remains incompletely understood with no specific treatment available (*6, 19*). Infection with HIV leads to the production of IFNs which can interfere with viral replication. IFNα and -β, constitute the type I IFNs and play a major role as the first line of host defense against HIV in the brain (*20*). We have shown previously that intranasal treatment with IFNβ prevents *in vitro* and *in vivo* neuronal damage triggered by HIVgp120, contingent on the presence of IFNAR1 and CCL4 (*6*). However, in the absence of neuroprotective levels of IFNβ, IFNAR1 (the receptor for type I IFNs) can contribute to HIVgp120 induced neuronal injury and neurocognitive and memory impairment, presumably by permitting signaling of IFNα (*7*). The present study shows that the baseline level of IFNβ is crucial to maintaining normal neuronal function, while the knockout of IFNβ in HIVgp120 mice partially diminishes in a sex-dependent fashion some aspects of neuronal injury. One possible explanation is that IFNβKO also prevents regulation of factors that can contribute to neuronal injury, such as IFNα (*12*).

Behavioral testing confirmed that 9-10 month-old HIVgp120 mice have impaired recognition memory while, in contrast to their 11-14 month-old counterparts (*7*), spatial memory is still functional if they express IFNβ. Our study also reveals that IFNβ deficiency itself can have a detrimental effect on these cognitive functions. Moreover, unlike our previous observation with 11-14 month-old HIVgp120tg mice, we did not find any sex-dependent differences in NOR and BM tests of the mice aged 9-10 months (*1, 7*). In this

study only WT mice had intact recognition memory. Novel object recognition involves hippocampus and perirhinal cortex (*28, 29*). Therefore, the behavioral phenotype fits with the damage to MAP2$^+$ neurites and SYP$^+$ presynaptic terminals in cortex and hippocampus of both sexes. In contrast, the compromised recognition memory in IFNβ deficient mice is not entirely reflected by neuronal and synaptic injury since a reduction of neurites was only observed in the cortex of female IFNβKO mice and a loss of SYP$^+$ presynaptic terminals was only observed in the cortex and hippocampus of male IFNβKO mice. Moreover, the changes in IFNβKO were not as pronounced as seen in the HIVgp120 and IFNβKO-HIVgp120tg mice. The role of IFNβ in maintaining normal neurites and presynaptic terminals warrants further examination.

The BM test of spatial memory is sensitive to impaired hippocampal function (*30*) and not significantly affected in the 9-10 month-old HIVgp120 and IFNβKO mice in contrast to the IFNβKO-HIVgp120 mice, suggesting that the combination of neurotoxic viral protein with lack of protective IFNβ worsens impairment of spatial learning. A possible explanation is the persistence of damage in hippocampal neuronal dendrites seen in HIVgp120 and IFNβKO-HIVgp120 mice while the ameliorated injury to SYP$^+$ presynaptic terminals associated by IFNβKO is not sufficient to protect the mice from impaired spatial learning. In fact, the IFNβ-expressing HIVgp120 mice perform comparably in the spatial memory task to their IFNβKO counterparts despite a more pronounced loss of SYP$^+$ presynaptic terminals. Thus, IFNβ may support spatial memory in a yet uncharacterized fashion even if synapses are compromised. Alternatively, SYP$^+$ presynaptic terminals may not be functionally normal in the absence of IFNβ, which could explain the differences in

the expression of multiple components of the here investigated four major neurotransmission systems.

In contrast to the behavioral assessments, the immunohistochemistry data shows pronounced sex- and brain region-dependent effects of IFNβ deficiency. The loss of presynaptic terminals in both cortex and hippocampus of males suggests that the baseline level of IFNβ is required to maintain neuronal homeostasis. On the other hand, no reduction of presynaptic terminals was observed in female cortex or hippocampus due to IFNβ deficiency. The diminished injury of SYP$^+$ presynaptic terminals was specific to the hippocampus of IFNβKO-HIVgp120 mice of both sexes. The decreasing trend in the expression level of HIVgp120 mRNA in the hippocampus of IFNβ-deficient males and females could explain, at least in part, the protection observed in the hippocampus. Our lab has previously observed that the effect of IFNAR1 on damage to SYP$^+$ presynaptic terminals varied by brain region and sex, and the hippocampus was more protected in females than males (*7*).

The other prominent pathological hallmarks of HIV brain pathology are astrocytosis and microgliosis (*1, 6*). IFNβ ablation does not prevent astrocytosis induced by HIVgp120 in male and female cortex and male hippocampus, as judged by GFAP expression. This finding is in line with our previously published work (*7*). However, a significant increase in GFAP expression was observed in the female hippocampus of IFNβKO-HIVgp120tg mice, which indicates that IFNβ limits astrocytosis in a sex-dependent mechanism which warrants further investigation. On the other hand, IFNβ ablation ameliorated the HIVgp120 induced microgliosis in both cortex and hippocampus of females but not males. The lower

101

numbers of microglial cells in female hippocampus could also explain the protection observed for presynaptic terminals in female hippocampus, which is in line with our previous observation in CCR5-deficient HIVgp120 mice (*9*). On the other hand, the reduced numbers of microglia in female cortex were not sufficient to provide protection of presynaptic terminals, suggesting the involvement of an additional IFNβ-dependent mechanism that counteracts synaptic injury in the presence of microglial activation.

Our previous study has shown a sex effect on expression of viral envelope protein gp120 in the brain with an increase in males of IFNAR1-deficient mice (*7*). Here we investigated the RNA expression of HIVgp120 in both the brain regions and in line with the earlier observation, only male IFNβKO-HIVgp120 mice showed higher expression of HIVgp120, and only in cortex, suggesting a sex specific effect of the IFNα/β-IFNAR1 axis that warrants further study. The transgenic expression of viral envelope gp120 is also known to upregulate several other components of the innate immune response, such as CCL2, -3, -4, -5, CXCL10 and LCN2. The β-chemokines CCL3, -4 and -5 are natural ligands of HIV co-receptor CCR5 that suppress HIV-1 infection (*17*). In addition, we have shown that CCL4 and CCL5 can protect neurons from HIVgp120 induced neuronal injury (*6, 22*). Interestingly, IFNβ ablation affected the RNA expression level of CCL4 only in female hippocampus and that of CCL5 in male hippocampus of HIVgp120 mice revealing a sex effect on the expression of these antiviral and neuroprotective chemokines. Also, CCL3 was upregulated only in IFNβKO-HIVgp120 female hippocampus. Overall, upregulation of β chemokines only in the hippocampus may contribute to the partial protection observed for presynaptic terminals. In contrast, IFNβ deficiency does not affect

the expression level of these β-chemokine in the cortex which in part can explain the lack of protection seen in the cortex. Strikingly the absence of IFNβ resulted in loss of presynaptic terminals in both brain regions in males and loss of MAP2$^+$ neurites only in female cortex, suggesting that a baseline amount of IFNβ is necessary to maintain neuronal homeostasis.

CCL2 is upregulated in HIVgp120 mice and while IFNβ ablation did not influence expression in male cortex, a significant downregulation occurred in the hippocampus of IFNβKO-HIVgp120 male mice. In the cortex and hippocampus of female, IFNβKO-HIVgp120 mice, there was a noticeable trend towards a reduction in expression of CCL2.. That finding may at least in part explain the lower microglial count observed in the female cortex and hippocampus. The protection of presynaptic terminals in the hippocampus but not in the cortex of IFNβKO-HIVgp120 animals is similar to our previous observations in IFNAR1KO mice, where we observed sexual dimorphism in CCL2 expression, suggesting that additional sex-dependent factors regulate CCL2 (*7*). CXCL10 has been implicated in HIV neuropathogenesis and our study indicated that the CXCL10 level remains unaffected by the absence of IFNβ, possibly contributing to the loss of MAP2$^+$ neurites in cortex and hippocampus (*31*). However, a significant, albeit slight, decrease in CXCL10 levels was observed in female hippocampus in IFNBKO-HIVgp120 compared to HIVgp120 mice, which however was not sufficient to protect against damage to MAP2$^+$ neurites.

We have recently shown that exogenous, transnasally administered IFNβ can increase the expression level of CXCL11 in HIVgp120 brain and knocking out IFNAR1 can completely abrogate the chemokine's expression in the hippocampus, implicating the type

103

I IFN response as a necessary component for regulation of CXCL11 (*6, 7*). Although knocking down IFNβ in HIVgp120 mice does not affect the expression level of CXCL11 in the male cortex or hippocampus of either sex, a noteworthy upregulation was observed in the female cortex of IFNβKO-HIVgp120 mice, suggesting an IFNβ-independent of type I IFN signaling. IFNα may continue to signal through the IFNAR1 receptor and could be an inducer of CXCL11 production. In the cortex, the absence of IFNβ inhibits the HIVgp120-triggered expression of MX1, DDX58, IRF7, and IRF9 at the RNA level, indicating it requires IFN signaling and IRF7 seems most dependent on IFNβ signaling. In contrast, the lack of IFNβ does not impact the mRNA level of IRF3, indicating that other factors can increase its expression in HIVgp120 mice in a sex-dependent manner. The RNA induction of MX1, RIG-I, IRF7 and IRF9, which is responsible for the anti-viral state induced by type I IFNs, and protein level of STAT1, which is responsible for JAK/STAT signaling to activate ISGs, all were abrogated in HIVgp120 mice lacking IFNβ. This suggests that the type I IFN response to the viral trigger but not the baseline expression is abolished in both brain structures following ablation of IFNβ (*6, 7, 25*). On the other hand, the pSTAT3 expression and STAT3 transcript either trends towards or is significantly upregulated in the cortex of IFNβKO-HIVgp120 compared to the HIVgp120 animals. STAT3 in the CNS is implicated in shunting neuronal progenitors away from differentiating into neurons and more preferentially into astrocytes, thus providing a possible explanation for astrocytosis (*32*). However, the absence of IFNβ did not result in any notable changes in protein levels of phospho-STAT3 and total STAT3 in the cortex. These findings do not exclude that IFNβ may play a role in regulating STAT3 expression

in the brain in the context of HIV infection but show that IFNβ is not required for increasing STAT3 levels. Further research is needed to fully elucidate the mechanisms governing STAT3 function in the brain in the presence and absence of HIV.

We recently showed a role for LCN2 in behavioral impairment, neuronal damage and microglia activation in HIVgp120 mice (*1*). Here, we observed an increase in the transcript level of LCN2 in cortex of IFNβKO-HIVgp120 mice and in female hippocampus, which provides a potential, additional explanation for neuronal injury associated with a more pronounced behavioral deterioration compared to the other genotypes.

Expression of genes related to neurotransmission is also affected by IFNβ-deficiency in a sex-dependent fashion in both cortex and hippocampus. HIVgp120 and IFNβKO with and without gp120 altered the different components of GABAergic, glutaminergic, dopaminergic, and serotonergic neurotransmission systems compared to WT controls. Notably, females displayed alteration of more pre- and post- synaptic components in comparison to males in both cortex and hippocampus suggesting a more pronounced effect of endogenous IFNβ in females. While sexual dimorphism in the components of neurotransmission systems is in line with our earlier studies (*1, 7*), it is the first time we observe more pronounced changes in females. Subjecting the gene expression data to IPA, we identified sex differences in top gene networks that are affected by HIVgp120 and IFNβ deficiency in cortex and hippocampus. Interestingly, CREB1 scored high enough to be included in the networks for cortex and hippocampus of males but not females. However, IPA predicted CREB binding protein (CREBP) as the major upstream regulator in cortex and hippocampus of both sexes, which is in line with our studies on the role of IFNAR1

105

suggesting the involvement of CREB1 in the IFN response (*7*). In a separate earlier study, we observed a network linking CREB1 and p38MAPK, and CREB1 is known to be regulated by p38MAPK and ERK1/2 (*1*). Here we show the sex-independent effect of MAPK signaling and the increase of phospho-p38 in cortex of HIVgp120tg brain corresponding with neuronal injury, while downregulation of p38 activity in the IFNβKO mice appears insufficient to provide neuronal protection. The persistent neuronal damage may be explained by the concomitant inhibition of phosphorylated and total ERK1/2 signaling in the cortex of IFNβ deficient mice with and without HIVgp120. We and others have shown previously that activation of ERK1/2 is one of the key signaling pathways contributing to neuronal protection (*7, 23*). In contrast, active and total p38 levels remain unchanged in the hippocampus of HIVgp120 and IFNβKO mice, a finding in line with our earlier study of the role of IFNAR1 (*7*). Thus, the diminished injury seen in the hippocampal pre-synaptic terminals of IFNβKO-HIVgp120 mice might result from increased ERK1/2 signaling. On the other hand, the downregulation of active ERK1/2 in the IFNβKO mice below the baseline level may explain the pre-synaptic terminal damage seen in male IFNβKO hippocampus. The dysregulation of MAPK singling pathways in neurocognitive disorders is widely recognized (*33*) and our data support the notion IFNβ affects the balance of all MAPK signaling that is vital to achieve neuroprotection.

A study conducted with macaques has demonstrated that IFNβ can inhibit the continued replication of SIV within macrophages, indicating that IFNβ may be able to regulate SIV replication within the CNS (*34*). Additionally, IFNβ was shown to prevent HIV-1 infection in primary cultures of human fetal microglia as well as production of chemokines CCL3,

106

CCL4, and CCL5 (*35*). Minagawa et al. (1989), reported high levels of human IFNβ in the sera of HIV-1 infected patient, especially asymptomatic carriers (*36*). Another study has shown increased IFNβ gene expression in the gut, but not in blood, in persons with HIV-1 infection compared to age/gender-matched uninfected controls (*37*). These reports suggest that the IFN response might differ in various parts of the body during chronic HIV-1 infection. Surprisingly, existing literature on IFNβ signaling in people living with HIV (PLWH) with HAND/HAD is very limited and more research is needed to clarify the specific impact of IFNβ signaling on neurocognition of PLWH.

On the other hand, the levels of IFN-α in the cerebrospinal fluid are higher in individuals with HAD compared to those without HAD (*38-40*). Recent research has shown that both type I and type II interferon response genes are activated in the brains of HIV patients without neurocognitive impairment, as well as in HIV patients with HIV encephalitis (HIVE), particularly in white matter, frontal cortex, and basal ganglia (*41, 42*). The earlier study reported that genes related to the IFN response, such as CD163 (cluster of differentiation 163), PSMB8 (proteosome subunit beta type 8), GBP1 (guanylate binding protein 1) and BTN3A3 (butyrophilin subfamily 3 member A3) were significantly upregulated in the white matter, frontal cortex and basal ganglia of HIV infected individual with neurocognitive impairment with HIVE compared to those without neurocognitive impairment (*41*). The latter study found that HIV patients with neurocognitive impairment but without HIVE did not show activation of IFNs, but they did have increased expression of chemokines, cytokines and β-defensins in the white matter (*42*). These findings indicate

107

complex interaction between IFN response, neurocognitive impairment and HIV infection which warrants further research.

The present study has a limitation since we employed a transgenic HIVgp120 mouse model, which is known to closely recapitulate hallmarks of early HIV infection in brain and development of encephalitis. While this model provides valuable insights into the neurological effects of HIV during the initial stages, the findings observed in this system may not fully represent the experience of PLWH who have mild HAND and are on effective ART. The majority of PLWH access cART and experience milder forms of HAND. Future research in human cohorts in combination with additional new models are warranted to expand on the potential translational implications of our findings.

5. Conclusions

In summary, our findings show that endogenous IFNβ is important for normal memory dependent behavioral performance and modulates neuropathology in HIVgp120tg brains, indicating that its absence facilitates neurocognitive impairment and development of neuropathology. Moreover, in the absence of HIV, endogenous IFNβ appears to play a vital role in maintaining neuronal homeostasis and memory function.

Ethics approval and consent to participate

Not applicable.

Availability of data or materials

The data generated during this study are available from the corresponding author upon reasonable request. The new mouse line will be shared through material transfer agreements (MTA).

Competing Interest

The authors declare no competing interest.

Abbreviations

Actb: Actin Beta; ANOVA: Analysis of variance; BM: Barnes maze test; BSA: Bovine serum albumin; BCA: Bicinchoninic acid; BTN3A3: Butyrophilin subfamily 3 member A3; CNS: Central nervous system; CREB1: cAMP responsive element binding protein 1; CD163: cluster of differentiation 163; DS: Dopamine serotonin; Gapdh: Glyceraldehyde-3-Phosphate Dehydrogenase; Gusb: Glucuronidase Beta; GFAP:Glial fibrillary acidic protein; GG: GABA Glutamate; GBP1: Guanylate binding protein 1; Hsp90ab1: Heat Shock Protein 90 Alpha Family Class B Member 1; HIVgp120tg: HIVgp120 transgenic mouse; HIV: Human immunodeficiency virus; HAND: HIV-associated neurocognitive disorder; IFN: Interferon; IFNβ: Interferon beta; IPA: Ingenuity Pathway Analysis;ISGs: Interferons stimulated genes; IFNβKO: IFNβ gene knockout; IFNAR: Interferon type 1 (IFN-α/β) receptor; Iba1: Ionized calcium-binding adaptor molecule 1; JNK: cJun N-terminal kinase; JAK-STAT:Janus kinase-signal transducer and activator of transcription; LCN2: Lipocalin; LDT: Light/dark transfer; LMA: Locomotor activity; MAPK: Mitogen-activated protein kinases; MAP-2: Microtubule-associated protein 2; NOR: Novel object recognition; OM: Optomotor; PSMB8: Proteosome subunit beta type 8; PLWH: People living with HIV; Syp: Synaptophysin; SIV: Simian immunodeficiency virus; STAT1: Signal transducer and activator of transcription 1; TSRI: The Scripps Research Institute's; WHO: World health organization; WT: Wild type

REFERENCES FOR CHAPTER TWO

1. D. Ojeda-Juarez *et al.*, Lipocalin-2 mediates HIV-1 induced neuronal injury and behavioral deficits by overriding CCR5-dependent protection. *Brain Behav Immun* **89**, 184-199 (2020).

2. D. Saylor *et al.*, HIV-associated neurocognitive disorder--pathogenesis and prospects for treatment. *Nat Rev Neurol* **12**, 234-248 (2016).

3. J. E. Bell, An update on the neuropathology of HIV in the HAART era. *Histopathology* **45**, 549-559 (2004).

4. M. Kaul, J. Zheng, S. Okamoto, H. E. Gendelman, S. A. Lipton, HIV-1 infection and AIDS: consequences for the central nervous system. *Cell Death Differ* **12 Suppl 1**, 878-892 (2005).

5. W. Ru, S. J. Tang, HIV-associated synaptic degeneration. *Molecular brain* **10**, 40 (2017).

6. V. E. Thaney *et al.*, IFNbeta Protects Neurons from Damage in a Murine Model of HIV-1 Associated Brain Injury. *Sci Rep* **7**, 46514 (2017).

7. H. Singh *et al.*, A pivotal role for Interferon-α receptor-1 in neuronal injury induced by HIV-1. *Journal of Neuroinflammation* **17**, 226 (2020).

8. S. M. Toggas *et al.*, Central nervous system damage produced by expression of the HIV-1 coat protein gp120 in transgenic mice. *Nature* **367**, 188-193 (1994).

9. R. Maung *et al.*, CCR5 knockout prevents neuronal injury and behavioral impairment induced in a transgenic mouse model by a CXCR4-using HIV-1 glycoprotein 120. *J Immunol* **193**, 1895-1910 (2014).

10. E. C. Borden *et al.*, Interferons at age 50: past, current and future impact on biomedicine. *Nat Rev Drug Discov* **6**, 975-990 (2007).

11. L. Alammar, L. Gama, J. E. Clements, Simian Immunodeficiency Virus Infection in the Brain and Lung Leads to Differential Type I IFN Signaling during Acute Infection. *The Journal of Immunology* **186**, 4008-4018 (2011).

12. L. Erlandsson *et al.*, Interferon-beta is required for interferon-alpha production in mouse fibroblasts. *Curr Biol* **8**, 223-226 (1998).

13. M. M. Hoefer *et al.*, Combination of methamphetamine and HIV-1 gp120 causes distinct long-term alterations of behavior, gene expression, and injury in the central nervous system. *Exp Neurol* **263**, 221-234 (2015).

14. K. J. Livak, T. D. Schmittgen, Analysis of Relative Gene Expression Data Using Real-Time Quantitative PCR and the 2−ΔΔCT Method. *Methods* **25**, 402-408 (2001).

15. K. E. Medders, N. E. Sejbuk, R. Maung, M. K. Desai, M. Kaul, Activation of p38 MAPK is required in monocytic and neuronal cells for HIV glycoprotein 120-induced neurotoxicity. *J Immunol* **185**, 4883-4895 (2010).

16. S. Lee, D. K. Lee, What is the proper way to apply the multiple comparison test? *Korean J Anesthesiol* **71**, 353-360 (2018).

17. F. Cocchi *et al.*, Identification of RANTES, MIP-1 alpha, and MIP-1 beta as the major HIV-suppressive factors produced by CD8+ T cells. *Science* **270**, 1811-1815 (1995).

18. R. K. Berg *et al.*, Genomic HIV RNA induces innate immune responses through RIG-I-dependent sensing of secondary-structured RNA. *PLoS One* **7**, e29291 (2012).

19. H. Singh, J. Koury, M. Kaul, Innate Immune Sensing of Viruses and Its Consequences for the Central Nervous System. *Viruses* **13**, (2021).

20. V. E. Thaney, M. Kaul, Type I Interferons in NeuroHIV. *Viral Immunol* **32**, 7-14 (2019).

21. Y. Koga *et al.*, Roles of Cyclic AMP Response Element Binding Activation in the ERK1/2 and p38 MAPK Signalling Pathway in Central Nervous System, Cardiovascular System, Osteoclast Differentiation and Mucin and Cytokine Production. *Int J Mol Sci* **20**, (2019).

22. M. Kaul, S. A. Lipton, Chemokines and activated macrophages in HIV gp120-induced neuronal apoptosis. *Proc Natl Acad Sci U S A* **96**, 8212-8216 (1999).

23. I. Mocchetti, A. Bachis, Brain-derived neurotrophic factor activation of TrkB protects neurons from HIV-1/gp120-induced cell death. *Crit Rev Neurobiol* **16**, 51-57 (2004).

24. J. W. Schoggins *et al.*, A diverse range of gene products are effectors of the type I interferon antiviral response. *Nature* **472**, 481-485 (2011).

25. T. Doyle, C. Goujon, M. H. Malim, HIV-1 and interferons: who's interfering with whom? *Nat Rev Microbiol* **13**, 403-413 (2015).

26. B. Yang, S. Akhter, A. Chaudhuri, G. D. Kanmogne, HIV-1 gp120 induces cytokine expression, leukocyte adhesion, and transmigration across the blood-brain barrier: modulatory effects of STAT1 signaling. *Microvasc Res* **77**, 212-219 (2009).

27. S. Dziennis, N. J. Alkayed, Role of signal transducer and activator of transcription 3 in neuronal survival and regeneration. *Rev Neurosci* **19**, 341-361 (2008).

28. D. G. Mumby, A. Tremblay, V. Lecluse, H. Lehmann, Hippocampal damage and anterograde object-recognition in rats after long retention intervals. *Hippocampus* **15**, 1050-1056 (2005).

29. B. D. Winters, S. E. Forwood, R. A. Cowell, L. M. Saksida, T. J. Bussey, Double dissociation between the effects of peri-postrhinal cortex and hippocampal lesions on tests of object recognition and spatial memory: heterogeneity of function within the temporal lobe. *J Neurosci* **24**, 5901-5908 (2004).

30. R. Paylor, Y. Zhao, M. Libbey, H. Westphal, J. N. Crawley, Learning impairments and motor dysfunctions in adult Lhx5-deficient mice displaying hippocampal disorganization. *Physiol Behav* **73**, 781-792 (2001).

31. V. J. Sanders *et al.*, Chemokines and receptors in HIV encephalitis. *AIDS* **12**, 1021-1026 (1998).

32. T. Li *et al.*, Targeted inhibition of STAT3 in neural stem cells promotes neuronal differentiation and functional recovery in rats with spinal cord injury. *Exp Ther Med* **22**, 711 (2021).

33. E. K. Kim, E. J. Choi, Pathological roles of MAPK signaling pathways in human diseases. *Biochim Biophys Acta* **1802**, 396-405 (2010).

34. S. A. Barber, D. S. Herbst, B. T. Bullock, L. Gama, J. E. Clements, Innate immune responses and control of acute simian immunodeficiency virus replication in the central nervous system. *J Neurovirol* **10 Suppl 1**, 15-20 (2004).

35. R. Kitai, M. L. Zhao, N. Zhang, L. L. Hua, S. C. Lee, Role of MIP-1beta and RANTES in HIV-1 infection of microglia: inhibition of infection and induction by IFNbeta. *J Neuroimmunol* **110**, 230-239 (2000).

36. T. Minagawa *et al.*, Detection of high levels of immunoreactive human beta-1 interferon in sera from HIV-infected patients. *Life Sci* **45**, iii-vii (1989).

37.	G. Le Dreau *et al.*, [Diagnosis of mediastinal neuro-endocrine tumor using endosonography guided transesophageal puncture biopsy]. *Gastroenterol Clin Biol* **22**, 87-90 (1998).

38.	A. Krivine *et al.*, Measuring HIV-1 RNA and interferon-alpha in the cerebrospinal fluid of AIDS patients: insights into the pathogenesis of AIDS Dementia Complex. *J Neurovirol* **5**, 500-506 (1999).

39.	O. Perrella *et al.*, Transforming growth factor beta-1 and interferon-alpha in the AIDS dementia complex (ADC): possible relationship with cerebral viral load? *Eur Cytokine Netw* **12**, 51-55 (2001).

40.	M. B. Rho *et al.*, A potential role for interferon-alpha in the pathogenesis of HIV-associated dementia. *Brain Behav Immun* **9**, 366-377 (1995).

41.	B. B. Gelman *et al.*, The National NeuroAIDS Tissue Consortium brain gene array: two types of HIV-associated neurocognitive impairment. *PLoS One* **7**, e46178 (2012).

42.	P. P. Sanna, V. Repunte-Canonigo, E. Masliah, C. Lefebvre, Gene expression patterns associated with neurological disease in human HIV infection. *PLoS One* **12**, e0175316 (2017).

CHAPTER THREE:

EphB2-mediated ephrin-B reverse signaling on microglia drives an inflammatory, but antiviral response in HIV

Jeffrey Koury[1], Hina Singh[1,2], Samantha Sutley-Koury[1], Dominic Fok[1], Xinru Qiu[3], Ricky Maung[1,2], Benjamin B. Gelman[4,5], Iryna Ethell[1], Marcus Kaul[1,2]*

[1]Division of Biomedical Sciences, School of Medicine, University of California, Riverside, 900 University Ave, Riverside, CA, 92521, USA

[2]Infectious and Inflammatory Disease Center, Sanford Burnham Prebys Medical Discovery Institute, 10901 North Torrey Pines Road, La Jolla, CA, 92037, USA

[3]Division of Genetics, Genomics and Bioinformatics, University of California, Riverside, 900 University Ave, Riverside, CA, 92521, USA

[4]Department of Pathology, University of Texas Medical Branch, 301 University Blvd, 77555-0419 Galveston, TX USA

[5]Department of Neuroscience and Cell Biology, University of Texas Medical Branch, 301 University Blvd, 77555-0419 Galveston, TX USA

***Corresponding author**: Marcus Kaul, Division of Biomedical Sciences, School of Medicine, University of California, Riverside, 900 University Ave, Riverside, CA, 92521, USA. Tel: (951) 827-7774. E-mail: marcus.kaul@medsch.ucr.edu

A version of this chapter will be submitted for publication (manuscript in preparation).

3.1. ABSTRACT

HIV Associated Neurocognitive Disorder (HAND) is a condition of cognitive and neurological impairments associated with pathological inflammation and a loss of synaptic integrity and function. Although therapeutics exist to increase the lifespan of people living with HIV (PLWH), they are not effective at preventing HIV induced neuronal damage and the prevalence of HAND remains unchanged. In this study, we highlight the increase in expression of ephrin-B/EphB in *post-mortem* brain of PLWH, correlating with proviral DNA, viral RNA and inversely with abstract executive function and verbal fluency. Increased expression of ephrin-B/EphB is also observed in brains of a transgenic mouse model of neuroHIV suggesting the upregulation can be driven, at least in part, by viral gp120 envelope protein and type I interferon, IFNβ. Additionally, we show induction of ephrin-B1 expression in microglia following type I interferon activation. Given the previously reported impact of EphB2 on inflammation in the periphery, the functional role of EphB2-mediated ephrin-B reverse signaling on microglia was assessed for a pro-inflammatory and antiviral signature. We found that EphB2 treated microglia secreted inflammatory factors and induced contact-independent neurotoxicity. Finally, knockdown of microglial ephrin-B1, an EphB2 binding partner, shows a partial alleviation of the microglial pro-inflammatory signature and neurotoxicity. Altogether our study suggests that elevated EphB2, and its reverse signaling through ephrin-B1 in microglia contribute to neuroinflammation and neurotoxicity in neuroHIV.

3.2. INTRODUCTION

HIV-associated neurocognitive disorder (HAND) is a condition characterized by cognitive and neurological impairments that occur from HIV infection and is found in up to 55% of people living with HIV (PLWH) (*1*). Symptoms range from mild cognitive deficits to severe dementia, manifesting in various ways, including deficits with memory, attention, concentration, language, decision-making, depression and motor skills (*2*). The exact mechanisms behind HAND or HIV induced neuronal injury are not fully understood, but several factors contribute to its development, namely chronic inflammation, release of viral proteins and glutamate excitotoxicity (*3*). Additionally, it is widely accepted that macrophages and microglia are key mediators of HIV induced inflammation and neurotoxicity. Notably, one pathological characteristic of neuroHIV is the presence of multinucleated microglial cells (*4*). Furthermore, depletion of microglia alone is sufficient to abrogate HIVgp120 induced neurotoxicity in a HIV mouse model and primary cortical cultures (*5*). Additionally, leveraging a transgenic mouse model expressing HIV protein gp120 (HIVgp120tg) (*6*), in combination with analysis of human tissues, previous studies have implicated the innate immune system, specifically the type I interferon response, in neuroHIV (*7*). Here we propose a novel mechanism driving the neuroinflammation, but also the antiviral response, observed in neuroHIV mediated by innate immune activation of ephrin-B/EphB.

Ephrins and Eph receptors belong to a family of receptor tyrosine kinases that play crucial roles in various physiological processes, including embryonic development, neural connectivity and, although less recognized, inflammation (*8*). Both ephrins and Eph

117

receptors are membrane-bound proteins, which interact in a cell-cell contact dependent manner and have a unique ability to signal bidirectionally (7). As it pertains to inflammation in the CNS, EphB2 deletion in a mouse stroke model was reported to decrease proinflammatory CCL2 and IL-6 in the ischemic zone, while EphB2 binding to astrocytic ephrin-Bs activated NF-kB signaling, suggesting a chronic inflammatory role for EphB2 (*9*). The role of astrocytic ephrin-B1 was also reported in a mouse model of traumatic brain injury (TBI), showing suppression of TBI-induced STAT3 phosphorylation by astrocyte-specific ablation of ephrin-B1 and upregulation of STAT3 induced by the activation of ephrin-B1 in astrocytes (*10*). However, the functional role of EphB/ephrin-B signaling in microglia has not been explored, which is of particular importance in the context of neuroinflammation and neurodegenerative disease as microglia are the key inflammatory mediators in the CNS.

In this study, we highlight the elevated expression of EphB2 in both the CNS of PLWH and in HIVgp120tg mice and report an up-regulation of ephrin-B1, specifically on microglia, in the hippocampus and cortex of HIVgp120tg animals. Our data support the pro-inflammatory impact of EphB2 reverse signaling and the role of microglial specific ephrin-B1 in mediating an inflammatory response. Finally, we show that EphB2 mediated ephrin-B activation in microglia triggers the release of neurotoxins affecting neuronal survival in iPSC derived neuronal/astrocytic co-cultures. Our study suggest that the elevated EphB2 levels in the CNS of PLWH contribute to the chronic inflammation, driving the neuropathology associated with HAND, and that therapeutics targeting EphB2-mediated ephrin-B signaling in microglia may minimize these deleterious effects (*11*).

3.3. MATERIALS AND METHODS

qRT-PCR of human samples

RNA from the middle frontal gyrus (neocortex) of HIV$^+$ patients and non-infected controls were isolated and prepared by Dr. Benjamin Gelman's laboratory (UTMB Galveston, TX) as a component of the National NeuroAIDS Tissue Consortium (NNTC). Investigators were blinded to HIV pathology status of the patients. All samples were coded, and qRT-PCR was performed as previously described (*12-14*). Briefly, 500ng of RNA from the middle frontal gyrus was reverse transcribed using SuperScript II reverse transcriptase (Invitrogen, USA) following the manufacturer's instructions. QRT-PCR was performed using Power PCR SYBR Green master mix (Cat#: 4367659, Applied Biosystems) on the QuantStudio 6 Flex System (Applied Biosystems). The results obtained were analyzed using the $2^{-\Delta\Delta Ct}$ method and normalized to β-actin.

Mouse models

HIVgp120tg mice were kindly provided by Dr. Lennart Mucke (Gladstone Institute of Neurological Disease, University of California, San Francisco, CA). Wild-Type, HIVgp120tg animals and IFNβ treated animals for immunohistochemistry were all 3-4 months old and male. Recombinant mouse IFNβ intranasal treatment was performed once a week over a 4 week time period as reported in a previous study (*14*). IFNβ global knockout animals were kindly provided by Dr. Tomas Leanderson (Lund University, Lund, SE) and were 9-12 months old when both males and females were analyzed.

Immunohistochemistry of HIVgp120tg and IFNβ treated animals

Immunohistochemistry was performed according to previously published protocols from our lab (*14-17*). Briefly, 3–4-month-old WT, HIVgp120tg or IFNβ treated animals were anesthetized and brains were quickly removed and fixed for 72 h at 4 °C in 4% paraformaldehyde. Brains were sectioned using a vibratome to generate 40-μm-thick sagittal brain sections. Sections were subsequently stained with ephrin-B1 (R&D Systems, AF473), Iba1 (Wako, Cat#019-19741,1:1000) and GFAP (Cell Signaling Technology, Cat#3670, 1:1000). Immunolabeled sections were mounted on glass slides with vectashield and overlaid with coverslips. Slides for analysis were imaged using a Zeiss LSM 880 confocal microscope. Image analysis was accomplished using imageJ by taking total mean intensity of ephrin-B1 in the CA1 of the hippocampus or generating regions of interest around microglia and assessing mean intensity of ephrin-B1 of hippocampal microglia.

Culturing and treatment of HMC3

HMC3 were purchased from ATCC (Cat#CRL-3304) and cultured in EMEM, 10% FBS and 1% Pen/Strep. HMC3 cells were cultured in a 12 well (RNA) or 6 well (protein). Cells were treated with lipofectamine RNAiMAX + ephrin-B1 siRNA (Life Technologies, ephrin-B1 silencer select Cat#4392420) or negative control siRNA (12 well- 12.5pmol, 6 well- 25pmol) for 48 hours, followed by pre-clustered EphB2-Fc (R&D, Cat# 5189-B2-050, 2ug/ml) for either 24 hours (RNA or secretome) or 15 minutes (protein lysate) before lysing the cells. Pre-clustering is done for 1 hour on ice by combining equal amounts of EphB2-Fc (R&D, Cat# 5189-B2-050) or Ctrl-Fc (R&D, Cat#110-HG) and Goat anti Human IgG (JacksonImmuno, Cat #109-005-003), and mixing every 15 minutes. For

western blot studies, cells are switched to serum free media 1 hour before treatment with pre-clustered EphB2-Fc. Following EphB2 treatment for the appropriate time, supernatants were collected and stored at -80C for future experiments. For RNA studies, lysis was done on ice for 15 minutes with RLT buffer (Qiagen) + 1% B-ME. For protein studies, lysis was performed using RIPA Buffer with protease and phosphatase inhibitors. Treatment of HMC3 with IFNβ used human recombinant interferon beta 1a (3,000 U/ml) (PBL Assay Science, Cat#11415-1) or 0.001% BSA (vehicle control) for 24 hours, and for IRF7 knockdown studies cells were treated for 48 hours prior to IFNβ treatment with RNAiMAX + IRF7 siRNA (life technologies, silencer select Cat#5194563, 12.5 pmol) or negative control siRNA.

Isolation of mRNA and RT-PCR from mouse tissue and human in vitro cells

RNA of murine cerebral cortex was isolated using the Qiagen RNeasy Lipid Tissue Midi Kit (Qiagen) and hippocampal RNA and HMC3 RNA were isolated using Qiagen Mini Kit (Qiagen) according to the manufacturer's instructions. qRT-PCR was performed as described above for human samples and previously reported (*12, 14*). The results obtained were analyzed using the $2^{-\Delta\Delta Ct}$ method and relative amounts of mRNA of every gene were calculated by normalizing to internal control GAPDH.

Immunoblotting

Western blotting using protein lysates from HMC3 treated cells was conducted as previously published (*18*). Briefly, 16 µg of protein was added to 4X LDS sample buffer and 10X reducing agent (Invitrogen) and boiled for 5 min. Samples were loaded and run in a 15 well 4-12% SDS-PAGE gel (Invitrogen) for electrophoretic separation. Following

transfer to PVDF membrane, membranes were blocked with 5% bovine serum albumin (BSA) solution and subsequently incubated overnight at 4˚C with primary antibodies as follows: rabbit phosphorylated NF-kB (1:1000; Cell Signaling Technology, Cat#3031S); rabbit total NF-kB (1:1000; Cell Signaling Technology, Cat#8242S); and GAPDH (1:20,000; Ambion, Cat#4300). Membranes were then incubated with secondary antibody in 5% BSA: goat anti-rabbit (1:2000; CST, Cat#7074) and goat anti-mouse (1:25,000; Pierce, Cat#1858413) secondary antibodies conjugated with horseradish-peroxidase. SuperSignal Dura chemiluminescent detection kit (Pierce) was used to visualize bound antibodies. Membranes were imaged using the ChemiDoc™ XRS+ imager. Densitometry analysis was performed using ImageJ 1.53a software (http://rsb.info.nih.gov/nih-image/).

Bulk RNA Sequencing

RNA collected from *in vitro* studies (HMC3) were first bioanalyzed using the Agilent 2100 Biosystem or Tapestation in the UC Riverside Genomics Core. Samples with RIN > 9.0 were used for downstream bulk RNA sequencing at the UC San Diego (UCSD) genomics core. RNA sequencing was performed on the Illumina NovaSeq 6000, using an rRNA depletion, Paired End (PE100) and 25M reads per sample. FASTQ files were then processed through the reference cDNA sequences for the human genome (GRCh38), which were downloaded from the Ensembl database (Release 109). Following the retrieval of this file, we utilized the Kallisto [PMID: 27043002] software to generate an index that facilitates rapid transcript quantification. This index was created by employing Kallisto's index function on the downloaded cDNA FASTA file. For quantification, we executed the kallisto quant command. The output includes estimates of transcript abundances, making

it amenable to downstream analyses including differential gene expression studies. Read counts/TPM were converted into log2Fc using the DESeq2 script including a pre-filtering step of reads < 10 (*19*). Annotation was done on Galaxy using the Human Genome ChR38.109 reference. Visualization of the differentially expressed genes was done using a multitude of tools/scripts including enhancedvolcano script and Ingenuity Pathway Analysis (IPA) for pathway and networks analysis. P value cutoff and log2FC cutoff was set to 0.05 and 0.4, respectively. ShinyGO 0.77 was used for GO Enrichment of biological processes, using the top 300 differentially upregulated genes with an FDR < 0.05 cutoff.

LegendPlex

Supernatants from vehicle, EphB2-Fc, ephrin-B1 siRNA and ephrin-B1 siRNA + EphB2-Fc treated microglia collected following 24-hour treatment were used for multiplex analysis, without dilution. Three different LegendPlex panels were used, according to manufacturer's protocol, to get a comprehensive inflammatory and anti-viral profile including LegendPlex Human Vascular Inflammation Panel 1 (13-plex) (BioLegend, Cat#740551), LegendPlex Human Proinflammatory Chemokine Panel 1 (13-plex) (BioLegend, Cat#740984) and Human Anti-Virus Response Panel (13-plex) (BioLegend, Cat#740349). LegendPlex beads were read on a Novocyte Quanteon flow cytometer and subsequently analyzed using BioLegend LegendPlex Data Analysis Software Suite to generate Mean Fluorescence Intensities (MFI) and calculate concentrations. 5 parameter logistic regression (5PL) was performed for each analyte assessed, and concentrations (pg/mL) were generated using these standard curves.

Neurotoxicity Assay and Analysis

iCell Glutamatergic Neurons (iGluta, Fujifilm CDI, Cat#1060) and iCell Astrocytes (iAstro, Fujifilm, CDI, Cat#1037) were co-cultured at a ratio of 6:1 in black walled clear bottom 96 well plates for imaging (Corning, Cat#353219) previously coated in 0.1% PEI and geltrex. The 96 well were coated with PEI for 1 hour at 37°C, then washed and dried overnight, followed by 1 hour at 37°C of geltrex (Life Technologies, Cat#A1569601). After 7 days of culture, with 50% media changes occurring every 2-3 days, cell-free condition media from microglia treated cells, or aggregated EphB2 only control, were transferred to the co-culture for 24 hours before 4% PFA fixation for 25 minutes at 4°C. Cells were permeabilized with 0.2% triton X-100, blocked with 10% goat serum and stained with Hoechst Dye (1:150), mouse MAP-2 (Sigma, Cat#M4403, 1:500) and rabbit NeuN (Millipore/Sigma, Cat#ABN78, 1:500). Secondary Antibodies: goat anti-rabbit AF488 (Invitrogen, Cat#A11034, 1:200) and goat anti-mouse rhodamine red (JacksonImmunoResearch, Cat#115-295-146, 1:200). Cells were imaged in a 96 well black walled plate with a 40X objective and counted for MAP-2/NeuN double positive cells. The average of the number of MAP-2/NeuN positive cells in the vehicle treatment was defined as 100% neuronal survival.

Statistical analysis

Analysis of histopathological data, mRNA expression, Western blotting data, and correlation analysis were performed using Prism 9 software (GraphPad Software, Inc., CA, USA), Comparisons of multiple groups employed either One-Way or Two-Way analysis of variance (ANOVA) followed by Tukey's post hoc test. Comparison of two groups used

student's t-test. *P*-values < 0.05 were considered statistically significant. For human samples, Pearson correlations were calculated to determine significance of correlation.

3.4. RESULTS

EphB2 is differentially expressed in PLWH with brain pathology and its levels correlate with poorer cognitive performance.

Given that neuroinflammation is a hallmark characteristic of neuroHIV, and previous studies in other diseases implicate EphB2 in inflammation in other diseases (*20, 21*), we first investigated, if EphB2 is elevated in the CNS of PLWH by analyzing mRNA expression in neocortex (middle frontal gyrus) of non-infected controls (N = 46), PLWH (N = 63), PLWH without brain pathology (N = 44) and PLWH with brain pathology (N = 19). The analysis of EphB2 mRNA expression shows that its levels are preferentially elevated in PLWH with brain pathology (p < 0.0001) compared to controls and PLWH without brain pathology (**Fig 3.1A**). In this context, Brain Pathology is defined by the presence of multinucleated giant cells or microglial nodules, highlighting microglia as a potential key target and/or cellular source for EphB2. In PLWH, EphB2 mRNA levels positively correlate with log HIV DNA (r = 0.297, p = 0.017) and log HIV RNA (r = 0.384, p = 0.002) viral load. Additionally, levels of EphB2 mRNA inversely correlated with neurocognitive tests including abstract executive domain T score (r = -0.44, p = 0.001) and verbal fluency domain T score (r = -.334, p = 0.015) (**Fig 3.1B-E**). These findings support a possible role for EphB2/ephrin-B signaling in driving brain pathology, increased HIV viral load, and poorer cognitive scores in PLWH. As brain pathology is defined by a

pathological presentation of microglial nodules or multinucleated giant cells, we hypothesized that EphB2 may be acting specifically on microglial cells.

HIVgp120 and IFNβ regulate ephrin-B/EphB in the cortex and hippocampus, potentially through IRFs in microglia.

EphB2 and ephrins signal bidirectionally and therefore we utilized HIVgp120tg mice to assess the cell specific expression of the binding partner of EphB2, ephrin-B1, that can act as both ligand and receptor. In addition, we investigated mechanisms that could be regulating ephrin-B/EphB expression in the CNS. To investigate whether HIV viral proteins or a type I interferon response can regulate ephrin-B/EphB expression, we assessed the mean intensity of ephrin-B1 immunoreactivity in the CA1 hippocampus, specifically in Iba1$^+$ microglia, in 3–4-month-old mice, constitutively expressing the HIV envelope protein gp120 or treated intranasally with recombinant IFNβ (a type I interferon). HIVgp120tg animals show a prominent type I interferon response, including activation of interferon regulator factors (IRFs) and antiviral interferon stimulated genes (ISGs). Transgenic HIVgp120s elicit a type I interferon response, and so both HIVgp120tg mice and IFNβ treated non-tg mice were assessed to determine the role of the type I interferon response in the regulation of ephrin-B1/EphB levels. Indeed, both the HIVgp120 transgene and IFNβ treatment alone increased the expression of ephrin-B1 in the CA1 of the hippocampus, suggesting that viral envelope protein gp120, and specifically the antiviral response, may promote ephrin-B1 expression (**Fig 3.2B**). Inversely, ablation of IFNβ resulted in a significant decrease in both ephrin-B1 and EphB2 transcript levels in the

hippocampus (**Fig 3.2D**). Consistent with our proposed hypothesis that EphB/ephrin-B signaling in microglia drives HIV brain pathology, microglial-specific ephrin-B1 immunoreactivity was positively regulated by both HIVgp120 and IFNβ (**Fig 3.2A, 3.2C**). Similar effects were also observed in human cells as the treatment of HMC3 human microglia *in vitro* with recombinant human IFNβ (3,000 U/ml) induced elevated transcript levels of both ephrin-B1 ($p<0.001$) and EphB2 ($p<0.05$) approximately 1.5-fold compared to vehicle control (**Fig 3.2E**).

As IFNβ is well known to propagate a type I interferon response, we observed an increase in expression of IRF7 mRNA transcript levels in the PLWH with brain pathology compared to uninfected controls, similar to the increase in EphB2 mRNA expression in the same group (**Fig 3.3A**, $P < 0.001$ PLWH with brain pathology vs uninfected). Correlations in the neocortex of PLWH also revealed a very robust positive correlation between ephrin-B1 (**Fig 3.3B**, $r= 0.58$, $p= 4\times10^{-6}$), EphB2 (**Fig 3.3C**, $r= 0.554$, $p= 8\times10^{-6}$) and the type I interferon master regulator, IRF7, suggesting a strong association between ephrin-B/EphB and type I interferon. IRF7 transcript levels are also prominently induced in the cortex and hippocampus of the HIVgp120tg animals, and this upregulation is dependent on the activation of type I interferon IFNβ signaling (**Fig 3.3D**). With the discovery that IFNβ induced ephrin-B/EphB expression, and the strong correlation between the levels of ephrin-B1/EphB2 and type I master regulator IRF7, we wanted to determine next if IRF7 was a key mediator in this IFNβ induced activation of ephrin-B/EphB. HMC3 human microglia were transfected with IRF7 siRNA (12.5 pmol) using RNAiMAX transfection reagent 48 h prior to treatment with IFNβ (3,000 U/mL) for 24 h. To our surprise, knocking down

IRF7 in microglia (**Fig 3.3E**) did not reduce expression of EphB2, but rather increase its expression, as well as other type I interferon genes including IFIT1 and endogenous IFNβ itself, suggesting that IRF7 exerts negative feedback on IFNβ expression (**Fig 3.3F-H**). Although IRF7 does not seem to be mediating the IFNβ induced activation of EphB2, the ablation of IRF7 alone does induce activation of NF-kB transcripts which in turn may be contributing to the IFNβ induced activation of EphB2 **(Supplementary Fig 3.3).** This is plausible because the EphB2 gene contains binding sites for NF-kB near it's transcriptional start site (*21*).

The data also suggests that the presence of HIVgp120 viral envelope protein and the type I interferon response, specifically IFNβ, is sufficient to induce ephrin-B/EphB expression in the CNS, particularly microglial cells. Although the functional role of EphB/ephrin-B signaling in neurodevelopment synapses have been characterized, its role in CNS inflammation is poorly understood and the few studies describing the role of EphB2/ephrin-B have largely focused on the peripheral immune response (*20, 22*). Thus, we assessed next to what extent elevated EphB2 in the CNS may be inducing inflammation and more specifically if microglia are a cellular source of the resulting inflammation.

EphB2-mediated ephrin-B reverse signaling induces a robust transcriptional antiviral and pro-inflammatory signature in human microglia.

To determine the function of EphB2/ephrin-B signaling in microglia, we treated HMC3 human microglia with pre-clustered human recombinant EphB2-Fc (2ug/ml) for 24 h to induce ephrin-B reverse signaling in microglia. RNA-sequencing revealed that human

microglia treated with pre-clustered EphB2 exhibited a pro-inflammatory antiviral gene expression signature. GO enrichment analysis revealed upregulation of gene expression associated with biological processes, including type I interferon response and cytokine mediated signaling and response **(Fig 3.4A).** Assessment of highly differentially expressed genes (log2FC cutoff = 0.4, P value < 0.05) revealed a pro-inflammatory and antiviral signature in EphB2- vs vehicle-treated microglia, including upregulation of IL-6, IFITM3, RIG-I, IRF7, and C3 **(Fig 3.4B, 3.4C)**. The network analysis showed a prominent activation of the type I interferon response and subsequent antiviral response in parallel to the pro-inflammatory cytokine/chemokine response in EphB2-treated microglia. Finally, transcript levels of specific inflammatory genes were confirmed using qRT-PCR including IL-6 and CD68, suggesting a pro-inflammatory/pro-phagocytic state for the microglia **(Fig 3.4D, 3.4E).** Additionally, an 8-fold increase of NF-kB phosphorylation was observed in EphB2- vs vehicle-treated microglia **(Supplementary Fig. 3.4),** with canonical NF-kB related genes differentially expressed (i.e. IL-6, TNFa, IL-1B) warranting an additional future investigation of downstream cytokine or chemokine production. Our findings highlight a novel function of ephrin-B reverse signaling, at least in microglia, to prime the innate immune system by activating viral detectors (RIG-I), antiviral effector proteins (IFITM3), complement (C3) and master regulator of the type I interferon response (IRF7).

EphB2-mediated ephrin-B1 reverse signaling in human microglia induces a pro-inflammatory secretome profile, and microglial ephrin-B1 knockdown mutes the response.

EphB2 treatment of human microglia activated a multitude of genes downstream of the NF-kB signaling pathway based on the RNAseq data, and thus, we examined the profile of secreted products. Considering a significant increase in microglial ephrin-B1 immunoreactivity in the presence of HIVgp120 or IFNβ, we next assessed whether the effects of EphB2 on NF-kB signaling and cytokine responses in microglia are mediated through ephrin-B1 by knocking down microglial ephrin-B1. Ephrin-B1 was knocked down in human microglia via siRNA treatment for 48-h followed by a 24-h treatment of microglia with pre-clustered EphB2-Fc for secretome analysis. NF-kB associated markers are upregulated in EphB2 treated microglia, based on RNAseq, and NF-kB is well recognized for its role as a transcriptional activator of various pro-inflammatory genes including pro-inflammatory cytokines (*23*). Thus, using the LegendPlex multiplex bead-based system, secreted cytokine and chemokine profiles were interrogated at scale following EphB2-Fc and ephrin-B1 siRNA treatment of microglia. The results reveal EphB2 mediated ephrin-B reverse signaling onto microglia drives a pro-inflammatory secretome profile **(Fig 3.5A)** of factors, including IP-10/CXCL10 (**Fig 3.5B**), GM-CSF (**Fig 3.5C**), CCL11 (**Fig 3.5D**), and MMP-9 (**Fig 3.5E**) that is partially alleviated by microglial ephrin-B knockdown. The third highest scoring network (Ingenuity Pathway Analysis) from RNA sequenced microglia shows, compared to EphB2 stimulation alone, the reduction of microglial ephrin-B1 in the presence of EphB2 blunts activation of pro-

inflammatory or NF-kB regulated molecules including, IL1B, CXCL10, and RELA (**Fig 3.5F**). Taken together, EphB2-mediated ephrin-B reverse signaling onto microglia results in secreted pro-inflammatory cytokines and chemokines and this effect is partially prevented by the knockdown of microglial ephrin-B1.

Pro-inflammatory factors secreted from microglia following the treatment with EphB2 are sufficient to induce neurotoxicity.

Because the microglial secretome clearly displayed a pro-inflammatory phenotype following EphB2 treatment, and hampered by microglial ephrin-B1 knockdown, we wanted to assess the impact of these secreted products on neurons. Human iPSC derived glutamatergic neurons and human iPSC derived astrocytes were co-cultured (iGluta/iAstrocyte) at ratio of 6:1 **(Fig 3.6A)** and were then incubated with 50% cell free conditioned media from vehicle, EphB2, ephrin-B1 siRNA and ephrin-B1 siRNA + EphB2 treated microglia. Afterwards, neurons were co-stained for MAP-2 (red) and NeuN (green), and neuronal survival was determined based on the counts of MAP-2/NeuN double positive cells **(Fig 3.6B).** Neuronal survival was significantly reduced following incubation with EphB2 treated microglial conditioned media. However, ephrin-B1 knockdown in microglia partially alleviated the EphB2 induced neuronal death (ephrin-B1 siRNA + EphB2-CM vs EphB2-CM, $p < 0.001$), presumably by preventing the secretion of microglial proinflammatory, neurotoxic components. The presence of other ephrins on microglia, and the partial knockdown of ephrin-B1 are factors that may explain the inability of ephrin-B1 knockdown to completely preserve neuronal survival at baseline level **(Fig 3.6B).**

However, given some potential, intrinsic toxicity from the transfection protocol, and potentially from ephrin-B1 siRNA alone, comparison of ephrin-B1 siRNA + EphB2-CM vs ephrin-B1 siRNA-CM showed no statistically significant change, indicating the microglia knockdown of ephrin-B1 may be sufficient to prevent neurotoxicity resulting from EphB2-Fc treated microglial conditioned media. Taken together, our data suggest that ephrin-B1 signaling in microglia, at least partially, drives the secretion of neurotoxic factors in response to clustered EphB2 exposure.
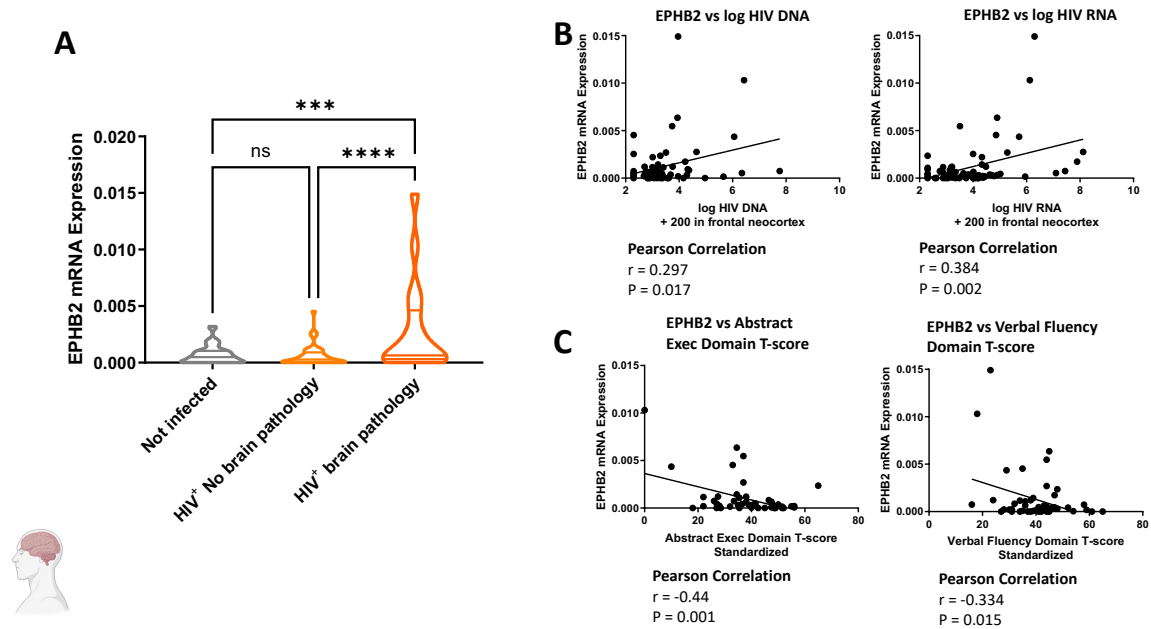
Figure 3.1. EphB2 is differentially expressed in human neocortex (middle frontal gyrus) of PLWH with brain pathology and ephrin genes strongly correlate with HIV load and neurocognitive performance. (A) Relative gene expression levels of EphB2 using mRNA from the middle frontal gyrus (neocortex) of the following groups of individuals: Not-infected (N = 46) and HIV+ (N = 63), HIV no brain pathology (N = 44) and HIV brain pathology (N = 19). The relative gene expression levels of EPHB2 in HIV+ (N = 63) patient's cortex was used to calculate Pearson correlations for **(B)** log HIV DNA/RNA load and **(C)** two domains of neurocognitive performance**.** Values in graph are mean ± SEM; n.s., non-significant, * P ≤ 0.05, ** P ≤ 0.01, *** P ≤ 0.001, **** P ≤ 0.0001, One-Way ANOVA followed by Tukey's post hoc test. The schematic graphic indicating human brain related data are presented was created with BioRender software (BioRender.com).
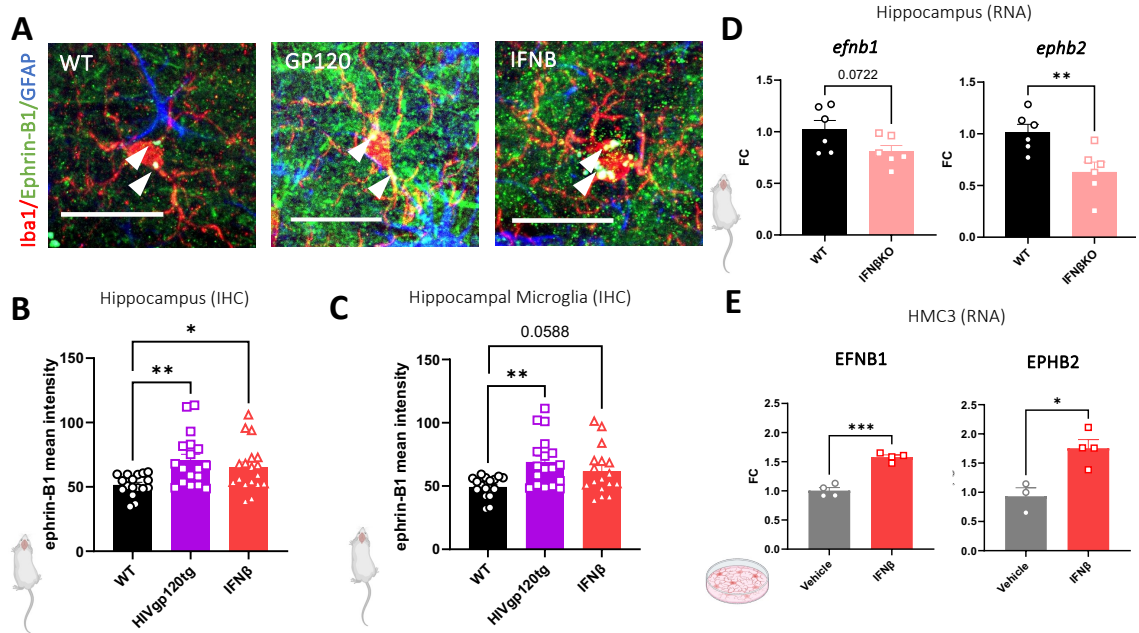
Figure 3.2. HIVgp120 and IFNβ regulate total and microglial specific ephrin-B1 expression in hippocampus. (A) Sagittal brain section stained for astrocytic GFAP (blue), microglial Iba1 (Red) and ephrin-B1 (Green). Values are Mean Intensity of ephrin-B1 fluorescence in total CA1 **(B)** or microglia gated **(C)**. All mice for IHC are male, aged 3 – 4 months. IFNB indicates intranasal treatment with the cytokine. N = 3 per genotype. **(C)** Analysis of mRNA expression of ephrin genes in the hippocampus of WT and IFNβKO. Relative mRNA expression was calculated by normalizing to *Gapdh* using the $2^{-\Delta\Delta Ct}$ method. RNA of IFNβKO and WT mice for qRT-PCR was from hippocampus of males and females, n = 6 (female n = 3; male n = 3) per genotype. Values are mean ± SEM; n.s., non-significant, * P ≤ 0.05, ** P ≤ 0.01, *** P ≤ 0.001, **** P ≤ 0.0001, One-Way ANOVA followed by Tukey's post hoc test. **(E)** Increase in EFNB1 and EPHB2 mRNA expression following 24-hour IFNβ treatment in human microglial HMC3 cells. N = 3-4 experiments, 2 technical replicates averaged per experiment. Values are Mean ± SEM; n.s. = non-significant, * P < 0.05, ** P < 0.01, *** P < 0.001, **** P < 0.0001, students t-test. Graphics created with Biorender software.
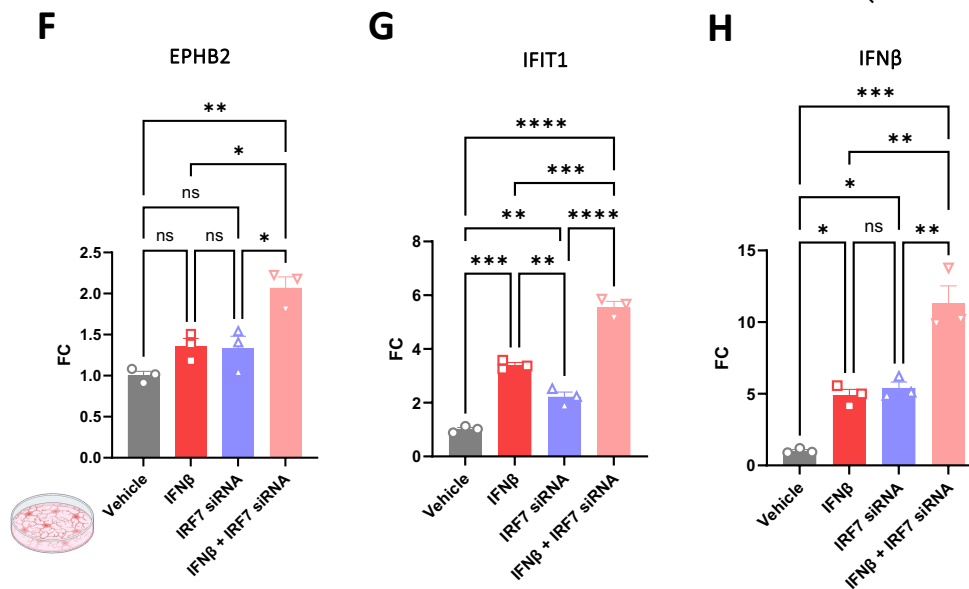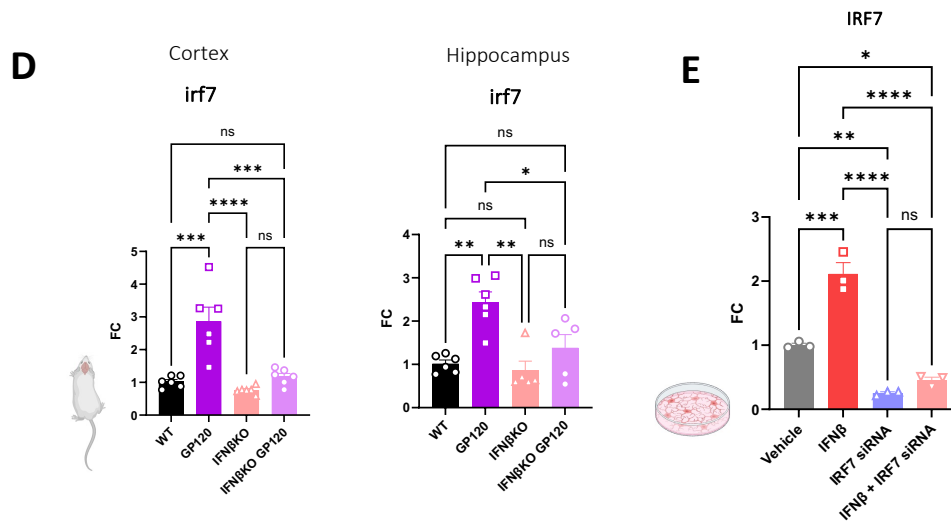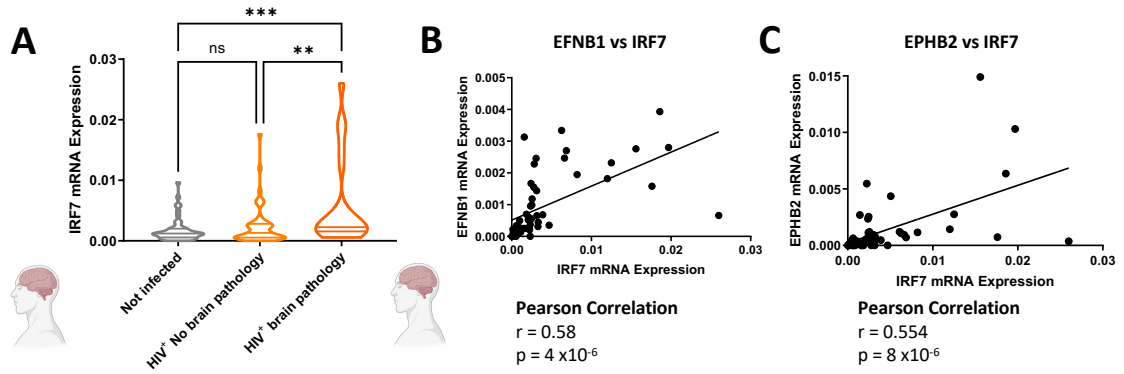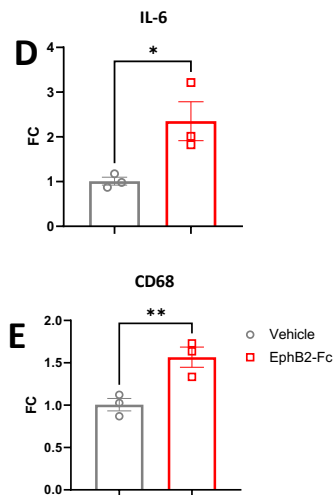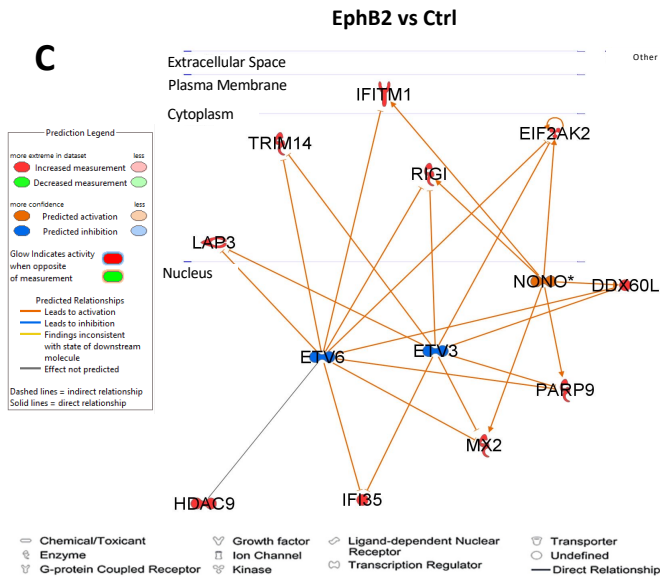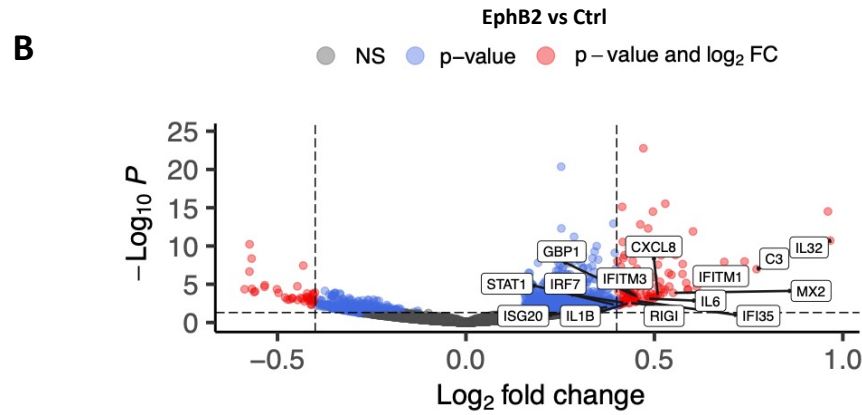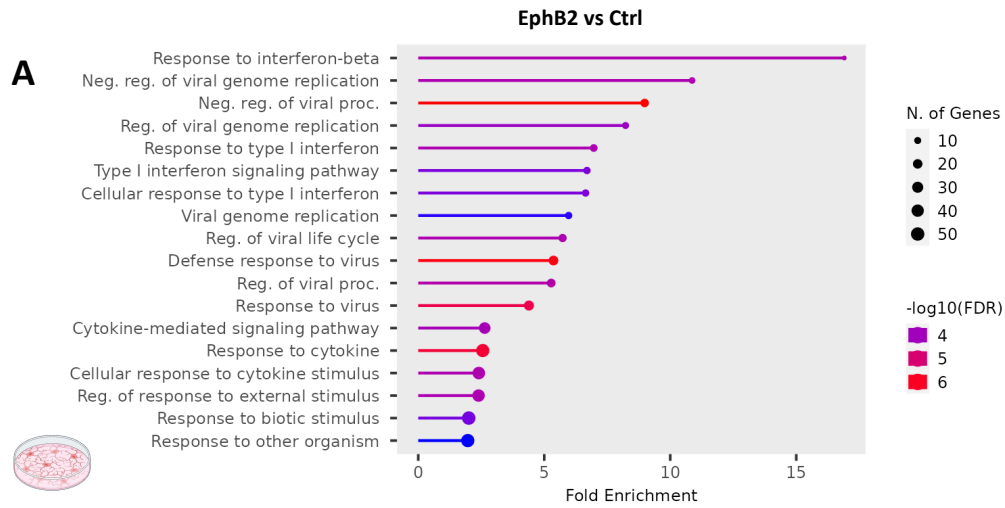
Figure 3.3. IRF7 is differentially expressed in human neocortex (middle frontal gyrus) of PLWH with Brain Pathology, correlates with ephrin-B/EphB genes and regulates ephrin-B/EphB. (A) Relative gene expression levels of IRF7 using mRNA from the middle frontal gyrus (neocortex) of Non-infected (N = 46) and HIV+ (N = 63), HIV No Brain Pathology (N = 44) and HIV Brain Pathology (N = 19). Relative gene expression levels of HIV+ (N = 63) patient's cortex was used and Pearson correlations were calculated for IRF7 vs **(B)** EFNB1 **(C)** and EPHB2. **(D)** Relative gene expression levels of IRF7 from the cortex and hippocampus of 9-month-old WT, HIVgp120tg, IFNβKO and IFNβKO HIVgp120tg mice. N = 6 (N = 3 male, N = 3 female) per genotype. Expression normalized to Beta-Actin. **(E)** IRF7, **(F)** EPHB2 **(G)** IFIT1 and **(H)** IFNβ mRNA expression following 48-hour IRF7 siRNA or negative control siRNA treatment followed by 24-hour IFNβ treatment or 0.001% BSA vehicle in HMC3. N = 3 biological replicates, 2 technical replicates averaged per experiment. Values are Mean ± SEM; n.s. = non-significant, * P < 0.05, ** P < 0.01, *** P < 0.001, **** P < 0.0001, Two Way ANOVA followed by Tukey's post hoc test. Graphics created in Biorender.com.

A EphB2 vs Ctrl

Response to interferon-beta
Neg. reg. of viral genome replication
Neg. reg. of viral proc.
Reg. of viral genome replication
Response to type I interferon
Type I interferon signaling pathway
Cellular response to type I interferon
Viral genome replication
Reg. of viral life cycle
Defense response to virus
Reg. of viral proc.
Response to virus
Cytokine-mediated signaling pathway
Response to cytokine
Cellular response to cytokine stimulus
Reg. of response to external stimulus
Response to biotic stimulus
Response to other organism

Fold Enrichment

N. of Genes
10
20
30
40
50

-log10(FDR)
4
5
6

B EphB2 vs Ctrl

NS   p−value   p − value and log₂ FC

$-Log_{10} P$

Log₂ fold change

GBP1, CXCL8, IL32, C3, IFITM1, STAT1, IRF7, IFITM3, MX2, ISG20, IL1B, RIGI, IL6, IFI35

C EphB2 vs Ctrl

Extracellular Space
Plasma Membrane
Cytoplasm
Nucleus

IFITM1, EIF2AK2, TRIM14, RIGI, LAP3, NONO*, DDX60L, ETV6, ETV3, PARP9, MX2, HDAC9, IFI35

D IL-6

FC

*

E CD68

FC

**

Vehicle
EphB2-Fc

Figure 3.4. EphB2 reverse signaling in microglia activates antiviral and inflammatory genes and pathways. Bulk RNA sequencing of HMC3 microglia treated with EphB2-Fc or Ctrl-Fc for 24 hours. **(A)** GO Enrichment of EphB2 vs Ctrl using the top 300 upregulated genes. **(B)** Volcano plot of differentially expressed genes of EphB2 vs Ctrl samples (0.4 log2Fc and 0.05 p-value cutoff). **(C)** Network analysis using Ingenuity Pathway Analysis (IPA) of the third highest scoring network (antiviral network). Blue indicates predicted down-regulated while red reflects up-regulated genes respectively. **(D-E)** mRNA transcript levels of IL-6 and CD68 from EphB2 treated microglia. RNA sequencing; N = 3 biological replicates. qRT-PCR; N = 3 biological replicates, 2 technical replicates averaged per biological replicate. Values are Mean ± SEM; * $P \leq 0.05$, ** $P \leq 0.01$, *** $P \leq 0.001$, **** $P \leq 0.0001$, n.s., non-significant, student's t-test.

A Secretome of human microglia

Vehicle / EphB2 / ephrin-B1 siRNA / ephrin-B1 siRNA + EphB2

Eotaxin, MCP-1, MIG, ENA-78, MIP-3a, GROa, I-TAC, IL-1B, IL-6, TNFa, IP-10, IFN-lambda1, IL-8, IFNa2, GM-CSF, IL-10, IFN-γ, ICAM-1, VCAM-1, MMP-9

Z-Score

B IP-10

C GM-CSF

D Eotaxin/CCL11

E MMP-9

ephrin-B1 siRNA
EphB2-Fc

F EphB2 vs Ctrl   EphB2 + ephrin-B1 siRNA vs Ctrl

139
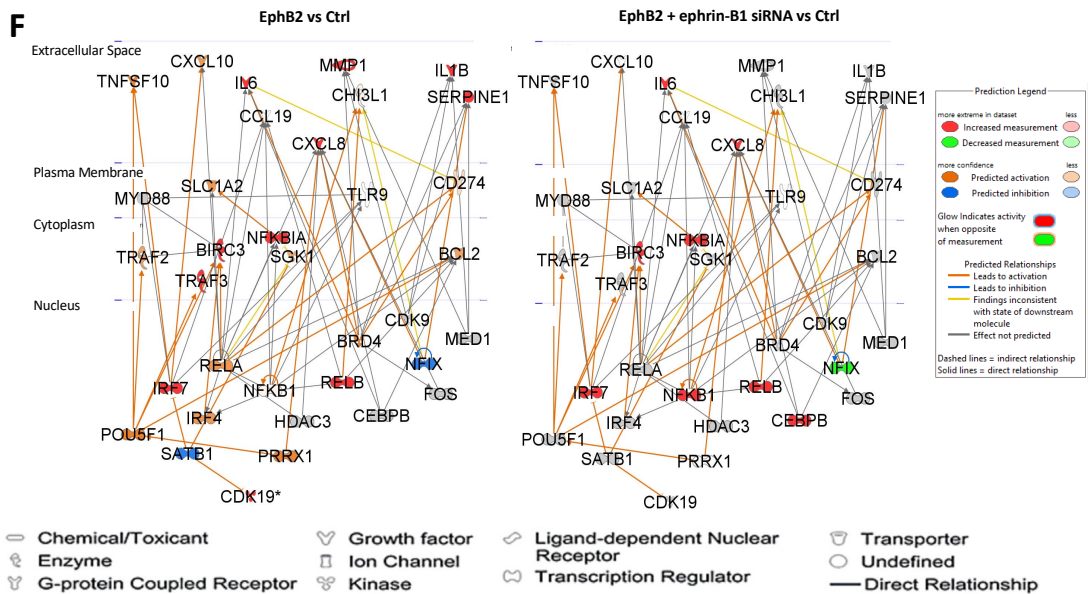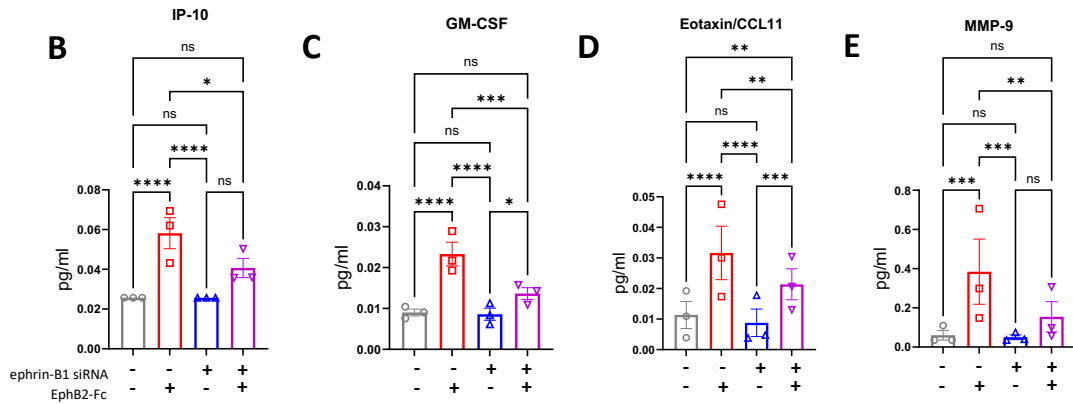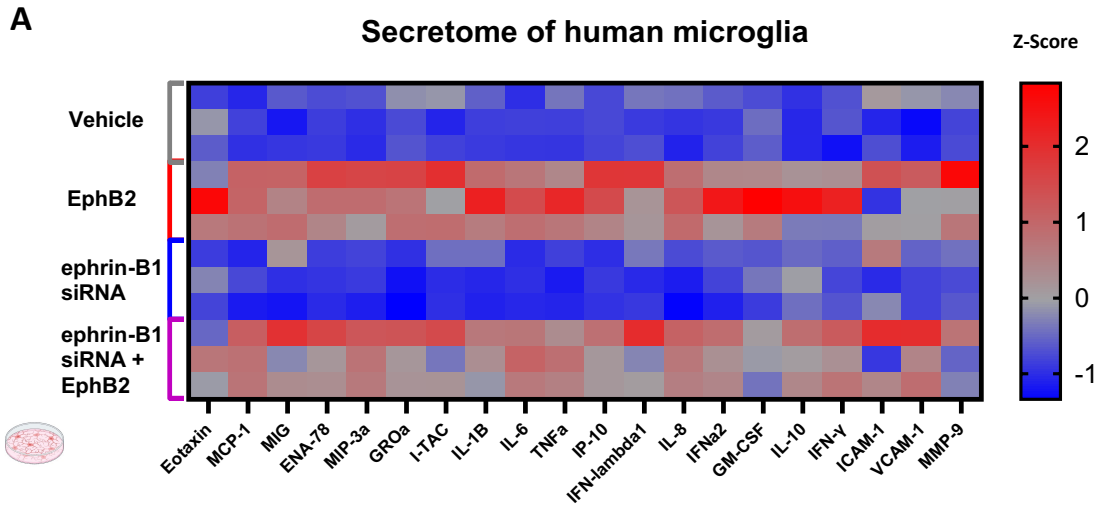
Figure 3.5. EphB2 reverse signaling produces a pro-inflammatory cytokine/chemokine secretome profile, while knockdown of microglial specific ephrin-B1 hampers EphB2 induced inflammatory response. (A) Multiplexed analysis of supernatants following 48-hour treatment of ephrin-B1 siRNA or scramble siRNA + 24-hour EphB2-Fc (2ug/ml) or control-Fc (2ug/ml) treatment in HMC3 human microglia using LegendPlex bead assay. N = 3 biological replicates. 2 technical replicates per biological replicate averaged. Heatmap values are z score based on averaged MFI of each technical replicate per experiment. **(B-E)** representative protein concentrations of IP-10, GM-CSF, CXCL1 and MMP-9 from the LegendPlex bead assay **(F)** Network analysis of the third highest scoring network for EphB2 vs Ctrl, and EphB2 + ephrin-B1 siRNA vs Ctrl (Ingenuity Pathway Analysis) to determine the network level changes from reducing ephrin-B1 during EphB2 mediated activation of microglia. Green indicates downregulated while red reflects upregulated genes respectively, and blue indicates predicted down-regulated while orange reflects predicted up-regulated genes respectively. Components without color represent genes without experimentally determined expression levels. * P < 0.05, ** P < 0.01, *** P < 0.001, **** P < 0.0001, n.s. = non-significant, Two-Way ANOVA followed by Tukey's post hoc test.
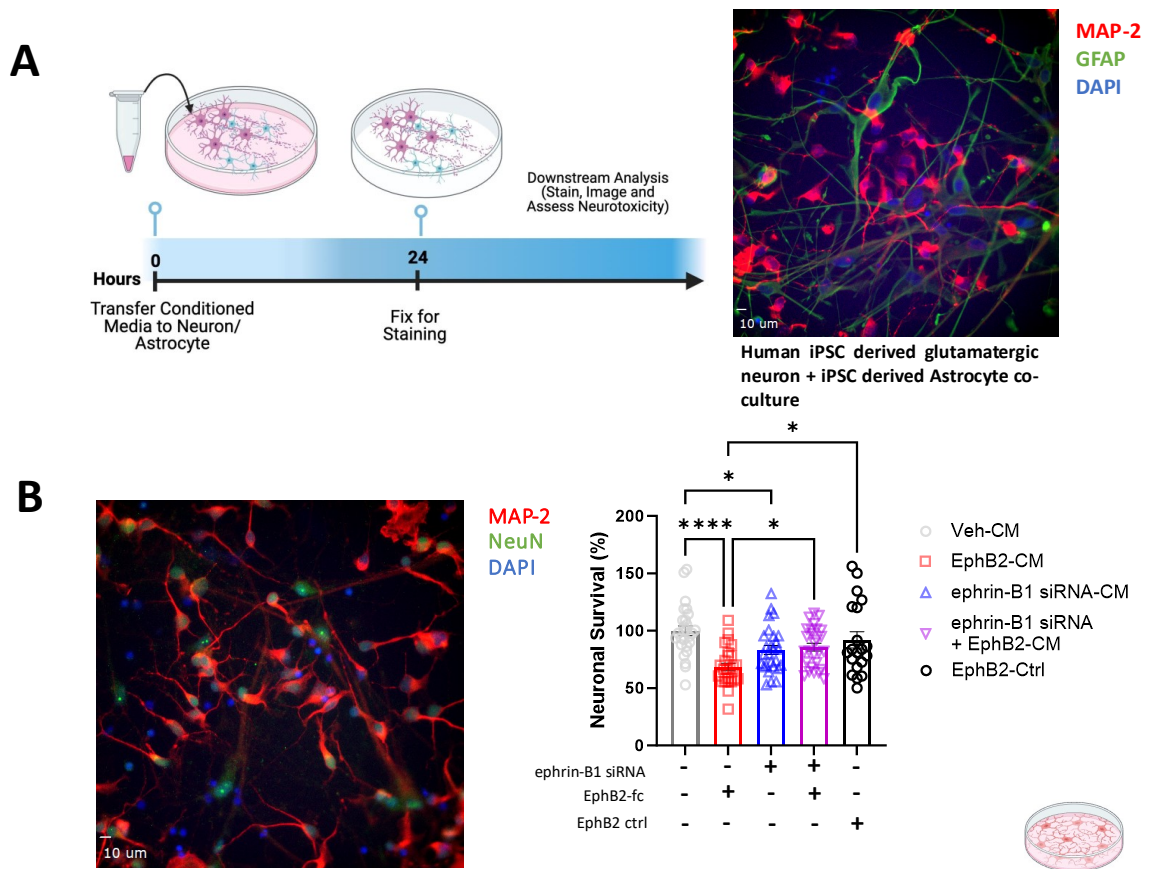
Figure 3.6. Secreted factors from EphB2 activated microglia induce neurotoxicity. (A) Timeline beginning with microglial conditioned media (CM) transfer and representative image of iGluta/iAstrocyte (6:1 neuron to astrocyte) co-cultures stained with MAP-2 for dendrites (red), GFAP for Astrocytes (green) and Hoechst Dye (Blue). **(B)** iGluta/iAstrocyte co-cultures were exposed for 24 hours to 50% cell-free conditioned media from treated microglia. HMC3 microglia were previously treated for 48 hours with RNAiMAX reagents and negative control (scramble siRNA) or ephrin-B1 siRNA, then stimulated for 24 hours with pre-clustered EphB2-Fc or ctrl-Fc before supernatants were collected. Neurotoxicity was assessed with MAP-2/NeuN double positive neuron counts following 24 hours exposure to 50% cell-free microglia conditioned media. Co-cultures of iGluta/iAstrocyte exposed to media conditioned by vehicle-treated microglia (Veh-CM) were used to define 100% neuronal survival. Values are Mean ± SEM; N = 3 independent co-culture experiments, with CM from N = 3 independent HMC3 EphB2 stimulation experiments. An average of approximately 1000 cells were counted per treatment. * P < 0.05, ** P < 0.01, *** P < 0.001, **** P < 0.0001, n.s. = non-significant, Two Way ANOVA followed by Tukey's post hoc test. Graphics created with Biorender software.
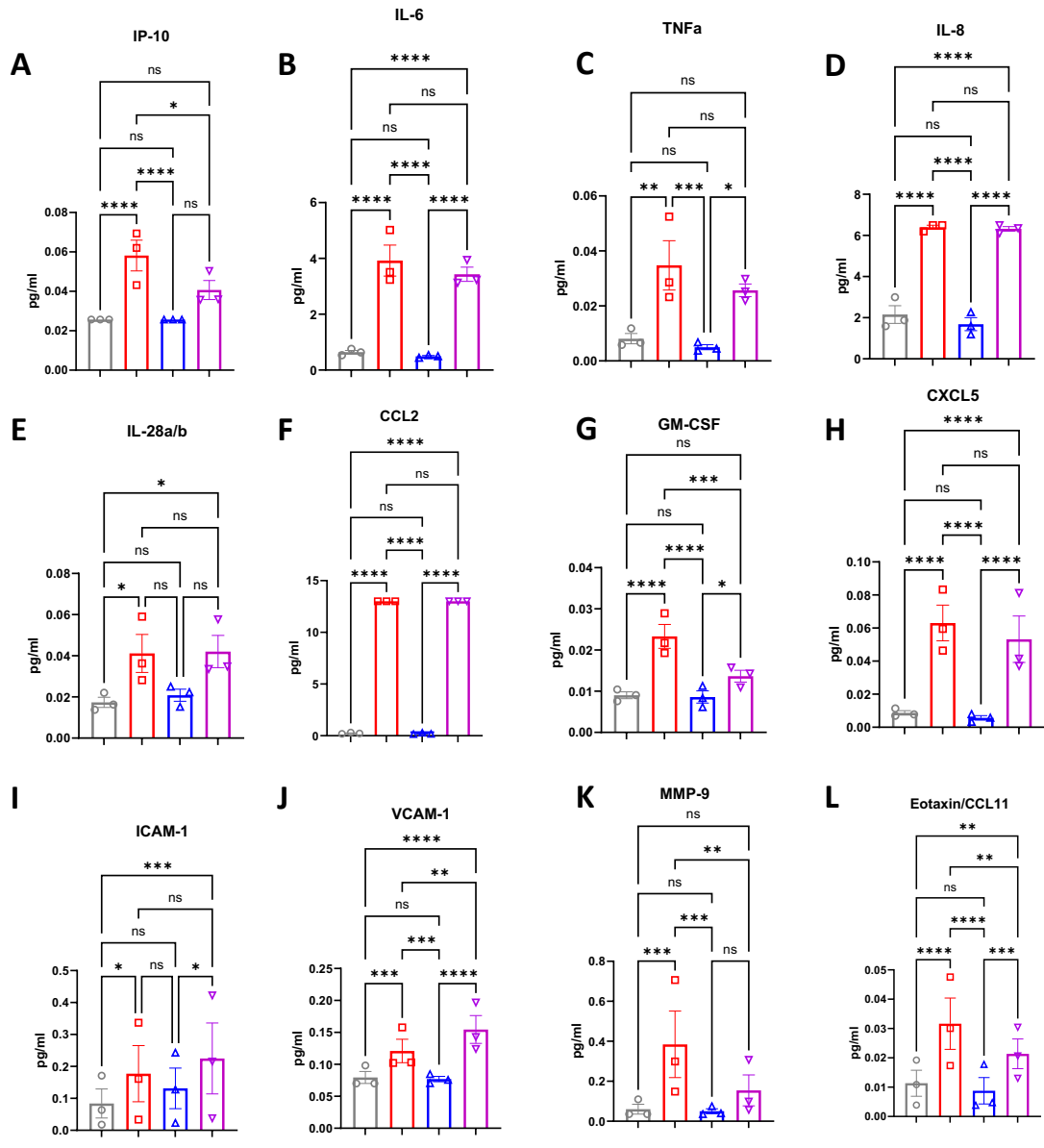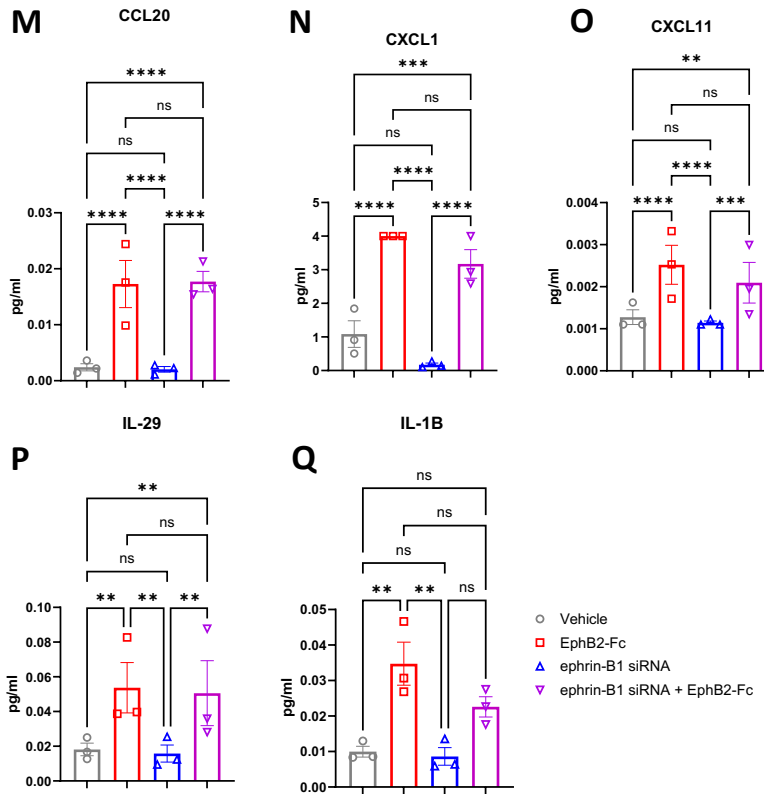
SUPPLEMENTARY FIGURES

Gene Name	Species	Forward	Reverse	Final Concentration
Irf7	Mouse	CACCCCCATCTTCGACTTCA	CCAAAACCCAGGTAGATGGTGTA	5uM
Efnb1	Mouse	ACCCTAAGTTCCTAAGTGGGA	CTTGTAGTACTCGTAGGGC	20uM
Ephb2	Mouse	TACATCCCCCATCAGGGTGG	GCCGGATGAATTTGGTCCGC	20uM
Gapdh	Mouse	AGGTCGGTGTGAACGGATTTG	TGTAGACCATGTAGTTGAGGTCA	20uM
Actin	Mouse	ACGGCCAGGTCATCACTATTG	CAAGAAGGAAGGCTGGAAAAGA	20uM
IRF7	Human	CATTCCTGGCACACACACAT	AAGCCCTTCTTGTCCCTCTC	20uM
EFNB1	Human	GTCCTACTACTGAAGCTACG	CTCTTGGACGATGTAGACAG	20uM
EPHB2	Human	GCAGTGTCCATCATGCATC	AGTACTGCAGCTCATAGTCC	20uM
IL6	Human	CTCCAGGAGCCCAGCTATGA	CCCAGGGAGAAGGCAACTG	20uM
HEAL	Human	TGCCTTTGCACAAGCTCTTC	TGCTGCAATAACCAGGTGTC	20uM
CD68	Human	TAGCTGGACTTTGGGTGAGG	CTCTCTGTAACCGTGGGTGT	20uM
IFNβ	Human	TTGACATCCCTGAGGAGATTAAGC	TTAGCCAGGAGGTTCTCAACAATAG	20uM
IFIT1	Human	GGAAACACCCACTTCTGTCTTACTG	ATTTGGATCATTTGTGCCTTGTAG	20uM
GAPDH	Human	GTCTCCTCTGACTTCAACAGCG	ACCACCCTGTTGCTGTAGCCAA	20uM
ACTIN	Human	CATGTACGTTGCTATCCAGGC	CTCCTTAATGTCACGCACGAT	20uM

Supplementary Table 3.1. qRT-PCR primers list. List of forward and reverse sequences for primers used for qRT-PCR including gene target name, species, forward primer sequence, reverse primer sequence and final concentration used.
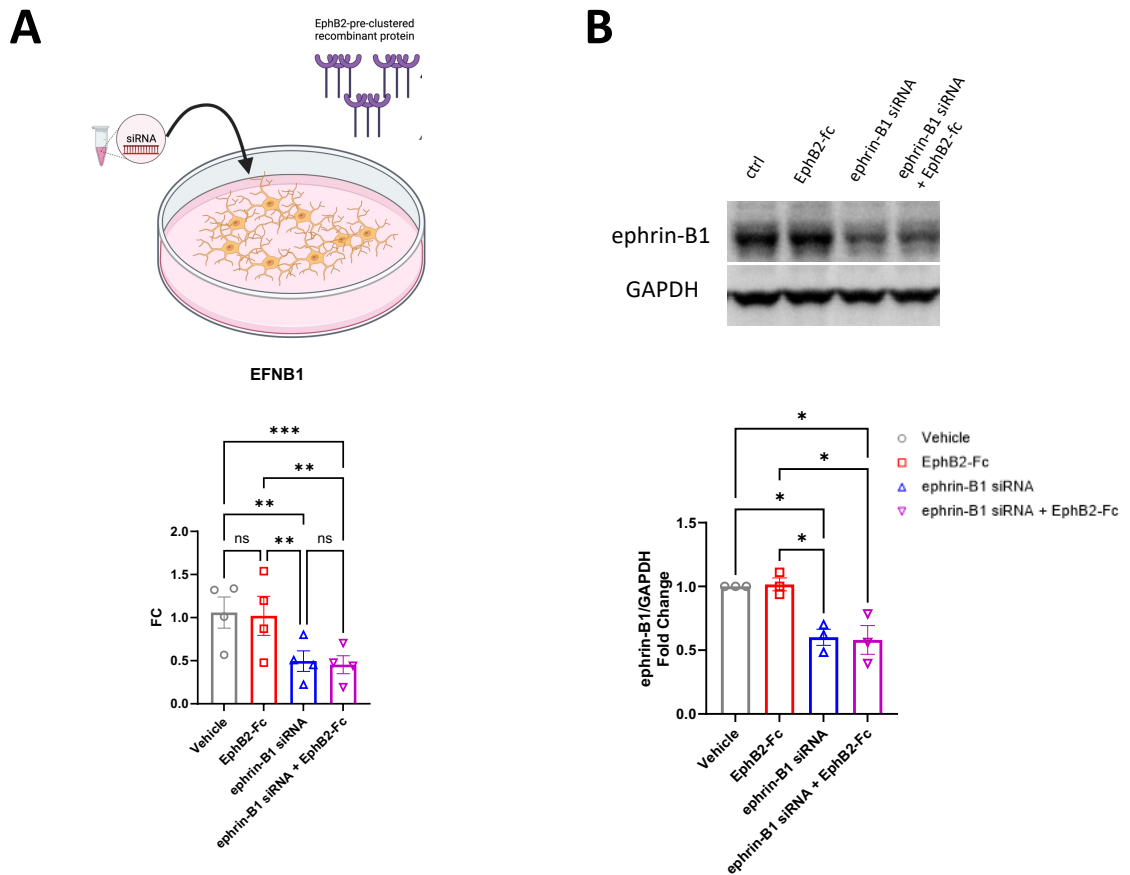
Supplementary Figure 3.1. Ephrin-B1 siRNA downregulates ephrin-B1 at the mRNA and protein level. (A) QRT-PCR analysis of EFNB1 using isolated RNA of human microglial HMC3 cells following 48-hour treatment with ephrin-B1 siRNA or scramble siRNA + 24-hour ephB2-Fc (2ug/ml) or control-Fc (2ug/ml) treatment. Fold change of EFNB1 transcript levels and **(B)** ephrin-B1 protein expression normalized to GAPDH. N = 3-4 biological replicates. 6-8 total technical replicates. Representative images taken at 40X magnification. Values are Mean ± SEM with n.s. = non-significant, * P < 0.05, ** P < 0.01, *** P < 0.001, **** P < 0.0001, Two-Way ANOVA followed by Tukey's Post Hoc.

A IP-10

B IL-6

C TNFa

D IL-8

E IL-28a/b

F CCL2

G GM-CSF

H CXCL5

I ICAM-1

J VCAM-1

K MMP-9

L Eotaxin/CCL11

CXCL1

CXCL11

IL-29

IL-1B

144

Supplementary Figure 3.2. Concentrations of all statistically significantly differentially regulated proteins detected with LegendPlex assays (comparing EphB2 vs Vehicle treatments). Multiplexed analysis of supernatants following 48-hour treatment of ephrin-B1 siRNA or scramble siRNA + 24-hour ephB2-Fc (2ug/ml) or control-Fc (2ug/ml) treatment of human HMC3 microglia using a LegendPlex bead assay. Panels (**A-Q**) include pro-inflammatory cytokines, pro-inflammatory chemokines, and antiviral markers represented in Figure 3.4A and other markers that were statistically significant when comparing EphB2 vs vehicle-treated cells. N = 3 biological replicates. 2 technical replicates per biological replicate averaged. Representative protein concentrations are Mean ± SEM, * P < 0.05, ** P < 0.01, *** P < 0.001, **** P < 0.0001, n.s. = non-significant, Two-Way ANOVA followed by Tukey's Post Hoc.
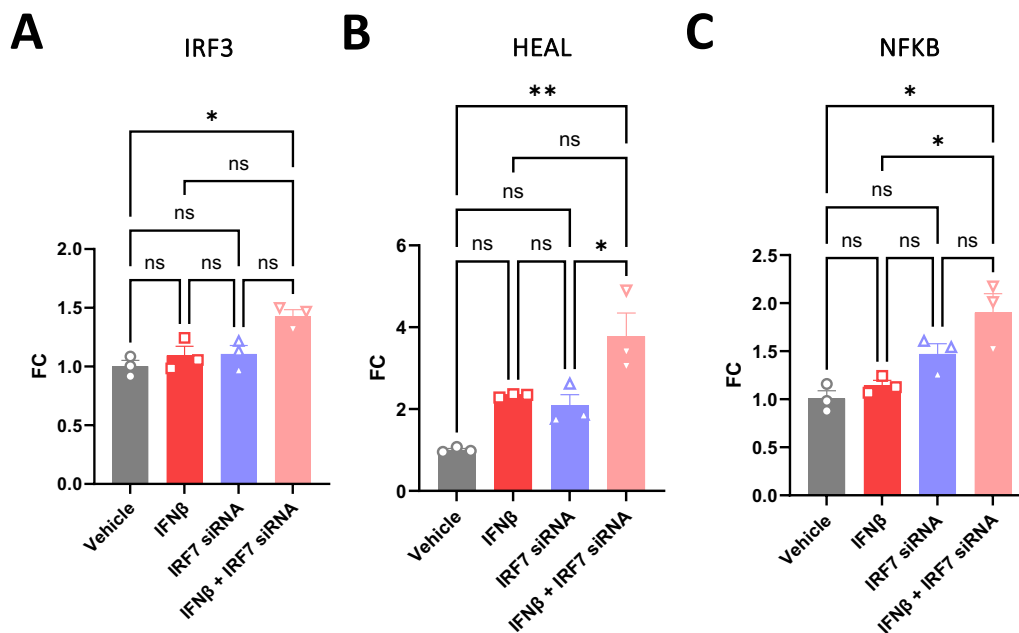
Supplementary Figure 3.3. IRF7 knockdown potentiates IFNβ induced IRF3, HEAL and NFKB mRNA expression. Relative RNA expression of **(A)** IRF3, **(B)** HEAL and **(C)** NFKB in HMC3 microglia following 48-hour IRF7 siRNA knockdown followed by IFNB treatment (3000U/ml). Expression normalized to GAPDH. N = 3 biological replicates per treatment. Values are Mean $\pm$ SEM with * P < 0.05, ** P < 0.01, *** P < 0.001, **** P < 0.0001, Two Way ANOVA followed by Tukey's post hoc test.
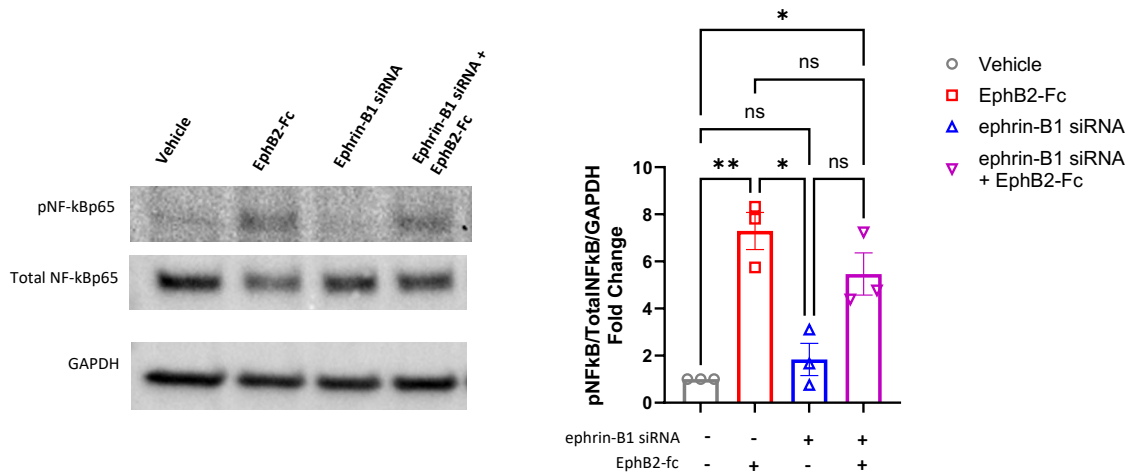
Supplementary Figure 3.4. EphB2 treatment activates NF-kB signaling. Representative western blot of phospho-NF-kB, total NF-kB and GAPDH. The graph shows fold change normalized to vehicle control of phospho-NF-kB normalized to Total NF-kB then to GAPDH. N = 3 biological replicates per treatment. Values are Mean $\pm$ SEM with * P < 0.05, ** P < 0.01, *** P < 0.001, **** P < 0.0001, Two Way ANOVA followed by Tukey's post hoc test.

3.5. DISCUSSION

In this paper, we show for the first time (1) ephrin-B/EphB is induced by the presence of HIV viral envelope protein gp120, and by treatment with both recombinant human and mouse IFNβ, a prominent type I interferon. Namely, (2) EphB2 was found to be elevated in the CNS of PLWH who have brain pathology, but not those without brain pathology, highlighting EphB2 as a potential biomarker to discern the two groups. However, it was unclear what the implications of this abundance of EphB2 in the brain were on microglia. Our study showed in microglia, (3) EphB2-mediated ephrin-B reverse signaling induces a presumably NF-kB mediated pro-inflammatory and antiviral response sufficient to cause non-contact dependent neurotoxicity.

Prior to this study, the regulators of ephrin-B/EphB in the CNS were poorly described, particularly in microglia, and the role of EphB2/ephrin-B signaling in microglia altogether. Here, we highlight HIVgp120 expression and especially IFNβ as key regulators of ephrin-B1, and inducers of EphB2. Expression of type I interferon master regulator, IRF7, correlates with ephrin-B1 and EphB2 in the cortex of PLWH, and is regulated by IFNβ in the brain of a mouse model. However, ablating IRF7 from human microglia and stimulating with IFNβ paradoxically resulted in enhanced activation of EphB2 and other antiviral factors like IFIT1 and IFNβ transcripts. IRF7, among three other IRFs, IRF1, -3, and -5, operates as a positive regulator of the type I interferon gene transcription (*24*). However, knockdown of IRF7 resulting in increased IFNβ production suggests that IRF7 may also provide a negative feedback signal. It is also possible that ablation of IRF7 resulted in the induction and activation of other IRFs, as shown in our study, IRF3 transcript levels being

induced **(Supplementary Fig 3.3)**, which may promote the activation of downstream IFN inducible factors and potentially EphB2. Additionally, it has been described that the ratio of IRF3 to IRF7 impacts preference towards homo vs heterodimerization, ultimately adjusting the landscape and binding affinity to interferon stimulated response elements (ISREs) on downstream targets (*25*). Ablation of IRF7 skews the ratio in favor of IRF3, and thus alters the landscape of activation potentially leading to the potentiation of interferon molecules seen here, such as IFIT1, IFNβ itself and even EphB2. Moreover, one study has shown that EphB2's regulatory region contains multiple binding sites for NF-kB (*21*). The ablation of IRF7 alone in microglia was sufficient to activate NF-kB transcripts, which was further potentiated by IFNβ treatment, which may suggest the induction of EphB2 transcripts following IRF7 siRNA knockdown could be mediated via this NF-kB activation **(Supplementary Fig 3.3)**. This is a plausible assumption as the EPHB2 gene contains binding sites near it's transcriptional start site for NF-kB (*21*).

NeuroHIV, and prevalence of HAND, can persist at times even when the viral load has become undetectable (*2*). Antiretroviral therapies extend lifespan of PLWH and suppress viral replication; however, they do not eliminate the virus allowing for viral protein products to continue to breakthrough and cause inflammation and neurodegeneration (*2*). The elevated EphB2 observed in the brains of people living with HIV who have brain pathology may provide insights on the persistent neurocognitive problems that PLWH face. In HIV, in a cohort of almost 2000 PLWH, worse executive function was associated with lack of full virologic suppression (*26*). EphB2's inverse correlation with Abstract Executive and Verbal Fluency T-scores **(Fig 3.1B)** suggests a deleterious association with

EphB2 and neurocognitive performance, resembling those seen in non-virologically suppressed individuals. Specifically, in PLWH with brain pathology, the pathological feature distinguishing higher cortical expression of EphB2 was the presence of multinucleated giant cells or microglial nodules highlighting microglia as the presumed key perpetrators to investigate **(Fig 3.1).**

Additionally, we observed that type I interferons, namely IFNβ, induce ephrin-B/EphB **(Fig 3.2)** but in a circular fashion where EphB2 mediated ephrin-B1 reverse signaling on microglia in turn generates an antiviral, type I interferon response. In GO Enrichment analysis of RNAseq data of EphB2 treated microglia vs Ctrl, some of the most enriched biological processes included "Response to Interferon Beta", "Regulation of Viral Life Cycle" and other cytokine response **(Fig 3.4A)**. Differential gene expression analysis **(Fig 3.4B)** and network analysis clearly shows a broad and robust type I interferon response, including activation of IRF7, IFITM3, RIG-I, MX2, IFI35 as seen by network analysis of the 3rd highest scoring network (**Fig 3.4C**). Therefore, it is possible that there is a previously unrecognized positive feedback loop, but it is unclear what is mediating the IFNβ triggered ephrin-B/EphB activation. Beyond the previously discussed NF-kB binding sites, transcription factor binding sites on human EFNB1 (Genecards ID: GC0XP068828) include IRF4, IRF5 and TRIM25 (a regulator of the RIG-I viral cytoplasmic detector). Additionally, for human EPHB2 (Genecards ID: GC01P022710) transcription factor binding sites are found for IRF4, STAT5, RELB. This suggests a potential route through other IRFs, such as IRF4 or IRF5, not IRF7, that provide the intermediary for IFNβ to enhance ephrin-B/EphB activation.

To fend off the virus, this EphB2 induced response seems to be a non-canonical, novel, mechanism for the host to drive an antiviral phenotype in a seemingly positive feedback loop given ephrin-B1/EphB2's own activation by IFNβ. However, what remains unclear is what impact the chronic presence of elevated EphB2 in the CNS has on inflammation and the subsequent impact on neuronal function and survival. Acute EphB2 treatment of microglia, as shown with the RNAseq and secretome experiments in this study, activates NF-kB signaling and induces a unique cytokine/chemokine profile, which we show to be neurotoxic (*27, 28*). Indeed, the transfer of conditioned media from microglia stimulated with EphB2-Fc shows non-contact dependent neurotoxicity presumably stemming from the secreted cytokines/chemokines of microglia. This presents itself as a potentially novel mechanism for HIV induced neuronal damage, and plausibly other neurodegenerative diseases where inflammatory activation of microglia is a root cause. The inflammatory signature of EphB2 treated microglia overlaps with a hallmark immune signature in the brain of various HIV models and PLWH, including CCL2, CXCL10, IL-1B, TNFa, IL-6, MMP-9 and others **(Fig 3.5B)** (*29-31*). Of particular note, MMP-9, is upregulated in the CNS of HIV infected individuals (*32*) and various neuroHIV models and associated with blood-brain barrier leakiness through reduced vascular tight junction proteins and presumably enhanced peripheral immune infiltrates and viral entrance into the CNS (*33, 34*). TNFa serves a similar role to MMP-9 in opening a paracellular route through the blood brain barrier for HIV infected macrophages, where chemoattractive signals from activated microglia, including CCL2 and CXCL10, further perpetuate the infiltration into the CNS (*35*). Additionally, in an HIVgp120 model, IL-6 expression has been shown to be NF-kB

dependent, with the ability of NF-kB specific siRNAs, and IKK-2 and IKKB inhibitors to block induction of IL-6 by gp120 (*36*).

Neurotoxicity is a pathological phenomenon seen in neuroHIV that was also observed through conditioned media transferred from EphB2-Fc treated microglia alone to neurons, which we presume is a consequence of the assortment of pro-inflammatory secreted factors (IL-6, CXCL10, TNFa, IL-1B etc) **(Fig 3.5B)**. However, to control for the transfer of leftover EphB2 in the microglia conditioned media, an EphB2 only control (EphB2-ctrl) containing only EphB2-Fc was transferred to the iGluta/iAstrocyte co-cultures showing a loss of neuron survival, but not to the extent of the EphB2-CM. Astrocytic ephrin-B1 was previously shown to play a role in remodeling synapses through astrocytic STAT3, potentially mediated by EphB2 signaling to ephrin-B1 on astrocytes, therefore addition of EphB2 only to iGluta/iAstrocyte cultures may cause some neuronal damage via astrocytes. However, microglial EphB2-CM reduced neuronal survival by a higher percentage compared to the EphB2-control ($P<0.05$) suggesting that secreted products, likely pro-inflammatory in nature, exacerbated neurotoxicity. IL-6, for example, is elevated in microglia following EphB2 treatment but also in the brains of PLWH and is associated with HIV induced depression. Physiologically chronic exposure of IL-6 has shown to elicit behavioral abnormalities (seizures and ataxia) and abnormal EEG function in the hippocampus (*29, 37, 38*). More recent studies provide a novel mechanism by which IL-6 induces changes in neuronal iron uptake and transport pathways that result in neurodegenerative iron sequestration (*39*). CXCL10 (also known as IP-10), a prominently secreted factor from EphB2 activated microglia is one of many factors we observed that

152

have been previously described to be neurotoxic. CXCR3, the receptor for CXCL10, is present on neurons, and following CXCL10 activation in a polyinosinic-polycytidylic acid (PIC) model, CXCL10 was shown to induce hyperexcitability, with CXCR3 inhibition attenuating seizure hypersensitivity induced by PIC challenge (*40, 41*). Additionally, elevated TNF-a and IL-1B have been observed in the CSF of PLWH with HAD, with the capacity to both induce neuronal injury via release of neurotoxic molecules including ceramide and L-cysteine (*41-43*).

As with many viral infections, controlling HIV and neuroHIV is a balancing act of limiting the infection without having rampant inflammation. Both runaway viral activation and runaway antiviral response need to be managed to prevent long term bystander neuronal dysfunction. Completely ablating EphB2 is likely a poor therapeutic strategy, as it plays an important cellular function such as NMDA receptor recruitment and maintenance of healthy and mature neural spines in the hippocampus (*44*). Targeting microglial ephrin-B1, and plausibly other microglial ephrin-Bs, may serve as a more viable option to minimize the deleterious neuroinflammation seen in the CNS in viral encephalitis stemming from HIV or potentially other viruses.

A potential limitation of the study is that the model for human microglia, HMC3 cells, are immortalized microglia and thus may not be the most representative of native physiological microglia. The use of alternative models including iPSC derived microglia or primary human microglia may prove to be a more appropriate *in vitro* model. Additionally, in our study, ephrin-B1 siRNA knockdown reduces expression by approximately 50% (**Supplementary Fig 3.1**), therefore reverse signaling through ephrin-

153

B1 can still occur just at a reduced level. This is seen by only partial neuroprotective effects of ephrin-B1 siRNA following EphB2 treatment when microglia conditioned media was transferred onto iGluta/iAstrocyte co-cultures. Additionally, EphB2 can bind to other ephrin-Bs, and uniquely some ephrin-As. Therefore, it's not surprising that simply targeting ephrin-B1 doesn't prevent EphB2 from signaling through other alternative ephrin ligands on microglia (*45*). Thus, the ablation of ephrin-B1 on microglia may only provide a partial signaling blockade and partial alleviation of the detrimental bystander neuronal effects stemming from EphB2-mediated ephrin-B1 reverse signaling on microglia.

In conclusion, the study firstly suggests soluble EphB2 as a potential biomarker to distinguish between PLWH with or without brain pathology. EphB2, and ligand ephrin-B1, activation can directly stem from type I interferon signaling as shown by the robust differential expression of ephrin-B1/EphB2 on microglia following IFNβ stimulation. The function of the elevated EphB2 in the CNS, at least through EphB2-mediated ephrin-B reverse signaling to microglia, is to perpetuate the antiviral response, but also produce and secrete pro-inflammatory products. Although the antiviral response is crucial to reduce the viral burden, the pro-inflammatory protein products are likely culprits for non-contact dependent neurotoxicity. Microglial mediated neuroinflammation has been the suggested perpetrator for a plethora of neurodegenerative diseases including Alzheimer's Disease, and Parkinson's Disease, etc (*46*). This study opens the door to a novel microglial signaling pathway that may be modulated to shed light on and potentially quell the physiological, pathological, and clinical symptoms associated with inflammatory neurodegenerative diseases.

AUTHOR CONTRIBUTIONS

FUNDING

ACKNOWLEDGEMENTS

REFERENCES FOR CHAPTER THREE

1. N. Sacktor *et al.*, Prevalence of HIV-associated neurocognitive disorders in the Multicenter AIDS Cohort Study. *Neurology* **86**, 334-340 (2016).

2. R. J. Ellis, M. J. Marquine, M. Kaul, J. A. Fields, J. C. M. Schlachetzki, Mechanisms underlying HIV-associated cognitive impairment and emerging therapies for its management. *Nature Reviews Neurology* **19**, 668-687 (2023).

3. M. Kaul, G. A. Garden, S. A. Lipton, Pathways to neuronal injury and apoptosis in HIV-associated dementia. *Nature* **410**, 988-994 (2001).

4. P. Castellano, L. Prevedel, E. A. Eugenin, HIV-infected macrophages and microglia that survive acute infection become viral reservoirs by a mechanism involving Bim. *Scientific Reports* **7**, 12866 (2017).

5. W. Ru *et al.*, Microglia Mediate HIV-1 gp120-Induced Synaptic Degeneration in Spinal Pain Neural Circuits. *J Neurosci* **39**, 8408-8421 (2019).

6. S. M. Toggas *et al.*, Central nervous system damage produced by expression of the HIV-1 coat protein gp120 in transgenic mice. *Nature* **367**, 188-193 (1994).

7. R. Maung *et al.*, CCR5 knockout prevents neuronal injury and behavioral impairment induced in a transgenic mouse model by a CXCR4-using HIV-1 glycoprotein 120. *J Immunol* **193**, 1895-1910 (2014).

8. T. K. Darling, T. J. Lamb, Emerging Roles for Eph Receptors and Ephrin Ligands in Immunity. *Front Immunol* **10**, 1473 (2019).

9. A.-S. Ernst *et al.*, EphB2-dependent signaling promotes neuronal excitotoxicity and inflammation in the acute phase of ischemic stroke. *Acta Neuropathologica Communications* **7**, 15 (2019).

10. A. M. Nikolakopoulou *et al.*, Astrocytic Ephrin-B1 Regulates Synapse Remodeling Following Traumatic Brain Injury. *ASN Neuro* **8**, 1-18 (2016).

11. A. J. Gill *et al.*, Heme oxygenase-1 deficiency accompanies neuropathogenesis of HIV-associated neurocognitive disorders. *J Clin Invest* **124**, 4459-4472 (2014).

12. R. Maung *et al.*, CCR5 knockout prevents neuronal injury and behavioral impairment induced in a transgenic mouse model by a CXCR4-using HIV-1 glycoprotein 120. *J Immunol* **193**, (2014).

13. M. M. Hoefer *et al.*, Combination of methamphetamine and HIV-1 gp120 causes distinct long-term alterations of behavior, gene expression, and injury in the central nervous system. *Exp Neurol* **263**, 221-234 (2015).

14. V. E. Thaney *et al.*, IFNβ Protects Neurons from Damage in a Murine Model of HIV-1 Associated Brain Injury. **7**, 46514 (2017).

15. H. Singh *et al.*, A pivotal role for Interferon-α receptor-1 in neuronal injury induced by HIV-1. *Journal of Neuroinflammation* **17**, 226 (2020).

16. V. E. Thaney *et al.*, IFNbeta Protects Neurons from Damage in a Murine Model of HIV-1 Associated Brain Injury. *Sci Rep* **7**, 46514 (2017).

17. D. Ojeda-Juárez *et al.*, Lipocalin-2 mediates HIV-1 induced neuronal injury and behavioral deficits by overriding CCR5-dependent protection. *Brain Behav Immun* **89**, 184-199 (2020).

18. K. E. Medders, N. E. Sejbuk, R. Maung, M. K. Desai, M. Kaul, Activation of p38 MAPK is required in monocytic and neuronal cells for HIV glycoprotein 120-induced neurotoxicity. *J Immunol* **185**, (2010).

19. M. I. Love, W. Huber, S. Anders, Moderated estimation of fold change and dispersion for RNA-seq data with DESeq2. *Genome Biology* **15**, 550 (2014).

20. P. N. Mimche *et al.*, EphB2 receptor tyrosine kinase promotes hepatic fibrogenesis in mice via activation of hepatic stellate cells. *Scientific Reports* **8**, 2532 (2018).

21. P. D. Pozniak, M. K. White, K. Khalili, TNF-α/NF-κB signaling in the CNS: possible connection to EPHB2. *J Neuroimmune Pharmacol* **9**, 133-141 (2014).

22. Z. Huang *et al.*, Key role for EphB2 receptor in kidney fibrosis. *Clin Sci (Lond)* **135**, 2127-2142 (2021).

23. T. Liu, L. Zhang, D. Joo, S. C. Sun, NF-κB signaling in inflammation. *Signal Transduct Target Ther* **2**, 17023- (2017).

24. K. Honda, A. Takaoka, T. Taniguchi, Type I Inteferon Gene Induction by the Interferon Regulatory Factor Family of Transcription Factors. *Immunity* **25**, 349-360 (2006).

25. K. K. Andrilenas *et al.*, DNA-binding landscape of IRF3, IRF5 and IRF7 dimers: implications for dimer-specific gene regulation. *Nucleic Acids Res* **46**, 2509-2520 (2018).

26. A. M. Anderson *et al.*, Better executive function is independently associated with full HIV suppression during combination therapy. *Aids* **33**, 2309-2316 (2019).

27. S. Hu, P. K. Peterson, C. C. Chao, CYTOKINE-MEDIATED NEURONAL APOPTOSIS. *Neurochemistry International* **30**, 427-431 (1997).

28. R. Mehla, S. Bivalkar-Mehla, M. Nagarkatti, A. Chauhan, Programming of neurotoxic cofactor CXCL-10 in HIV-1-associated dementia: abrogation of CXCL-10-induced neuro-glial toxicity in vitro by PKC activator. *Journal of Neuroinflammation* **9**, 239 (2012).

29. A. Mudra Rakshasa-Loots, H. C. Whalley, J. H. Vera, S. R. Cox, Neuroinflammation in HIV-associated depression: evidence and future perspectives. *Molecular Psychiatry* **27**, 3619-3632 (2022).

30. E. A. Nickoloff-Bybel, L. Festa, O. Meucci, P. J. Gaskill, Co-receptor signaling in the pathogenesis of neuroHIV. *Retrovirology* **18**, 24 (2021).

31. S. M. Ju *et al.*, Extracellular HIV-1 Tat up-regulates expression of matrix metalloproteinase-9 via a MAPK-NF-kappaB dependent pathway in human astrocytes. *Exp Mol Med* **41**, 86-93 (2009).

32. B. Sporer *et al.*, Presence of matrix metalloproteinase-9 activity in the cerebrospinal fluid of human immunodeficiency virus-infected patients. *J Infect Dis* **178**, 854-857 (1998).

33. J. P. Louboutin, B. A. Reyes, L. Agrawal, E. J. Van Bockstaele, D. S. Strayer, HIV-1 gp120 upregulates matrix metalloproteinases and their inhibitors in a rat model of HIV encephalopathy. *Eur J Neurosci* **34**, 2015-2023 (2011).

34. J. P. Louboutin, L. Agrawal, B. A. Reyes, E. J. Van Bockstaele, D. S. Strayer, HIV-1 gp120-induced injury to the blood-brain barrier: role of metalloproteinases 2 and 9 and relationship to oxidative stress. *J Neuropathol Exp Neurol* **69**, 801-816 (2010).

35. M. Fiala *et al.*, TNF-alpha opens a paracellular route for HIV-1 invasion across the blood-brain barrier. *Mol Med* **3**, 553-564 (1997).

36. A. Shah *et al.*, HIV-1 gp120 induces expression of IL-6 through a nuclear factor-kappa B-dependent mechanism: suppression by gp120 specific small interfering RNA. *PLoS One* **6**, e21261 (2011).

37. D. Alvarez-Carbonell *et al.*, Cross-talk between microglia and neurons regulates HIV latency. *PLoS Pathog* **15**, e1008249 (2019).

38. I. L. Campbell, Transgenic mice and cytokine actions in the brain: bridging the gap between structural and functional neuropathology. *Brain Res Brain Res Rev* **26**, 327-336 (1998).

39. J. K. Sterling *et al.*, Interleukin-6 triggers toxic neuronal iron sequestration in response to pathological α-synuclein. *Cell Rep* **38**, 110358 (2022).

40. T. J. Petrisko *et al.*, Neuronal CXCL10/CXCR3 Axis Mediates the Induction of Cerebral Hyperexcitability by Peripheral Viral Challenge. *Frontiers in Neuroscience* **14**, (2020).

41. N. A. Brabers, H. S. Nottet, Role of the pro-inflammatory cytokines TNF-alpha and IL-1beta in HIV-associated dementia. *Eur J Clin Invest* **36**, 447-458 (2006).

42. W. R. Tyor *et al.*, Cytokine expression in the brain during the acquired immunodeficiency syndrome. *Ann Neurol* **31**, 349-360 (1992).

43. H. A. Gelbard *et al.*, Neurotoxic Effects of Tumor Necrosis Factor Alpha in Primary Human Neuronal Cultures are Mediated by Activation of the Glutamate AMPA Receptor Subtype: Implications for AIDS Neuropathogenesis. *Developmental Neuroscience* **15**, 417-422 (1994).

44. M. Henkemeyer, O. S. Itkis, M. Ngo, P. W. Hickmott, I. M. Ethell, Multiple EphB receptor tyrosine kinases shape dendritic spines in the hippocampus. *J Cell Biol* **163**, 1313-1326 (2003).

45. Z. Yu *et al.*, EphrinB2-EphB2 signaling for dendrite protection after neuronal ischemia in vivo and oxygen-glucose deprivation in vitro. *J Cereb Blood Flow Metab* **41**, 1744-1755 (2021).

46. Q. Alam *et al.*, Inflammatory Process in Alzheimer's and Parkinson's Diseases: Central Role of Cytokines. *Curr Pharm Des* **22**, 541-548 (2016).

CHAPTER FOUR:

Optimizing iPSC Neuron/Astrocyte Differentiation and Microglial HIV Infection

4.1. iPSC derived Neuron and Astrocyte Differentiation

INTRODUCTION

In vitro human cultures present as a unique and viable model for studying neurodegenerative diseases and neurotoxicity. Induced pluripotent stem cell (iPSC) differentiated neurons allow for high yield production of a plethora of neuronal subtypes, which not only express the proper neuronal signatures but also functional responsiveness. Neuronal cultures in isolation show hyper-responsivity, for example following neurotoxic insult astrocytes minimized neurotoxicant-induced cytotoxicity as compared to neuron cultures alone, highlighting the critical need for co-cultured models including astrocytes (*1*). Moreover, astrocytic uptake of glutamate is a hallmark function of astrocytes, and cultures lacking astrocytes exhibit increased excitotoxicity and neuronal death (*2*). Furthermore, co-cultures also better mimic an *in-vivo* physiological model of the brain. In our studies, we focus on non-cell contact dependent mechanisms of neurotoxicity stemming from microglia, and thus require a co-culture of neurons and astrocytes, lacking microglia, to decipher the impact of secreted products specifically from microglia on neurons.

MATERIALS AND METHODS

Neural Progenitor Cells (NPCs)

NPCs were purchased from ATCC (Cat# ACS-5004) derived from ATCC-BYS012 Normal Human Induced Pluripotent Cells (Caucasian, Male). 6 well plates were precoated with 0.150 mg/ml of Matrigel for 1 hour at 37°C. NPCs were then thawed and expanded

in NPC media (StemDiff, StemCell Technologies, Cat#05833). NPCs were passaged only >85% confluence, using 50% accutase (StemCell Technologies, Cat#07920) + 50% DPBS. NPCs below passage 3 were used for further differentiation.

Neural Differentiation Protocols

Two protocols were employed to differentiate NPCs into Neuron and Astrocyte co-cultures. In the first protocol, a complete neural differentiation media (Pistollato et al 2017, ND media) was added to NPCs and a full media change was performed every 3 days. Briefly, ND media comprised Neurobasal media (Thermo-Fisher, Cat# 21103049), B-27 Supplement 50X (Thermo-Fisher, Cat# 17504044), N2 Supplements (Thermo-Fisher, 17502-048), Penicillin/Streptomycin (50U/mL final concentration), GDNF (Thermo-Fisher, PHC7045, 1ng/mL final concentration) and BDNF (Thermo-Fisher, PHC7074, 2.5ng/mL final concentration).

The second protocol differentiates NPCs into forebrain neurons using a Forebrain differentiation media for 5 days (StemCell Technologies, Cat# 08600) with daily full media changes, followed by forebrain maturation media (StemCell Technologies, Cat# 08605) with full media changes every 2-3 days.

QRT-PCR

Following differentiation, cells were lysed for 10 minutes on ice with Qiagen RLT buffer + 1% beta-mercaptoethanol. RNA was extracted using a Qiagen RNeasy Mini Kit (Qiagen, Cat#74104). Reverse transcription and qPCR were performed according to previously described protocols from the Kaul lab (*3, 4*). The results obtained were analyzed

using the $2^{-\Delta\Delta Ct}$ method and relative amounts of mRNA for each gene were calculated by normalizing to the internal control GAPDH.

RESULTS

To study contact and non-contact dependent mechanisms of neurotoxicity in humans, an appropriate model needs to be generated. Two differentiation protocols were employed to differentiate neural progenitor cells (NPCs) into neuron and astrocyte co-cultures. By morphological assessment, following the 2 differentiation protocols, NPCs showed a clear change in morphology from a small teardrop shaped stubby processes to elongated processes **(Fig 4.1).** Additionally, as compared to NPCs, both differentiation protocols showed higher mRNA expression of pan-neuron markers (i.e. MAP2, NEUN, SYP, TUBB3), indicating successful differentiation into neurons. To determine whether there was a proclivity to differentiate into excitatory or inhibitory neurons, an assortment of excitatory and inhibitory genes was screened, indicating the presence of a blend of excitatory (VGLUT1, VGLUT2, PSD95) and inhibitory neurons (VGAT, GABBRA2, GEPHYRIN) **(Fig 4.2)**. Additionally, the robust expression of GFAP likely indicates the presence of astrocytes in the culture; however, GFAP expression can also be prominently expressed in neural progenitors and radial glial cells (*5*).
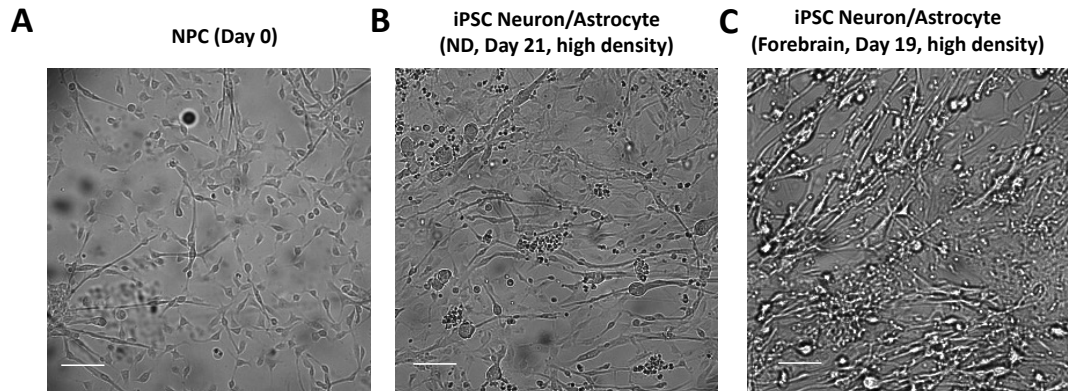
Figure 4.1. Brightfield microscopy images of NPCs differentiated into Neurons and Astrocytes. Brightfield representative images of **(A)** NPCs on day 0 prior to differentiation **(B)** iPSC derived neuron/astrocytes differentiated for 21 days using the ND media and **(C)** iPSC derived neuron/astrocytes differentiated for 19 days using the Forebrain Differentiation and Maturation Kit. Scale bar = 50µm. 10X magnification.
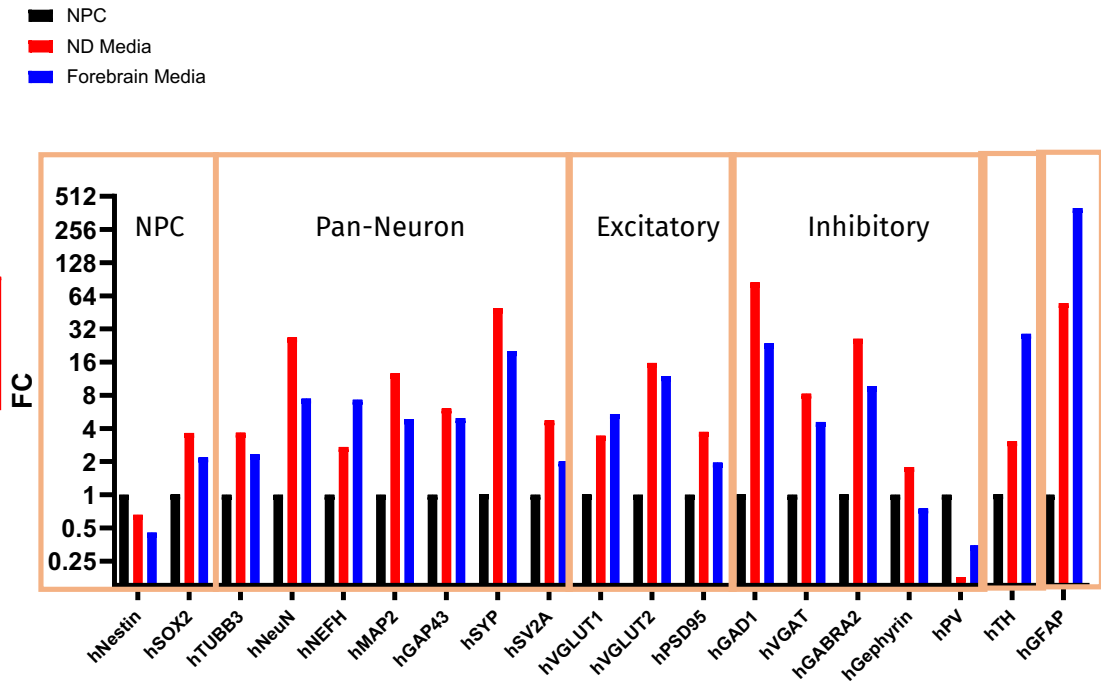
Figure 4.2. Characterization of NPCs differentiated into Neurons and Astrocytes.
qRT-PCR analysis of NPC, Pan-Neuron, Excitatory Neuron, Inhibitory Neuron, and Astrocytic gene categories of NPC (Black), ND media differentiated neurons/astrocytes (Red) and Forebrain media differentiated neurons/astrocytes (Blue). Values are fold change relative to NPC expression and normalized to GAPDH. N = 1 biological replicate with 2 technical replicates averaged per biological replicates.

165

Gene Name	Species	Forward	Reverse	Final Concentration
NESTIN	Human	TCAAGATGTCCCTCAGCC TGGA	AAGCTGAGGGAAGTCTTGGAGC	20uM
SOX2	Human	AAATGGGAGGGGTGCAAAAG	TTTTGCGTGAGTGTGGATGG	20uM
TUBB3	Human	CAACCAGATCGGGGCCAAGTT	GAGGCACGTACTTGTGAGAAGA	20uM
NEUN	Human	TACGCAGCCTACAGATACGCTC	TGGTTCCAATGCTGTAGGTCGC	20uM
MAP2	Human	TTTGGGCACACTCTTGTTGC	TTGCTTCCGTTGGCATTTCG	20uM
GAP43	Human	TGAGCAAGCGAGCAGAAAAG	TACAGCACAGCATGGTTGTC	20uM
SYP	Human	ACATGCAAGGAGCTGAGAGAC	AAACACGAACCACAGGTTGC	20uM
SV2A	Human	GCAACACGTTTTTCCGCAAC	TCAGACGGCTGTTCACAAAC	20uM
VGLUT1	Human	GCAAGTACATCGAGGACGCCAT	GCCACGATGATGGCATAGACTG	20uM
VGLUT2	Human	GAGAGGAGTAGACTGGCAACCA	CTGAAGACCAGCCAGTGTACTG	20uM
PSD95	Human	TCCACTCTGACAGTGAGACCGA	CGTCACTGTCTCGTAGCTCAGA	20uM
GAD1	Human	TGTCCAGGAAGCACCGCCATAA	TCCTTGACGAGAATGGCAGAGC	20uM
VGAT	Human	CTGGAACGTGACCAACGCCATC	TCATTCTCCTCGTACAGGCACG	20uM
GABRA2	Human	CCCAATGCACTTGGAGGATTTCC	AGAGCCATCAGGAGCAACCTGT	20uM
GEPHYRIN	Human	CTACACCAGTCCTGCTGTTGTC	CCACGAGAAATGATGGAGTCTGG	20uM
PV	Human	CTGATGGCTGCTGGAGACAAAG	GAGATTGGGTGTTCAGGGCAGA	20uM
TH	Human	TCAGAGCTGGACAAGTGTCATC	TGGAAGGCGATCTCAGCAATC	20uM
GFAP	Human	GCACGCAGTATGAGGCAATG	TAGTCGTTGGCTTCGTGCTT	20uM
GAPDH	Human	GTCTCCTCTGACTTCAACAGCG	ACCACCCTGTTGCTGTAGCCAA	20uM

Table 4.1. Primer list used for qRT-PCR to characterize iPSC derived neurons and astrocytes co-cultures.

DISCUSSION

Relative to NPCs, neuron/astrocyte co-cultures differentiated from both protocols expressed higher levels of pan-neuron, excitatory, inhibitory, and astrocytic markers. These findings indicate both differentiation protocols are a viable means to generate neuronal and astrocytic co-cultures. Generally, the ND media differentiated cultures were higher expressors of pan-neuronal markers (NEUN, MAP2, SYP) as compared to the Forebrain Media differentiated cultures. However, Forebrain Media differentiated cultures express ~4X more GFAP suggesting the Forebrain differentiated cultures to possibly contain more astrocytes and less neurons, as compared to ND media cultures **(Fig 4.2)**. Interestingly, the forebrain media supplier advertises the resulting cultures to contain less than 10% astrocytes. Based on morphological assessment, **(Fig 4.1)** the population of NPCs contained a fraction of already differentiated cells that may contain cells progressing through an astrocytic lineage. Alternatively, GFAP is expressed on radial glial cells and could indicate incomplete neuronal differentiation.

Some limitations of the study include the N = 1 biological replicate, making it impossible to determine whether the changes in gene expression are statistically significant. Additionally, the astrocytic marker used in the characterization was GFAP. Although it is a conventional marker for astrocytes, GFAP expressing neural progenitors exist and give rise to immature neurons making it difficult to ascertain whether, in our cultures, if these are radial glia or bona fide astrocytes. Alternative markers to verify the presence of mature astrocytes include S100B (which identifies GFAP+ cells that lose neural stem cell potential), Aldh1l1 or Glutamine synthetase (*6*).

4.2. HIV Infection Optimization

INTRODUCTION

HIV-1 infects macrophages in the periphery, which then traffic into the CNS through the blood brain barrier. Viral RNA has been detected in cerebrospinal fluid and brain tissue of people living with HIV as early as 2 weeks after initial inoculation (*7-9*). Notably, CCR5 (R5) preferring viruses allow for efficient entry and infection of macrophages and thus are the predominant strain found in the CNS (*10*). Although R5 HIV-1 viruses dominate the primary infection; a phenomena exists by which 50% of R5 viruses can transition to R5X4 viruses (preferring CCR5, but with less efficiency capable of CXCR4 usage) over time (*11*). Various strains may have different infection kinetics, be more prone to infecting microglia, and elicit a more prominent antiviral response in microglia. Therefore, when performing *in vitro* HIV infections, it is important to screen the various strains of HIV to determine how permissive microglia are to the strains and assess the host response from not only R5 HIV-1, but also X4 infection in microglia. In this section, both R5 (HIVBaL and SF162) and X4 (HIVIIIB) tropic strains of HIV-1 were screened in the infection of microglia. The goal of this section is to determine the differences in infectivity between strains and assess the capacity for an antiviral and Eph/ephrin response following infection.

MATERIALS AND METHODS

Ghost (3) CXCR4+ CCR5+ Cell Culturing and Infection.

Ghost (3) CCR5+ CXCR4+ (NIH HIV Reagent Program, Cat#ARP-3942) were cultured in a 12 well plate and grown until ~70% confluence. Ghost (3) CCR5+ CXCR4+ media contains DMEM + 10% FBS + 1% P/S + puromycin (1ug/ml), G418 (500ug/ml), hygromycin (100ug/ml). Cells were infected with either HIVIIIB or HIVBaL at 1, 0.1 and 0.01 MOI (NIH HIV reagent program). During inoculation, a 20ug/ul final concentration of polybrene was added to each well, and inoculation proceeded for 4 hours in 500uL of Ghost (3) CCR5+ CXCR4+ media without antibiotics. Inoculation was followed by 2 washes and infection proceeded for 2 days post infection (dpi).

HMC3 Cell Culturing and Infection

HMC3 (ATCC, Cat# CRL-3304) were cultured in a 12 well plate and grown to approximately 70% confluence. Cells were infected with either HIVIIIB, HIVBaL, HIVSF162 at 1, 0.1 or 0.01 MOI (NIH HIV reagent program). During inoculation, a 20ug/ul final concentration of polybrene was added to each well, as well as nucleosides dA (Sigma, cat# D8668), dT (Sigma, cat# T1895), dC (Sigma, cat# D0776), dG (Sigma, cat# D0901) at a final concentration of 2.5mM each. Inoculation proceeded for 4 hours in 500uL of HMC3 complete media (EMEM + 10% FBS + 1% P/S) followed by 2 washes. Infection proceeded for 14 dpi with full media changes occurring every day.

iMicroglia Cell Culturing and Infection

iPSC derived Microglia (iMicroglia, Fujifilm, Cat# C1110) were cultured in a 12-well PDL coated plate at ~125,000 cells/well. Cells were infected with either HIVIIIB,

HIVBaL, HIVSF162 at 1, 0.1 or 0.01 MOI (NIH HIV reagent program). During inoculation, a 20ug/ul final concentration of polybrene was added to each well, as well as nucleosides dA (Sigma, cat# D8668), dT (Sigma, cat# T1895), dC (Sigma, cat# D0776), dG (Sigma, cat# D0901) at a final concentration of 2.5mM each. Inoculation proceeded for 4 hours in 500uL of iMicroglia complete media (Fujifilm), followed by 2 washes. Infection proceeded for 12 dpi with 50% media changes occurring every 3 days.

P24 Assay

5% Triton X-100 was added to supernatants collected at the various time points, to a final concentration of 1% Triton X-100 to inactivate HIV. Virus-inactivated supernatants were then analyzed by p24 ELISA (Abcam, Cat# ab218268) according to manufacturer's protocol. Plate reading was performed on a PerkinElmer VICTOR X5 (2030 Multilabel Reader) at 450nm for 1 second. Absorbance values were converted to concentration (pg/ml) based on standard curve readings.

qRT-PCR

Cells were lysed with Qiagen RLT buffer + 1% beta-mercaptoethanol. RNA was extracted using a Qiagen mini kit, and reverse transcribed according to previously described protocols from the Kaul lab (*3, 4*). The results obtained were analyzed using the $2^{-\Delta\Delta Ct}$ method and relative amounts of mRNA of every gene were calculated by normalizing to internal control GAPDH.

Staining

HMC3 microglia were cultured in 96 well black walled plate and fixed with 4% paraformaldehyde. Cells were washed 3X with PBS and were blocked with 10% goat

serum and subsequently stained with mouse-CCR5 (R&D Systems, Cat#MAB183, 1:200), rabbit-CXCR4 (Sigma, Cat#AB1846, 1:500), rabbit-TMEM119 (Abcam, Cat#AB185333, 1:100) and mouse-Tubulin (Sigma, Cat#T-9026, 1:500) overnight at 4C in 5% goat serum. Secondary antibodies used were goat anti-mouse Rhodamine Red (1:50) and goat anti-rabbit AF488 (1:400). Cells were counterstained with Hoechst Dye 33343 (Invitrogen) for 5 mins and imaged using a Zeiss 200M fluorescence deconvolution microscope.

RESULTS

HIV indicator cells get infected with HIV and show strain specific responses.

HIV infection amounts were first optimized in Ghost (3) CCR5+ CXCR4+ cells, an indicator cell line stably transfected with a tat-dependent HIV-2 LTR-GFP construct. Following successful HIV infection, viral tat protein induced transcription of the HIV long terminal repeat (LTR) occurs activating GFP expression. Following 2 dpi with HIVIIIB (CXCR4-preferring) and HIVBaL (CCR5-preferring) GFP expression was evident **(Fig 4.3A).** Noticeably, when assessing the expression of viral gp120 protein and viral tat protein using qPCR, HIVIIIB resulted in ~10,000 X more gp120 expression in the host cell compared to HIVBaL. However, when assessing Tat mRNA expression using qPCR, HIVBaL resulted in 10X more Tat expression compared to HIVIIIB **(Fig 4.3B)**. Given the Tat dependence of the HIV-2 LTR-GFP, the higher Tat mRNA expression from HIVBaL unsurprisingly coincided with higher GFP expression from HIVBaL **(Fig 4.3A).** Additionally, the induction of type I interferon genes (IFNβ and IRF7) and ephrin-B1 were higher in HIVBaL compared to HIVIIIB **(Fig 4.3C, 4.3D).** These findings indicate both
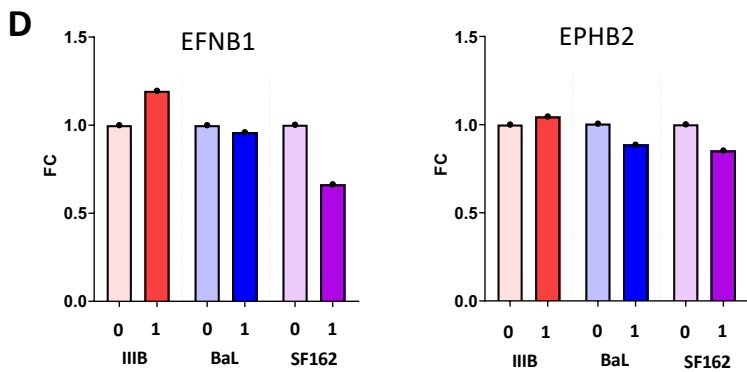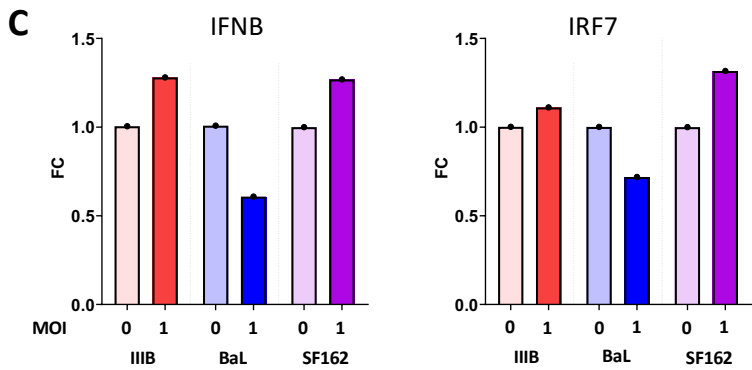
HIVIIIB (X4-preferring) and HIVBaL (R5-preferring) are capable of infection and elicit

a dose dependent antiviral and ephrin response.

A Neg Ctrl   IIIB – 1 MOI   BaL – 1 MOI

B GP120   TAT

C IFNB   IRF7

D EFNB1   EPHB2
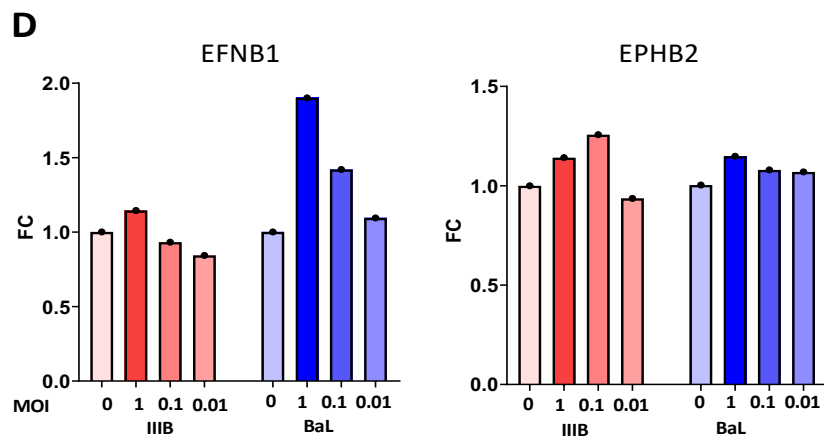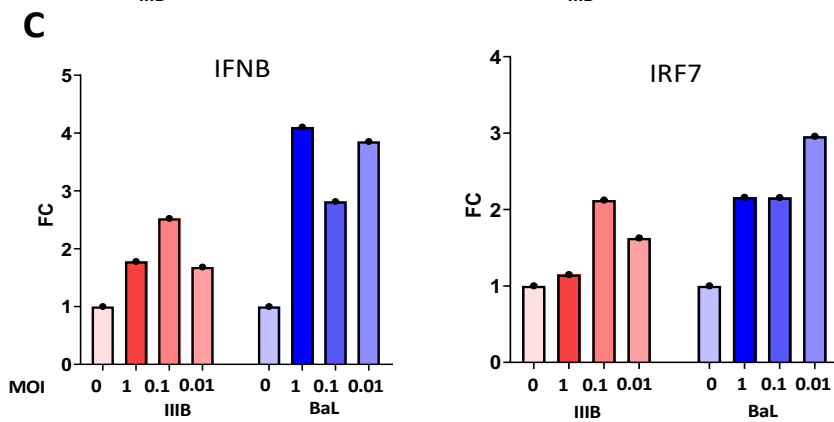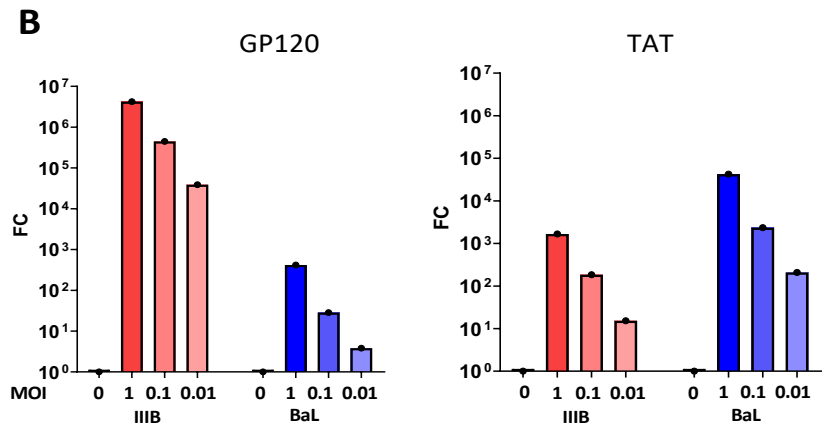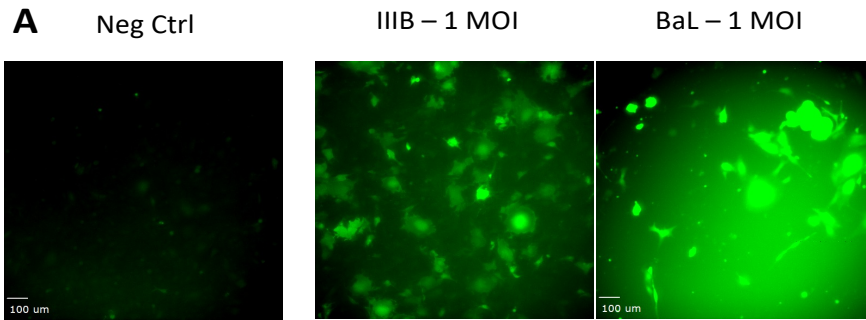
Figure 4.3. GHOST Cell Infection Optimization (IIIB, BaL). Ghost (3) CCR5+ CXCR4+ cells were infected with either HIVIIIB or HIVBaL at 1, 0.1 or 0.01 MOI. Following 2 dpi, **(A)** cells were imaged at 20X magnification for HIV dependent GFP expression. Scale bar = 100μm. Analysis of mRNA expression as fold change of **(B)** viral proteins, **(C)** type I interferon genes and **(D)** Eph/ephrin genes. Relative mRNA expression was calculated by normalizing to GAPDH using the $2^{-\Delta\Delta Ct}$. Values are fold change. N = 1 biological replicate, 2 technical replicates averaged per biological replicate.

HMC3 microglia do not get infected with HIV but iPSC derived microglia can get infected.

To test how permissive various in vitro models of microglia are to HIV infection, we first screened HMC3 microglia (our primary human microglial model) for the expression of CXCR4 and CCR5, two chemokine co-receptors required for HIV infection. HMC3 microglial cells express both CXCR4 and CCR5, which suggests that they should be able to be infected with HIV **(Fig 4.4A).** However, following HIV inoculation of HMC3 microglia with 3 different strains of HIV (HIVIIIB, HIVBaL, HIVSF162) at 3 different MOIs of 1, 0.1, 0.01 for 14 days, the presence of either viral gp120 and Tat mRNA at 14 dpi were undetectable (**Fig 4.4B**, 1 MOI concentration). I also did not detect any meaningful induction of type I interferon genes, IFNβ and IRF7 **(Fig 4.4C)** or ephrin related genes **(Fig 4.4D).** Additionally, p24 assay confirmed that at 6, 10 and 14 dpi there was no production of viral p24 into the supernatants of the HMC3 (data not shown). These results indicate that HMC3 microglia were not able to be infected with HIV even though they expressed the HIV receptors CXCR4 and CCR5 and would be an inappropriate model to assess HIV infection.

A Tub/CXCR4/DAPI   TMEM119/CCR5/DAPI

50 um   50 um

B

GP120

TAT

MOI

0 1 0 1 0 1
IIIB BaL SF162

C

IFNB

IRF7

MOI

0 1 0 1 0 1
IIIB BaL SF162

D

EFNB1

EPHB2

0 1 0 1 0 1
IIIB BaL SF162
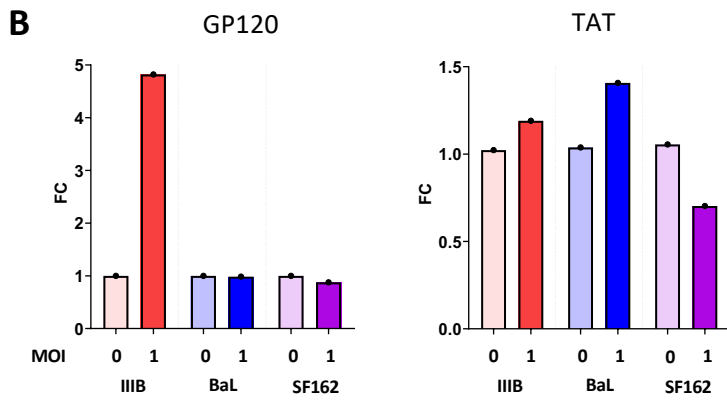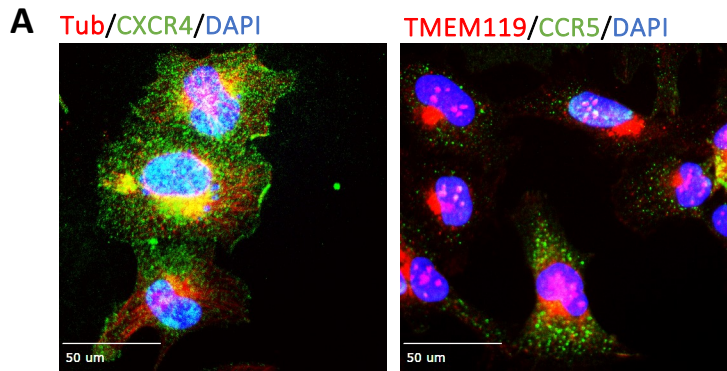
Figure 4.4. HMC3 Cell Infection Optimization. (A) Immunofluorescence labeling of HMC3 microglia with CXCR4 or CCR5 (green), Tubulin or TMEM119 (red) and Hoechst Dye (blue). HMC3 cells were infected with either HIVIIIB, HIVBaL or HIVSF162 at 1, 0.1 or 0.01 MOI. Following 14 dpi, analysis of mRNA expression as fold change of **(B)** viral proteins, **(C)** type I interferon genes and **(D)** Eph/ephrin genes. Relative mRNA expression was calculated by normalizing to GAPDH using the $2^{-\Delta\Delta Ct}$. Values are fold change. N = 1 biological replicate, 2 technical replicates averaged per biological replicate.

Given that HMC3 microglia were unable to be productively infected with three different strains of HIV, an alternative human microglial model was used to determine whether CCR5 or CXCR4 tropic HIV was capable of infecting microglia and what MOI was sufficient to produce detectable virus and elicit an antiviral response. IPSC derived microglia (iMicroglia, Fujifilm) were treated with HIV similarly to the HMC3s as described above. At 12 dpi, the microglia were assessed for presence of gp120 and Tat mRNA and showed high, but variable mRNA expression of gp120 and Tat that was influenced by HIV strain **(Fig 4.5A).** Additionally, when treated with MOI = 1, all strains showed detectable levels of p24 protein at 3, 6, 9 and 12 dpi, indicating that in contrast to HMC3 microglia, iPSC derived microglia can be productively infected with HIV **(Fig 4.5B).** HIVBaL p24 production exceeded the detection limit of the assay, while HIVIIIB and HIVSF162 peaked at 200pg/ml and 18pg/ml respectively. Peak production in the HIVIIIB and HIVSF162 strains peaked at 3 dpi and diminished at subsequent time points. Additionally, the strain specific p24 concentrations are in-line with Tat mRNA expression rather than gp120 mRNA expression, with HIVBaL leading to the highest production of p24 and expressor of Tat mRNA, followed by decreasing p24 production and Tat mRNA in HIVIIIB then HIVSF162. I found that HIVBaL infection of iPSC microglia produced the highest viral titer of all three strains, showing a ~3,000,000-fold increase in Tat mRNA expression (over background), compared to ~10,000-fold increase in Tat expression when treated with HIVIIIB, and ~500-fold increased Tat expression when treated with HIVSF162.
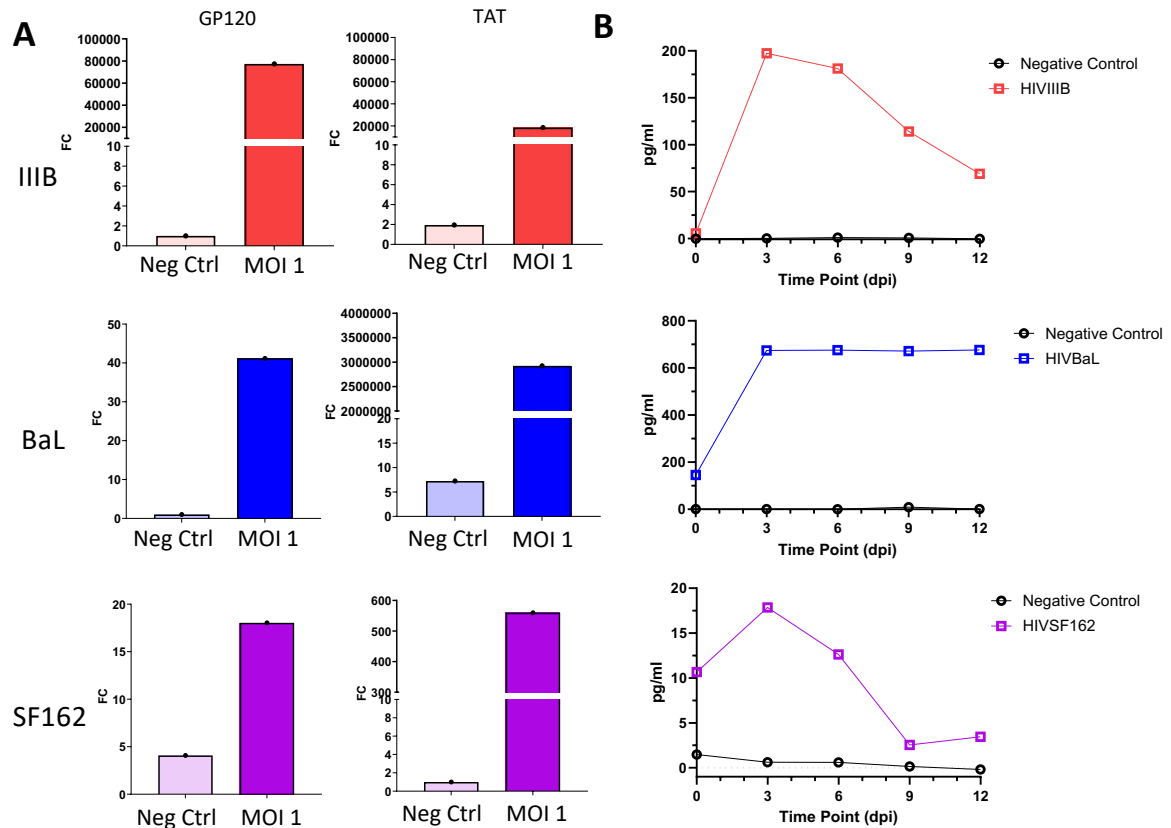
Figure 4.5. iMicroglia Cell Infection Optimization. iMicroglia cells were infected with either HIVIIIB, HIVBaL or HIVSF162 at 1 MOI. Following 12 dpi, analysis of mRNA expression as fold change of **(A)** viral proteins gp120 and Tat. **(B)** concentrations of p24 (pg/ml) from supernatants collected from HIV infected iMicroglia at 0, 3, 6, 9, 12 dpi. Relative mRNA expression was calculated by normalizing to GAPDH using the $2^{-\Delta\Delta Ct}$. Values are fold change. N = 1 biological replicate, 2 technical replicates averaged per biological replicate.

Gene Name	Species	Forward	Reverse	Final Concentration
GP120	viral	TGAGCCAATTCCCATACATTATTG	CCTGTTCCATTGAACGTCTTATTATTAC	20uM
TAT	Viral	GCATCCAGGAAGTCAGCCTA	TTGAGGAGGTCTTCGTCGCT	20uM
IRF7	Human	CATTCCTGGCACACACACAT	AAGCCCTTCTTGTCCCTCTC	20uM
EFNB1	Human	GTCCTACTACTGAAGCTACG	CTCTTGGACGATGTAGACAG	20uM
EPHB2	Human	GCAGTGTCCATCATGCATC	AGTACTGCAGCTCATAGTCC	20uM
IFNβ	Human	TTGACATCCCTGAGGAGATTAAGC	TTAGCCAGGAGGTTCTCAACAATAG	20uM
GAPDH	Human	GTCTCCTCTGACTTCAACAGCG	ACCACCCTGTTGCTGTAGCCAA	20uM

Table 4.2. Primer list used for qRT-PCR following HIV infection of HMC3 or iMicroglia.

DISCUSSION

To determine the MOI that should be used for in vitro infection of microglia, I infected the GHOST (3) CCR5+ CXCR4+ cell indicator line and found a dose dependent antiviral and Eph/ephrin response, as well as a dose dependent detectable viral gp120 and tat mRNA. Additionally, Ghost cells show a viral tropism-specific response. CXCR4 preferring HIVIIIB shows more detectable viral gp120 mRNA compared to HIVBaL, while CCR5 preferring HIVBaL shows more detectable Tat compared to HIVIIIB. Additionally, the more prominent antiviral and Eph/ephrin response, when analyzing mRNA transcript levels of IFNβ, IRF7 and ephrin-B1, stem from HIVBaL. The higher detectable Tat mRNA in the GHOST cell, at 2 dpi, may be the key viral protein driving the antiviral and ephrin response.

I tested whether two microgial cell lines could be productively infected with HIV and found that HMC3 could not be infected but iMicroglia could be robustly infected. HMC3 microglia showed expression of chemokine co-receptors CXCR4 and CCR5. However, following 4 hour inoculation and 14 days post infection, I was unable to detect viral gp120/Tat mRNA or p24 protein, indicating that these cells were not productively infected with HIV. This is inline with previous studies highlighting the inability of HMC3 to be infected due to the lack of CD4 expression **(Fig 4.4)** (*12, 13*).

In contrast, I was able to productively infect iPSC derived microglia with CXCR4 and CCR5 tropic HIV **(Fig 4.5)**. P24 assay reveals peak viral production at 3 dpi, and begins to decline towards negative control by 12 dpi. This may be due to the innate activation of an antiviral response, such as production of IFIT1, IFNβ, IRF7 and others I have previously

181

observed. Alternatively, the rampant viral infection may be jeopardizing the survival of the cells resulting in fewer host cells to continue viral production. HIVBaL infection resulted in significantly higher titers (> 600pg p24/ml) well above the detection limit of the assay, and thus need to be diluted to obtain an accurate estimate on viral production kinetics.

Limitation of these preliminary experiments include the N = 1. As a consequence, no statistical assessment can be done and therefore it is uncertain whether there is meaningful differential expression on any p24 concentrations or mRNA transcript levels.

Taken together, these results indicate that HIV at 1 MOI is suitable to infect GHOST (3) CCR5+ CXCR4+ Cells, which show clear fluorescence and viral RNA within the cell, as well as an anticipated activation of type I interferon genes and even ephrin-B1 transcripts following infection. The observed ephrin-B1 upregulation is in line with previously reported observations seen in Chapter 3 of this dissertation, where transgenic HIVgp120 expression and IFNβ both induced ephrin-B1 immunoreactivity. These results also indicate that HMC3 microglia are unable to to be infected, at least by the tested viral strains, but iPSC derived microglia are susceptible to HIV infection and thus are a more suitable choice for future HIV infection experiments.

Going forward, iPSC-derived microglia can be used to investigate the impact of EphB2 treatment on HIV infection and viral production. In Chapter 3, RNAseq data from EphB2 treated microglia showed an enrichment of antiviral biological processes and differential expression of antiviral genes, suggesting it may impact viral infection or production. Thus, the unique ability of iPSC microglia to be infected by HIV presents as a viable model to assess the antiviral effects of EphB2.

REFERENCES FOR CHAPTER FOUR

1. U. De Simone, F. Caloni, L. Gribaldo, T. Coccini, Human Co-culture Model of Neurons and Astrocytes to Test Acute Cytotoxicity of Neurotoxic Compounds. *International Journal of Toxicology* **36**, 463-477 (2017).

2. S. Mahmoud, M. Gharagozloo, C. Simard, D. Gris, Astrocytes Maintain Glutamate Homeostasis in the CNS by Controlling the Balance between Glutamate Uptake and Release. *Cells* **8**, (2019).

3. R. Maung *et al.*, CCR5 knockout prevents neuronal injury and behavioral impairment induced in a transgenic mouse model by a CXCR4-using HIV-1 glycoprotein 120. *Journal of immunology (Baltimore, Md. : 1950)* **193**, (2014).

4. V. E. Thaney *et al.*, IFNβ Protects Neurons from Damage in a Murine Model of HIV-1 Associated Brain Injury. **7**, 46514 (2017).

5. K. Johnson *et al.*, Gfap-positive radial glial cells are an essential progenitor population for later-born neurons and glia in the zebrafish spinal cord. *Glia* **64**, 1170-1189 (2016).

6. E. Raponi *et al.*, S100B expression defines a state in which GFAP-expressing cells lose their neural stem cell potential and acquire a more mature developmental stage. *Glia* **55**, 165-177 (2007).

7. L. E. Davis *et al.*, Early viral brain invasion in iatrogenic human immunodeficiency virus infection. *Neurology* **42**, 1736-1739 (1992).

8. C. D. Pilcher *et al.*, HIV in body fluids during primary HIV infection: implications for pathogenesis, treatment and public health. *Aids* **15**, 837-845 (2001).

9. R. H. Enting *et al.*, Concentrations of human immunodeficiency virus type 1 (HIV-1) RNA in cerebrospinal fluid after antiretroviral treatment initiated during primary HIV-1 infection. *Clin Infect Dis* **32**, 1095-1099 (2001).

10. K. T. Arrildt *et al.*, Phenotypic Correlates of HIV-1 Macrophage Tropism. *J Virol* **89**, 11294-11311 (2015).

11. D. E. Mosier, How HIV changes its tropism: evolution and adaptation? *Curr Opin HIV AIDS* **4**, 125-130 (2009).

12.   S. B. H. Gumbs *et al.*, Human microglial models to study HIV infection and neuropathogenesis: a literature overview and comparative analyses. *J Neurovirol* **28**, 64-91 (2022).

13.   M. A. Rai *et al.*, Comparative analysis of human microglial models for studies of HIV replication and pathogenesis. *Retrovirology* **17**, 35 (2020).

CHAPTER FIVE:

Conclusions and Future Directions

5.1. CONCLUSION

Viral encephalitis is seen in a plethora of viral infections which originate in the periphery and penetrate through the blood brain barrier into the parenchyma of the CNS. Among these viruses is HIV, which can traffic into the CNS resulting in viral protein production and innate immune activation, leading to pro-inflammation and neurotoxicity. The underlying mechanism for neuroinflammation, and resulting neurocognitive deficits, remain only partially understood. Namely, mild forms of neurocognitive deficits persist regardless of nearly complete viral suppression. This dissertation characterizes the impact of a crucial innate immune type I interferon, IFNβ, deficiency on HIV-1 enveloped protein induced neuroHIV. Additionally, this dissertation describes novel findings elucidating the functional role ephrin-B/EphB, a differentially expressed family, following IFNβ treatment, in the neuroinflammatory response in HIV.

In Chapter Two, IFNβ depletion was investigated to determine IFNβ's role in HIVgp120 induced neuroHIV. Presence of endogenous IFNβ proved to be on one hand important for the maintenance of recognition and spatial memory, and post-synaptic neuronal integrity. However, in the hippocampus, IFNβ depletion showed an amelioration of the HIVgp120 induced pre-synaptic damage and microglial activation, pointing to brain region-dependent effects on neuropathology. In the presence of HIVgp120, IFNβ depletion showed a less activated type I interferon response based on IRF7, DDX58, MX1 and IRF9 transcript levels, and phospho-STAT1 protein among others. Additionally, it showed a reduction in pro-inflammatory cytokines/chemokines such as CXCL10 and CCL2. These findings suggest a pivotal role for endogenous IFNβ

in maintaining a robust antiviral response, modulating neuropathology and MAPK/STAT activation pathways. Moreover, the study identified independently of any HIVgp120 effect a critical role of baseline expression of IFNβ for normal brain function.

Chapter Three highlights the activation and functional role of EphB2 in HIV. Firstly, ephrin-B/EphB is induced in the presence of HIV viral envelope protein gp120, and by treatment with recombinant IFNβ, a prominent type I interferon. Specifically, EphB2 was elevated in the CNS of PLWH who have brain pathology, but not those without brain pathology, as well as in IFNβ treated human microglia. Ephrin-B1 was found to be elevated following IFNβ treated human microglia, and in HIVgp120tg or IFNβ treated mice. However, what was unclear was the implications of this abundance of EphB2 in the brain on microglia. Therefore, the second conclusion was EphB2-mediated ephrin-B reverse signaling induced a pro-inflammatory and antiviral response. Knockdown of microglial ephrin-B1, a binding partner to EphB2, only partially alleviated EphB2 mediated activation of microglia **(Table 5.1)**.

	Vehicle	EphB2 activated microglia	EphB2 activated microglia w/ ephrin-B1 knockdown
Cytokine Production	-	⬆⬆⬆	⬆
Chemokine Production	-	⬆⬆⬆	⬆
Antiviral Response	-	⬆⬆⬆	⬆

Table 5.1. Overview of the inflammatory and antiviral changes following EphB2 and ephrin-B1 knockdown. EphB2 treated microglia activate NF-kB, secrete pro-inflammatory cytokines/chemokines, and generate an antiviral response. Ephrin-B1 knockdown blunts these responses.

Furthermore, the transfer of conditioned media from EphB2-mediated ephrin-B1 reverse signaling on microglia to iPSC derived neuron and astrocyte co-cultures resulted in contact independent neurotoxicity. Altogether, the findings highlight EphB2 activation in the CNS of PLWH and warrants an investigation into other neurodegenerative diseases with an inflammatory component. Additionally, it points to EphB2 as an activator of NF-kB and a pro-inflammatory response capable of inducing neurotoxicity while simultaneously inducing an antiviral response. Finally, in Chapter Four, experiments to optimize microglial HIV infection were done to ultimately investigate the impact of EphB2 mediated ephrin-B reverse signaling on HIV permissiveness given microglia's prominent antiviral response following EphB2 treatment. These optimization studies are a pre-requisite for the future directions focused on elucidating the impact of EphB2 treatment specifically on HIV infection dynamics in microglia.

5.2. FUTURE DIRECTION

The primary novel discovery in this dissertation focuses on elucidating the inflammatory and antiviral role of EphB2, which is elevated in the CNS of PLWH or in presence of viral envelope protein gp120. However, it does not focus on the functional role of EphB2 during HIV infection. Future directions include firstly, determining the inflammatory products of HIV infected microglia, and whether they are sufficient to induce contact independent neuronal damage. Additionally, preliminary data in Fig 4.3 suggests HIVBaL may upregulate ephrin-B1 in Ghost cells which warrants studies confirming if this phenomenon also occurs on iPSC derived microglia, the primary viral reservoir in the CNS. Then assessing if EphB2 mediated ephrin-B reverse signaling on microglia renders microglia less permissive to HIV infection, given the activation of the antiviral response, and if this impacts inflammatory production and subsequent neuronal damage.

Furthermore, downregulation of EphB2's binding partner ephrin-B1 on microglia, using ephrin-B1 siRNA, resulted in reduced inflammatory production but not complete return to baseline. This warrants further investigation of knocking down ephrin-B2 and ephrin-B3 to target all potential EphB2 binding partners. Additionally, it remains uncertain how modulating ephrin-Bs *in vivo* impact inflammation, neurotoxicity and ultimately behavior to inform us on its potential role as a therapeutic. To this end, it would be useful to investigate a microglia specific ephrin-B1/B2/B3 siRNA or antisense oligonucleotide (ASO) delivered to HIV infected humanized mice, to determine its

impact on inflammatory production, antiviral response, and neurotoxicity in an *in vivo* HIV infection model.

Initial studies with pH sensitive particles (data not shown) and differential expression of CD68 suggest a potential positive regulation of phagocytosis by microglial ephrin-B1. Furthermore, a differentially expressed marker in microglia, IFITM3, following EphB2 treatment in microglia, has been recently implicated in microglia's role in synaptic engulfment. These preliminary findings point to a potentially more contact dependent mechanism by which microglial ephrin-B/EphB could be impacting neurons and synaptic engulfment. It is unclear whether increased engulfment is beneficial or detrimental for surrounding neurons given that this can be aberrant and prune healthy neurons or scavenge to remove compromised neurons and debris. Moreover, it's unclear whether this increased phagocytic/synaptic pruning by microglia has a proclivity towards excitatory vs inhibitory subtypes of neurons in HIV. Therefore, future studies are warranted assessing the extent EphB2 treated microglia's synaptic engulfment capacity, and the consequence of this engulfment on neuronal health.

As it stands, these studies provide the foundation and rationale for further exploration of ephrin-B/EphB's role in neuroinflammation and in a type I interferon response specifically on microglia. Beyond its role in neuroHIV, this newly discovered signaling in microglia may provide a novel mechanism for neuroinflammation in other neurodegenerative diseases that may not be of viral origin.